AD-A196 505

DTIC FILE COPY

TOPICAL MEETING ON

LASERS IN MATERIAL DIAGNOSTICS

Approved for public release;
distribution unlimited.

AIR FORCE OFFICE OF SCIENTIFIC RESEARCH (AFSC)
NOTICE OF TRANSMITTAL TO DTIC
This technical report has been reviewed and is
approved for public release IAW AFR 190-12.
Distribution is unlimited.
MATTHEW J. KERPER
Chief, Technical Information Division

DTIC
ELECTE
JUN 3 0 1988
S E D

TECHNICAL DIGEST SERIES VOLUME 7

FEBRUARY 11-12, 1987
ALBUQUERQUE, NEW MEXICO

88 6 29 091

Unclassified
SECURITY CLASSIFICATION OF THIS PAGE

REPORT DOCUMENTATION PAGE

Unclassified

1a. REPORT SECURITY CLASSIFICATION: Unclassified	1b. RESTRICTIVE MARKINGS
2a. SECURITY CLASSIFICATION AUTHORITY	3. DISTRIBUTION/AVAILABILITY OF REPORT: Approved for public release; Distribution unlimited
2b. DECLASSIFICATION/DOWNGRADING SCHEDULE	
4. PERFORMING ORGANIZATION REPORT NUMBER(S)	5. MONITORING ORGANIZATION REPORT NUMBER(S): AFOSR-TR- 88-0599
6a. NAME OF PERFORMING ORGANIZATION: Optical Society of America — 6b. OFFICE SYMBOL (If applicable)	7a. NAME OF MONITORING ORGANIZATION: AFOSR/NP
6c. ADDRESS (City, State, and ZIP Code): 1816 Jefferson Place, N.W. Washington, D.C. 20036	7b. ADDRESS (City, State, and ZIP Code): Bldg. 410 Bolling AFB, Washington, D.C. 20332-6448
8a. NAME OF FUNDING/SPONSORING ORGANIZATION: AFOSR — 8b. OFFICE SYMBOL (If applicable): NP	9. PROCUREMENT INSTRUMENT IDENTIFICATION NUMBER: AFOSR-87-0094
8c. ADDRESS (City, State, and ZIP Code): Bldg. 410 Bolling AFB, Washington, D.C. 20332-6448	10. SOURCE OF FUNDING NUMBERS: PROGRAM ELEMENT NO. 61102F; PROJECT NO. 2301; TASK NO. A1; WORK UNIT ACCESSION NO.

11. TITLE (Include Security Classification): Organization of the Topical Meeting on Lasers in Material Diagnostics

12. PERSONAL AUTHOR(S): Jarus W. Quinn

13a. TYPE OF REPORT	13b. TIME COVERED	14. DATE OF REPORT (Year, Month, Day)	15. PAGE COUNT
Final	FROM 01/01/87 TO 10/31/87	87/10/31	

16. SUPPLEMENTARY NOTATION

17. COSATI CODES			18. SUBJECT TERMS (Continue on reverse if necessary and identify by block number)
FIELD	GROUP	SUB-GROUP	DIAGNOSTICS, LASERS, OPTICS. (mgm)

19. ABSTRACT (Continue on reverse if necessary and identify by block number)

Semiconductor Lasers: Semiconductor diode lasers remain the subject of intensive worldwide development efforts with rapid progress being made in many areas of device design and performance. In addition to their use in optical fiber systems, other applications have been identified and lasers are being fabricated to meet many different system requirements. This meeting treated all aspects of laer design, development and characterization.

Lasers in Material Diagnostics: Laser and optical techniques are increasingly important for diagnostics of a wide variety of materials and processing technologies. Applications range from diagnostics of impurities and other defects in materials, to probes of dry-processing technologies for semiconductor device fabrication, to imaging techniques for patterning and analysis in VLSI manufacture. These techniques are being used both for analytic measurements and as tools to probe new materials and effects. This meeting brought together workers from all of these areas for the exchange of results and of new directions for research. (over)

20. DISTRIBUTION/AVAILABILITY OF ABSTRACT: ☒ UNCLASSIFIED/UNLIMITED ☐ SAME AS RPT ☐ DTIC USERS	21. ABSTRACT SECURITY CLASSIFICATION: Unclassified
22a. NAME OF RESPONSIBLE INDIVIDUAL: Dr. Howard R. Schlossberg	22b. TELEPHONE (Include Area Code): 202/767-4906 — 22c. OFFICE SYMBOL: NP

DD FORM 1473, 84 MAR — 83 APR edition may be used until exhausted. All other editions are obsolete.

SECURITY CLASSIFICATION OF THIS PAGE
Unclassified

SOUTHWEST OPTICS '87 CONFERENCE
REGISTRATION LIST

LASTNAME	FIRSTNAM	ORGANIZA	ADDRESS1	ADDRESS2	MAILCODE	COUNTRY	DIGEST
ABEY	ALBERT E.	LLNL	PO BOX 808, L-86	LIVERMORE, CA	94550	USA	O
AL-JUMAILY	GHANIM A.	BARR ASSOCIATES	2 LYBERTY WAY	WESTFORD, MA	01720	USA	O
ANTHIS	JOHN P.	SANDIA NATIONAL LABS	DIV 2531 PO BOX 5800	ALBUQUERQUE, NM	87185	USA	L
APFEL	JOE	OCLI	2789 NORTHPOINT	SANTA ROSA, CA	95407	USA	O
ARIESSOHN	PETER C.	WEYERHAEUSER COMPANY	WTC 2F22	TACOMA, WA	98477	USA	L
ASAWA	CHARLES K.	TRW ELECTRO OPTICS RES CTR	ONE SPACE PARK	REDONDO BH, CA	90278	USA	S
ASHBY	CAROL	SANDIA NATIONAL LABS	DIV 1126 PO BOX 5800	ALBUQUERQUE, NM	87185	USA	L
ATKINSON	GEORGE H.	UNIVERSITY OF ARIZONA	DEPT OF CHEMISTRY	TUCSON, AZ	85721	USA	L
AVINOR	MICHAEL	UNIVERSITY OF NEW MEXICO		ALBUQUERQUE, NM	87131	USA	S
BASS	MICHAEL	UNIV OF SOUTHERN CALIFORNIA	UNIVERSITY PARK	LOS ANGELES, CA	90089	USA	L
BECKER	MICHAEL F.	UNIVERSITY OF TEXAS	ELECTRICAL ENGN DEPT	AUSTIN, TX	28712	USA	L
BENOOW	BERNARD	BDM CORPORATION	1801 RANDOLPH SE	ALBUQUERQUE, NM	87106	USA	S
BERRY	MICHAEL	RICE UNIV DEPT OF CHEMISTRY	PO BOX 1892	HOUSTON, TX	77251	USA	L
BLACK	BOB S.		7111 MOJAVE NW	ALBUQUERQUE, NM	87120	USA	S
BOLCH	JAMES B.	UNITED TECH OPTICAL SYSTEMS	PO BOX 109660	W PALM BH, FL	33410	USA	O
BOTEZ	DAN	TRW ELECTRO OPTICS RES CTR	ONE SPACE PARK	REDONDO BH, CA	90278	USA	S
BOUTOUNAT	MARIELLE S.	UNIVERSITY OF ARIZONA	DEPT OF CHEMISTRY	TUCSON, AZ	85721	USA	L
BRANNON	PAUL J.	SANDIA NATIONAL LABS	DIVISION 1124	ALBUQUERQUE, NM	87185	USA	S
BREILAND	WILLIAM G.	SANDIA NATIONAL LABS	DIVISION 1126	ALBUQUERQUE, NM	87185	USA	L
BROOKS	BOB	TRW ELECTRO OPTICS RES CTR	ONE SPACE PARK, R1-2162	REDONDO BH, CA	90278	USA	S
BROST	GEORGE A.	F J SEILER RESEARCH LAB		USAF ACAD, CO	80840	USA	S
BROWNING	STEPHEN D.	OPTICAL COATING LAB INC	2789 NORTHPOINT PARKWAY	SANTA ROSA, CA	95407	USA	O
BRUECK	STEVE	UNIVERSITY OF NEW MEXICO	CTR FOR HIGH TECH MATERIALS	ALBUQUERQUE, NM	87131	USA	L
BURNHAM	ROBERT D.	AMOCO RESEARCH CENTER	PO BOX 400, MS-F4	NAPERVILLE, IL	60566	USA	S
CANTRELL	CYRUS D.	UNIV OF TEXAS AT DALLAS	PO BOX 830688	RICHARDSON, TX	75083	USA	S
CARNIGLIA	CHARLES K.	MARTIN MARIETTA	PO BOX 9316, INT AIRPORT	ALBUQUERQUE, NM	87119	USA	O
CARSON	SUSAN D.	BDM CORPORATION	1801 RANDOLPH RD SE	ALBUQUERQUE, NM	87106	USA	L
CARVER	GARY E.	AT&T - ERC	PO BOX 900	PRINCETON, NJ	08540	USA	L
CHEN	C. C.	BOEING ELECTRONICS COMPANY	PO BOX 24969	SEATTLE, WA	98124	USA	S
CHENG	WOOD-HI	ROCKWELL INTERNATIONAL	PO BOX 10462, MS 406-230	DALLAS, TX	75207	USA	S
CHERNG	CHUNG-PIN	UNIVERSITY OF NEW MEXICO	CTR FOR HIGH TECH MATERIALS	ALBUQUERQUE, NM	87131	USA	S
CHOW	WENG W.	HUGHES AIRCRAFT	1600 RANDOLPH CT SE	ALBUQUERQUE, NM	87131	USA	S
CHRISTENSEN	DAVID H.	BALL AEROSPACE SYSTEMS DIV	PO BOX 1062, MS-T03	BOULDER, CO	80302	USA	S
CHRISTMAN	JO-ANNE M.	JET PROPULSION LABORATORY	4800 OAK GROVE DRIVE	PASADENA, CA	91109	USA	S
CHUNG	KI-HYUN	UNIVERSITY OF NEW MEXICO	CTR FOR HIGH TECH MATERIALS	ALBUQUERQUE, NM	87131	USA	S
CHUNG	YUN C.	LOS ALAMOS NATIONAL LAB	PO BOX 1663, CLS-5, MS/E535	LOS ALAMOS, NM	87545	USA	S
COLEMAN	JAMES J.	UNIVERSITY OF ILLINOIS	DEPT OF ELECTRICAL ENG	URBANA, IL	61801	USA	S
COLTRIN	MICHAEL E.	SANDIA NATIONAL LABS	DIVISION 1126	ALBUQUERQUE, NM	87185	USA	L
COOPER	DONALD E.	ROCKWELL INTERNATIONAL	1049 CAMINO DOS RIOS	THOUSAND OAK,CA	91360	USA	L
COOPER	DAVID E.	SRI INTERNATIONAL	333 RAVENSWOOD AVENUE	MENLO PARK, CA	94025	USA	L
CROWE	VICTOR S.	ALBUQUERQUE T-VI	2632 GRANITE NW	ALBUQUERQUE, NM	87104	USA	O
CROWE	DAVID A.	EASTMAN KODAK CO FSD	901 ELMGROVE ROAD	ROCHESTER, NY	14616	USA	O
CZYZAK	STANLEY R.	FJSRL	US AIR FORCE ACADEMY	COLORADO SG, CO	80840	USA	S
DAHLHAUSER	KARL J.	US AIR FORCE	AFWL/ARBF	KIRTLAND AFB,NM	87117	USA	S
DALTON	DONALD A.	UNITED TECH OPTICAL SYSTEMS	5301 CENTRAL, STR 1617	ALBUQUERQUE, NM	87108	USA	O
DE HAINAUT	LINDA M.	UNIVERSITY OF NEW MEXICO		ALBUQUERQUE, NM	87108	USA	L
DE WILTON	ANGELA C.	NORTHERN TELECOM ELEC	PO BOX 3511 STATION E	OTTAWA ONTARIO	K1Y4H7	CANADA	L
DEFREEZ	RICHARD K.	OREGON GRADUATE CENTER	19600 NW VON NEWMANN DR	BEAVERTON, OR	97006	USA	S
DENTE	GREGORY	CONSULTANT	2100 ALVARADO NE	ALBUQUERQUE, NM	87110	USA	S
DEPATIE	DAVID A.	KIRKLAND AIR FORCE BASE	AFWL	ALBUQUERQUE, NM	87117	USA	S
DIADIUK	VICKY	MIT LINCOLN LABORATORY	PO BOX 73	LEXINGTON, MA	02173	USA	S
DONOVAN	TERRY M.	NAVAL WEAPONS CENTER		CHINA LAKE, CA	93555	USA	O
DREYFUS	RUSSELL W.	IBM T J WATSON RESEARCH CTR	PO BOX 218	YKTOWN HTS, NY	10598	USA	L
DUFFY	PHILIP B.	LLNL	PO BOX 808, L-86	LIVERMORE, CA	94550	USA	O
DUPUIS	RUSSELL D.	AT&T BELL LABORATORIES	ROOM 7C327	MURRAY HILL, NJ	07974	USA	S

SOUTHWEST OPTICS '87 CONFERENCE
REGISTRATION LIST

LASTNAME	FIRSTNAM	ORGANIZA	ADDRESS1	ADDRESS2	MAILCODE	COUNTRY	DIGEST
EASTMAN	DANIEL R.	PERKIN-ELMER	401 MAIN AVENUE	NORWACK, CT	00859	USA	D
EATON	LARRY R.	TRW ELECTRO OPTICS RES CTR	ONE SPACE PARK	REDONDO BH, CA	90278	USA	S
ENGLERT	THAD J.	UNIVERSITY OF WYOMING	DEPT OF ELECTRICAL ENG	LARAMIE, WY	82071	USA	D
ENGLERT	SUE E.	UNIVERSITY OF WYOMING	DEPT OF ELECTRICAL ENGNR	LARAMIE, WY	82071	USA	D
EPLER	JOHN E.	XEROX PARC	3333 COYOTE HILL ROAD	PALO ALTO, CA	94043	USA	S
FACEY	TERENCE A.	PERKIN ELMER	100 WOOSTER HEIGHTS ROAD	DANSBURY, CT	06810	USA	D
FAUCHET	PHILIPPE M.	PRINCETON UNIVERSITY	DEPT OF ELECTRICAL ENG	PRINCETON, NJ	08544	USA	L
FECK	DAVID W.		1925 19TH LOOP	KIRTLAND AFB,NM	87116	USA	L
FERGUSON	THOMAS R.	AFWL/ARBL	517 MONTCLAIRE SE	ALBUQUERQUE, NM	87108	USA	S
FIGUEIRA	JOSEPH F.	LOS ALAMOS NATIONAL LAB	MS J566	LOS ALAMOS, NM	87501	USA	D
FIGUEROA	LUIS	UNIVERSITY OF FLORIDA	ELEC ENG, 216 LARSEN	GAINESVILLE, FL	32611	USA	S
FINLAN	J. MICHAEL	GENERAL ELECTRIC	PO BOX 8555 M1334	PHILADELPHIA,PA	19101	USA	S
FLOHR	MARK C.	UNIVERSITY OF WYOMING	DEPT OF ELECTRICAL ENG	LARAMIE, WY	82071	USA	D
FONG	CHUE	UNIVERSITY OF NEW MEXICO	CTR FOR HIGH TECH MATERIALS	ALBUQUERQUE, NM	87131	USA	L
FOSTER	MIKE D.	SIEMENS TRANSMISSION SYSTEM	ONE CAMINO DE LENKURT, NE	ALBUQUERQUE, NM	87123	USA	S
FRAAS	LEWIS, M.	BOEING TECH	PO BOX 28969 MS 9Z 80	SEATTLE, WA	98124	USA	S
GERARDO	JAMES B.	SANDIA NATIONAL LABS	PO BOX 5800	ALBUQUERQUE, NM	87185	USA	S
GIBB	ROGER M.	STC/STANTEL	PAIGNTON	DEVON		UK	S
GILLMAN	JOEL M.	ALBUQUERQUE T-VI	525 BUENA VISTA ST	ALBUQUERQUE, NM	87106	USA	L
GLECKLER	ANTHONY D.	UNIVERSITY OF ARIZONA	OPTICAL SCIENCES CENTER	TUCSON, AZ	85712	USA	S
GOERINGER	DOUGLAS E.	OAK RIDGE NATIONAL LAB	PO BOX Y BLDG 9735	OAK RIDGE, TN	37831	USA	L
GOTTSCHO	RICHARD A.	AT&T BELL LABORATORIES	ROOM 1A-259	MURRAY HILL, NJ	07974	USA	L
GOURLEY	PAUL L.	SANDIA NATIONAL LABS	DIVISION 1143	ALBUQUERQUE, NM	87185	USA	S
GREENBERG	KENNETH E.	SANDIA NATIONAL LABS	DIVISION 1124	ALBUQUERQUE, NM	87185	USA	L
GRISCOM	DAVID L.	NAVAL RESEARCH LAB	CODE 6570	WASHINGTON, DC	20375	USA	D
GUEL	GRACIELA R.	UNIVERSITY OF NEW MEXICO	TAPY HALL 101	ALBUQUERQUE, NM	87131	USA	S
GUENTHER	ARTHUR H.	AIR FORCE WEAPONS LAB		KIRTLAND AFB,NM	87117	USA	D
HADLEY	G. RONALD	SANDIA NATIONAL LABS	DIVISION 1124	ALBUQUERQUE, NM	87185	USA	S
HALE	CHARLEY P.	SPECTRON/A TITAN COMPANY	2017 YALE BLVD SE	ALBUQUERQUE, NM	87106	USA	D
HAMAKER	HENRY C.	VARIAN ASSOC MSK-115	GILHANSEN WAY	PALO ALTO, CA	94303	USA	S
HARGIS	PHILIP J.	SANDIA NATIONAL LABS	DIVISION 1124	ALBUQUERQUE, NM	87185	USA	L
HARRISON	FRANCIS B.	LOS ALAMOS NATIONAL LAB	MS E-543	LOS ALAMOS, NM	87545	USA	D
HENRY	CHARLES H.	AT&T BELL LABORATORIES	600 MOUNTAIN AVENUE	MURRAY HILL, NJ	07974	USA	S
HERMAN	IRVING	COLUMBIA UNIVERSITY		NEW YORK, NY	10027	USA	L
HETHERINGTON	WILLIAM M.	UNIVERSITY OF ARIZONA	DEPT OF CHEMISTRY	TUCSON, AZ	85721	USA	L
HIGBY	PAIGE L.	NRL/SFA	1401 MCCORMICK DR	LANDOVER, MD	20785	USA	D
HILL	DAILY S.	MCDONNEL DOUGLAS OPTO CTR	350 EXECUTIVE BOULEVARD	ELMSFORD, NY	10523	USA	S
HILLMAN	PAUL D.	AFWL/ARBF	KIRTLAND AIR FORCE	ALBUQUERQUE, NM	87117	USA	S
HJELME	DAG R.	UNIVERSITY OF COLORADO	DEPT OF EE, CAMPUS BOX 425	BOULDER, CO	80309	USA	S
HO	PAULINE	SANDIA NATIONAL LABS	DIVISION 1126	ALBUQUERQUE, NM	87185	USA	L
HOGGE	CHARLES B.	AIR FORCE WEAPONS LAB	KIRTLAND AIR FORCE BASE	ALBUQUERQUE, NM	87111	USA	D
HOHIMER	JOHN P.	SANDIA NATIONAL LABS	DIVISION 1124	ALBUQUERQUE, NM	87185	USA	S
HOLLBERG	LEO W.	NATL BUREAU OF STANDARDS	325 BROADWAY	BOULDER, CO	80303	USA	S
HUTCHINSON	JAMES A.	UNIV OF CALIFORNIA, IRVINE	DEPT OF CHEMISTRY	IRVINE, CA	92717	USA	L
IACOVAZZI	ROBERT A.	MARTIN MARIETTA AEROSPACE	PO BOX 5837 MP 150	ORLANDO, FL	32806	USA	D
IMAI	HAJIME	FUJITSU LABORATORIES	10-1 MORINOSATO-WAKAMIYA	ATSUGI		JAPAN	S
INGLE	JEFFREY T.	DEPARTMENT OF DEFENSE	9800 SAVAGE ROAD	FORT MEADE, MD	20755	USA	S
JANSEN	MICHAEL	TRW ELECTRO OPTICS RES CTR	ONE SPACE PARK	REDONDO BH, CA	90278	USA	S
KAMINOW	IVAN P.	AT&T BELL LABORATORIES	BOX 400	HOLMDEL, NJ	07733	USA	S
KARR	THOMAS J.	LLNL	PO BOX 808, L-495	LIVERMORE, CA	94550	USA	D
KAWANISHI	HIDENORI	SHARP CORPORATION	2613-1 ICHINOMOTO-CHO	TENRI-SHI	632	JAPAN	S
KAY	BRUCE D.	SANDIA NATIONAL LABS	ORG 1841 PO BOX 5800	ALBUQUERQUE, NM	87185	USA	L
KEILBACK	KEVIN A.	UNIVERSITY OF ARIZONA	OPTICAL SCIENCES CENTER	TUCSON, AZ	85721	USA	D
KELLER	RICHARD A.	LOS ALAMOS NATIONAL LAB	4 LA ROSA CT	LOS ALAMOS, NM	87454	USA	L
KELLY	SHAWN L.	ROME AIR DEVELOPMENT CTR	RADC/OCSE	GRIFFISS AFB,NY	13441	USA	S

SOUTHWEST OPTICS '87 CONFERENCE
REGISTRATION LIST

LASTNAME	FIRSTNAM	ORGANIZA	ADDRESS1	ADDRESS2	MAILCODE	COUNTRY	DIGEST
KEMPI	DAVID J.	ROCKWELL INTERNATIONAL CORP	2309 RENARD PL SE,SUITE 207	ALBUQUERQUE, NM	87106	USA	L
KINDER	FLOYD A.	COMARCO	509 LAS POSAS	RIDGECREST, CA	93555	USA	D
KING	C. W.	HARSHAW/FILTROL PARTNERSHIP	6801 COCHRAN ROAD	SOLON, OH	44139	USA	D
KOCH	THOMAS L.	AT&T BELL LABORATORIES	CRAWFORDS CORNER ROAD	HOLMDEL, NJ	07733	USA	S
KRAMARSIC	ROMAN J.	BDM	1801 RANDOLPH ROAD SE	ALBUQUERQUE, NM	87106	USA	D
KULLENDORFF	NILS J.	RIFA ERICCSON, DEPT U/TY	S-16381	STOCKHOLM		SWEDEN	S
KUO	CHIEN-YU	AT&T BELL LABORATORIES	555 UNION BLVD, RM 2C-205	ALLENTOWN, PA	18103	USA	S
LACOURSE	JOANNE	GET LABORATORIES	40 SYLVAN ROAD	WALTHAM, MA	02254	USA	S
LAW	MARILYN A.	MARTIN MARIETTA	PO BOX 9316	ALBUQUERQUE, NM	87119	USA	D
LEE	SONG	UNIVERSITY OF FLORIDA	ELEC ENG, 216 LARSEN	GAINESVILLE, FL	32611	USA	S
LEE	T. P.	BELLCORE		RED BANK, NJ	07701	USA	S
LEGER	JAMES R.	MIT LINCOLN LABORATORY	244 WOOD STREET	LEXINGTON, MA	02173	USA	S
LEMAIRE	HERVE L.	UNIVERSITY OF ARIZONA	DEPARTMENT OF CHEMISTRY	TUCSON, AZ	85721	USA	S
LIAU	ZONG-LONG	MIT LINCOLN LABORATORY	PO BOX 73	LEXINGTON, MA	02173	USA	S
LOWDERMILK	HOWARD	LLNL	PO BOX 808	LIVERMORE, CA	94550	USA	S
LUO	JHY-MINH	UNIVERSITY OF NEW MEXICO	CTR FOR HIGH TECH MATERIALS	ALBUQUERQUE, NM	87131	USA	D
MACLEOD	ANGUS	UNIVERSITY OF ARIZONA	OPTICAL SCIENCES CENTER	TUCSON, AZ	85721	USA	S
MACOMBER	STEVEN N.	PERKIN-ELMER	100 WOOSTER HEIGHTS ROAD	DANBURY, CT	06810	USA	D
MAGEE	CARL J.	NASA LANGLEY RESEARCH CTR	MS-468	HAMPTON, VA	23665	USA	S
MANTE	JOSEPH L.	SIEMES RTL	105 COLLEGE ROAD EAST	PRINCETON, NJ	08540	USA	S
MARCHIANDO	JAY F.	NATL BUREAU OF STANDARDS		GAITHERSBURG,MD	20899	USA	S
MARION	JOHN E.	LLNL	L-456	LIVERMORE, CA	94550	USA	L
MASLEY	ANDREW J.	TRW ELECTRO OPTICS RES CTR	ONE SPACE PARK	REDONDO BH, CA	90278	USA	S
MCCRAE	JACK E.	KIRTLAND AIR FORCE BASE	AFWL/ARBE	KIRTLAND AFB,NM	87117	USA	S
MCCREADY	DAVID E.	MARTIN MARIETTA	PO BOX 9316	ALBUQUERQUE, NM	87119	USA	S
MCGARVEY	JOHN	BOEING ELECTRONICS	PO BOX 24969 MS 7J-05	SEATTLE, WA	98124	USA	D
MCINERNEY	JOHN G.	UNIVERSITY OF NEW MEXICO	CTR FOR HIGH TECH MATERIALS	ALBUQUERQUE, NM	87131	USA	S
MCNALLY	JAMES J.	USAF ACADEMY	USAF/DFP	COLORADO SGS,CO	80840	USA	S
MCNEIL	THOMAS E.	US AIR FORCE ACADEMY	4115 DOLPHIN CR.	COLORADO SPG,CO	80918	USA	D
MCNEIL	JOHN R.	UNIVERSITY OF NEW MEXICO	DEPT OF ELEC ENG	ALBUQUERQUE, NM	87131	USA	L
MELNGAILIS	IVARS	MIT LINCOLN LABORATORY	PO BOX 73	LEXINGTON, MA	02173	USA	L
MILAM	DAVID	LLNL	PO BOX 808	LIVERMORE, CA	94550	USA	S
MILEY	GEORGE H.	UNIVERSITY OF ILLINOIS	214 NEL 103 S GOODWIN	URBANA, IL	61801	USA	D
MORRISON	CHARLES B.	TRW ELECTRO OPTICS RES CTR	ONE SPACE PARK B 147 RM1393	REDONDO BH, CA	90278	USA	D
MOTT	JEFFREY	PERKIN-ELMER CORP	100 WOOSTER HEIGHTS ROAD	DANBURY, CT	06810	USA	S
MULLINS	BILL	UNIVERSITY OF NEW MEXICO	CTR FOR HIGH TECH MATERIALS	ALBUQUERQUE, NM	87131	USA	S
NELSON	ROY D.	BALL AEROSPACE	PO BOX 1062	BOULDER, CO	80306	USA	L
NEWMAN	PAUL R.	ROCKWELL INTERNATIONAL	1049 CAMINO DOS RIOS	THOUSAND OAK,CA	91360	USA	S
NEWMANN	DAVID K.	USAF ACADEMY	DEPT OF PHYSICS	COLORADO SGS,CO	80840	USA	L
NEWNAM	BRIAN E.	LOS ALAMOS NATIONAL LAB	MS J566	LOS ALAMOS, NM	87545	USA	S
NOLL	ROBERT J.	PERKIN ELMER	230 LOCKWOOD ROAD	FAIRFIELD, CT	06430	USA	D
O'BRIEN	JAMES J.	UNIVERSITY OF ARIZONA	DEPT OF CHEMISTRY	TUCSON, AZ	85721	USA	S
OCHOA	ELLEN	SANDIA NATIONAL LABS	DIVISION 8435	LIVERMORE, CA	94550	USA	L
ODOM	ROBERT W.	CHARLES EVANS & ASSOCIATES	301 CHESAPEAKE DRIVE	REDWOOD CITY,CA	94063	USA	L
OLSHANSKY	ROBERT	GTE LABORATORIES	40 SYLVAN ROAD	WALTHAM, MA	02254	USA	L
OSINSKI	MAREK A.	UNIVERSITY OF NEW MEXICO	CTR FOR HIGH TECH MATERIALS	ALBUQUERQUE, NM	87131	USA	S
OU	SIMON S.	TRW ELECTRO OPTICS RES CTR	ONE SPACE PARK	REDONDO BH, CA	90278	USA	S
OWYOUNG	ADELBERT	SANDIA NATIONAL LABS	DIVISION 1124	ALBUQUERQUE, NM	87185	USA	S
PAISLEY	DENNIS	LOS ALAMOS NATIONAL LAB	PO BOX 1663 MS P950	LOS ALAMOS, NM	87545	USA	S
PAPANNAREDDY	RAJAPPA	SOUTHERN METHODIST UNIV	ELEC ENG DEPT	DALLAS, TX	75275	USA	S
PARK	JONG-DAE	UNIVERSITY OF NEW MEXICO	CTR FOR HIGH TECH MATERIALS	ALBUQUERQUE, NM	87131	USA	S
PARTIN	JUDY K.	EG&G IDAHO INC	PO BOX 1625	IDAHO FALLS, ID	83415	USA	D
PCHELKIN	NICHOLAS R.	AIR FORCE WEAPONS LAB	AFWL/ARBF	KIRTLAND AFB,NM	87117	USA	S
PEEBLES	HENRY C.	SANDIA NATIONAL LABS		ALBUQUERQUE, NM	87185	USA	L
PENNEY	CARL N.	GENERAL ELECTRICS CORP	R & D CENTER	SCHENECTADY, NY	12345	USA	D

SOUTHWEST OPTICS '87 CONFERENCE
REGISTRATION LIST

LASTNAME	FIRSTNAM	ORGANIZA	ADDRESS1	ADDRESS2	MAILCODE	COUNTRY	DIGEST
PHILLIPS	HARVEY M.	MANAGEMENT TECHNOLOGY INT	3586 MARSHALL	RIVERSIDE, CA	92504	USA	S
PHILLIPS	DENNIS D.	MARTIN MARIETTA AEROSPACE	PO BOX 9316	ALBUQUERQUE, NM	87119	USA	D
PIERCE	BRUCE J.	SPI	PENTAGON	WASHINGTON, DC	20301	USA	D
PODLESNIK	DRAGAN V.	COLUMBIA UNIVERSITY	1220 MUDD, 500 W 120&L ST	NEW YORK, NY	10027	USA	L
POMPHREY	PATRICK J.	TRW	ONE SPACE PK, MS 01-1240	REDONDO BH, CA	90278	USA	D
PREIER	HORST M.	FRAUNHOFER GESELLSCHAFT	HEIDENHOFSTRASSE 8	FREIBURG	D-7800	FED REP GER	S
PRIMAS	LORI E.	JET PROPULSION LABORATORY	4800 OAK GROVE DRIVE	PASADENA, CA	91109	USA	S
QUERNS	JOHN F.	AFWL/ARBF	KIRTLAND AFB	KIRTLAND AFB,NM	87117	USA	S
RAJ	TILAK	MARTIN MARIETTA	PO BOX 9316	ALBUQUERQUE, NM	87109	USA	L
RAJA	YASIN	UNIVERSITY OF NEW MEXICO	CTR FOR HIGH TECH MATERIALS	ALBUQUERQUE, NM	87131	USA	L
RAJIC	SLOBODAN	ROCKWELL INTERNATIONAL	PO BOX 10462	DALLAS, TX	75207	USA	S
REDIKER	ROBERT H.	MASSACHUSETTS INST OF TECH	77 MASSACHUSETTS AVENUE	CAMBRIDGE, MA	02139	USA	S
REINHARDT	DIETER	CARL ZEISS	CARL ZEISS STR/POSTFACH	OBERKOCHEN	D-7082	FED REP GER	D
REISER	CHRISTOPHER	SANDIA NATIONAL LABS	DIVISION 1124	ALBUQUERQUE, NM	87185	USA	D
REYNOLDS	DONALD C.	AVIONICS LAB - WPAFB		DAYTON, OH	45433	USA	L
REZEK	EDWARD A.	TRW ELECTRO OPTICS RES CTR	ONE SPACE PARK	REDONDO BH, CA	90278	USA	S
RICE	WALTER H.	ALBUQUERQUE T-VI	525 BUENA VISTA SE	ALBUQUERQUE, NM	87106	USA	S
RICKS	DOUGLAS W.	NAVAL WEAPONS CENTER		CHINA LAKE, CA	93555	USA	D
ROSENCWAIG	ALLAN	THERMA-WAVE INC	47734 WESTINGHOUSE DRIVE	FREMONT, CA	94539	USA	L
ROYCHOUDHURI	CHANDRA	PERKIN ELMER	100 WOOSTER HEIGHTS	DANBURY, CT	06810	USA	S
SALZMAN	JOSEPH J.	BELL COMMUNICATIONS RES	331 NEWMAN SPRINGS ROAD	RED BANK, NJ	07701	USA	S
SANDERS	VIRGIL E.	LOS ALAMOS NATIONAL LAB	PO BOX 1663 MS-J566	LOS ALAMOS, NM	87545	USA	L
SARDAR	DHIRAJ K.	UNIV OF TEXAS , SAN ANTONIO		SAN ANTONIO, TX	78285	USA	D
SCHAUS	CHRISTIAN F.	UNIVERSITY OF NEW MEXICO	EECE, L2150	ALBUQUERQUE, NM	87131	USA	S
SCHLOSSBERG	HOWARD	AFOSR	BUILDING 410	BOLLING AFB, DC	20375	USA	L
SCHMELL	REED A.	MARTIN MARIETTA	9316 INTERNATIONAL AIRPORT	ALBUQUERQUE, NM	87119	USA	D
SCHROEDER	HOLGER	IBM ALMADEN RESEARCH CENTER	650 HARRY ROAD	SAN JOSE, CA	95120	USA	L
SCHULTZ	JOHN F.	AIR FORCE WEAPONS LAB	KIRTLAND AFB	ALBUQUERQUE, NM	87117	USA	S
SEO	DONG-SUN	UNIVERSITY OF NEW MEXICO	CTR FOR HIGH TECH MATERIALS	ALBUQUERQUE, NM	87131	USA	S
SERGANT	MOSHE	TRW ELECTRO OPTICS RES CTR	ONE SPACE PARK	REDONDO BH, CA	90278	USA	S
SHAGAM	RICHARD N.	SANDIA NATIONAL LABS	PO BOX 5800	ALBUQUERQUE, NM	87185	USA	D
SHIAH	TZENGHUEI	UNIVERSITY OF NEW MEXICO	409 SYCAMORE ST SE	ALBUQUERQUE, NM	87106	USA	S
SHIEH	CHAN-LONG	SIEMES RTL	105 COLLEGE ROAD EAST	PRINCETON, NJ	08540	USA	S
SINARD-NORMANDIN	MARTINE	NORTHERN TELECOM ELEC	PO BOX 3511 STATION C	OTTAWA ONTARIO	K1Y 4H7	CANADA	L
SMITH	MARK W.	UNIVERSITY OF ARIZONA	OPTICAL SCIENCES CENTER	TUCSON, AZ	85721	USA	L
SNAVELY	BENJAMIN B.	EASTMAN KODAK COMPANY	901 ELMGROVE RD, DEPT 394	ROCHESTER, NY	14650	USA	D
SOARES	SCHUBERT	UNIVERSITY OF NEW MEXICO	CTR FOR HIGH TECH MATERIALS	ALBUQUERQUE, NM	87131	USA	S
SODA	HARUHISA H.	FUJITSU LAB	10-1 MORINOSTAO-WAKAMIYA	ATSUGI	243-02	JAPAN	S
SOLTZ	BARBARA A.	MCDONNELL DOUGLAS	OPTO ELECTRONICS CENTER	ELMSFORD, NY	10977	USA	S
STAMNITZ	TIMOTHY C.	UNIVERSITY OF HAWAII	603 MILOKAI ST	KAILUA, HI	96734	USA	S
STANTON	ALAN C.	SOUTHWEST SCIENCES INC.	1570 PACHECO ST SUITE E-11	SANTA FE, NM	87501	USA	L
STEWART	ALAN F.	AIR FORCE WEAPONS LAB	AFWL/ARBD	KIRTLAND AFB,NM	87117	USA	D
STOWELL	W. KENT	USAF	AFWAL/AADO-2	WRIGHT AFB, OH	45433	USA	L
STRAND	JIM	IBM ALMADEN RESEARCH CENTER	650 HARRY ROAD	SAN JOSE, CA	95120	USA	L
STREIFER	WILLIAM	SPECTRA DIODE LABS	3333 NORTH FIRST ST	SAN JOSE, CA	94134	USA	S
STUKE	MICHAEL	MAX-PLANCK-INSTITUTE	PO BOX 2841	GOETTINGEN	D-3400	FED REP GER	L
SURGET	JEAN	ONERA	BP 72	CHATILLON CEDEX	92322	FRANCE	D
SWEATT	WILLIAM C.	SANDIA NATIONAL LABS	PO BOX 5800, DIV 7556	ALBUQUERQUE, NM	87185	USA	D
SWIMM	RANDALL T.	UNIV OF SOUTHERN CALIFORNIA	CENTER FOR LASER STUDIES	LOS ANGELES, CA	90089	USA	D
TALLANT	DAVID R.	SANDIA NATIONAL LABS	ORG 1823 PO BOX 5800	ALBUQUERQUE, NM	87185	USA	L
TAM	ANDREW C.	IBM ALMADEN RESEARCH CENTER	DEPT K07-803, 650 HARRY RD	SAN JOSE, CA	95120	USA	L
TARVIN	JEFFREY A.	SCHULUMBERGER-DOLL RESEARCH	OLD QUARRY ROAD	RIDGEFIELD, CT	06877	USA	D
THOMAS	IAN M.	LAWRENCE LIVERMORE NAT LAB	7000 EAST AVENUE L-483	LIVERMORE, CA	94550	USA	D
THOMPSON	WILLIAM E.	AIR FORCE WEAPONS LAB	AFWL/ARB	KIRTLAND AFB,NM	87117	USA	S
THORNTON	ROBERT L.	XEROX PARC	3333 COYOTE HILL ROAD	PALO ALTO, CA	94304	USA	S

SOUTHWEST OPTICS '87 CONFERENCE
REGISTRATION LIST

LASTNAME	FIRSTNAM	ORGANIZA	ADDRESS1	ADDRESS2	MAILCODE	COUNTRY	DIGEST
TIHANYI	PETER L.	MCDONNELL DOUGLAS OPTO CTR	350 EXECUTIVE BLVD	ELMSFORD, NY	10523	USA	S
TROTT	WAYNE M.	SANDIA NATIONAL LABS	DIVISION 1128	ALBUQUERQUE, NM	87185	USA	L
TURANO	ANDREW J.	RAYMOND ENGINEERING, INC.	217 SMITH STREET	MIDDLETOWN, CT	06457	USA	S
TYLER	WAYNE L.	MESA COMPANY	4508 ANDREW NE	ALBUQUERQUE, NM	87109	USA	S
UCHIYAMA	SEIJI S. U.	CHIBA UNIVERSITY	IMAGE SCI ENG, 1-33 YAYOICH	CHIBA	260	JAPAN	S
VARELA	JOSEPH R.	ALBUQUERQUE T-VI	110 COLUMBIA SE #52	ALBUQUERQUE, NM	87106	USA	S
VEDAMANIKAM	CHANDRAN P.		8221 CONNECTICUT NE	ALBUQUERQUE, NM	87110	USA	O
WACHTER	JOSEPH R.	LOS ALAMOS NATIONAL LAB	MS E540 LANL	LOS ALAMOS, NM	87545	USA	S
WAGNER	DAVID K.	MCDONNELL DOUGLAS CORP	350 EXECUTIVE BLVD	ELMSFORD, NY	10523	USA	L
WAKAO	KIYOHIDE K.	FUJITSU LAB LTD	10-1 MORINOSATO-WAKAMIYA	ATSUGI		JAPAN	S
WALL	DAIVD L.	SPECTRA-PHYSICS/LASER ANALY	25 WIGGINS AVENUE	BEDFORD, MA	01730	USA	S
WALPOLE	JAMES N.	MIT LINCOLN LABORATORY	240 WOOD STREET	LEXINGTON, MA	02173	USA	L
WALTHER	FREDERICK G.	MIT LINCOLN LABORATORY	BOX 73	LEXINGTON, MA	02173	USA	S
WANG	WILLIAM W.	UNIVERSITY OF NEW MEXICO	CTR FOR HIGH TECH MATERIALS	ALBUQUERQUE, NM	87131	USA	S
WANG	S. C.	LOCKHEED RESEARCH LABS	3251 HANOVER ST	PALO ALTO, CA	94304	USA	S
WATERS	ROBERT G.	MCDONNELL DOUGLAS OEC	350 EXECUTVIE BLVD	ELMSFORD, NY	10523	USA	S
WEEKS	ROBERT A.	VANDERBILT UNIVERSITY	PO BOX 1678-B	NASHVILLE, TN	37235	USA	S
WELCH	DAVID F.	SPECTRA DIODE LABS	3333 N. FIRST STREET	SAN JOSE, CA	94536	USA	O
WELFORD	DAVID	MIT LINCOLN LABORATORY	PO BOX 73	LEXINGTON, MA	02173	USA	S
WELLMAN	JOHN A.	EASTMAN KODAK COMPANY	901 ELMGROVE ROAD	ROCHESTER, NY	14650	USA	S
WESSEL	JOHN E.	THE AEROSPACE CORPORATION	PO BOX 92957	LOS ANGELES, CA	90009	USA	O
WHARTON	JOHN J.	DARPA	1400 WILSON BLVD	ARLINGTON, VA	22209	USA	L
WILCOX	JAROSLAVA Z.	TRW	ONE SPACE PARK	REDONDO BH, CA	90273	USA	O
WILHELMSEN	HARALD	MIT LINCOLN LABORATORY	WOOD STREET	LEXINGTON, MA	01741	USA	S
WILLIAMS	FORREST L.	UNM CTR FOR HIGH TECH MATLS	DEPT OF EECE	ALBUQUERQUE, NM	87131	USA	O
WILLIAMS	JAMES C.	AIR FORCE WEAPONS LAB	KIRTLAND AIR FORCE BASE	ALBUQUERQUE, NM	87117	USA	L
WILLIAMSON	ROD	SANDIA NATIONAL LABS	PO BOX 5800	ALBUQUERQUE, NM	87185	USA	S
WILLOUGHBY	CHARLES T.	TRW SPACE AND TECHNOLOGY	ONE SPACE PARK R1/1078	REDONDO BH, CA	90278	USA	L
WILSON	LOYOLA B.		3422 SMITH SE APT C	ALBUQUERQUE, NM	87106	USA	S
WILSON	KIMBERLEY A.	AIR FORCE	1020 VALENCIA SE #F6	ALBUQUERQUE, NM	87108	USA	S
WILSON	SCOTT R.	UNIV OF NEW MEXICO - CHTM	DEPT OF EECE	ALBUQUERQUE, NM	87131	USA	S
WOEHL	WALTER E.	US ARMY WHITE SANDS MIS RAN	1607 MEMORY LANE	ALAMOGORDO, NM	88310	USA	S
YANG	JANE J.	TRW	ONE SPACE PARK	REDONDO BH, CA	90278	USA	O
YARGER	FRED L.	NEW MEXICO HIGHLANS UNIV	SCH OF SCI AND TECH	LAS VEGAS, NM	87701	USA	S
YOUNGER	CHRIS L.	ALBUQUERQUE T-VI	11000 SKYLINE NE #9	ALBUQUERQUE, NM	87123	USA	L
ZAH	CHUNG-EN	BELL COMMUNICATIONS RES	NVC3X361 331 NEWMAN SGS RD	RED BANK, NJ	07701	USA	S
ZAIDI	SALEEM	UNIVERSITY OF NEW MEXICO	CTR FOR HIGH TECH MATERIALS	ALBUQUERQUE, NM	87131	USA	L
ZEDIKER	MARK S.	MCDONNELL DOUGLAS ASTRO	PO BOX 516	ST. LOUIS, MO	63166	USA	S
ZMUDZINSKI	CHARLES A.	UNIVERSITY OF ILLINOIS	DEPT OF ELECTRICAL ENG	URBANA, IL	61801	USA	S
ZYSKIND	JOHN L.	AT&T BELL LABORATORIES	PO BOX 400	HOLMDEL, NJ	07733	USA	S

Total registration: 260

L = Lasers in Materials Diagnostics
S = Semiconductor Lasers
O = Optics in Adverse Environments

AFOSR-TR- 88-0599

TOPICAL MEETING ON

LASERS IN MATERIALS DIAGNOSTICS

Summaries of papers presented at the
Laser in Materials Diagnostics Topical Meeting

February 11-12, 1987

Albuquerque, New Mexico

Sponsored by the

Lasers and Electro-Optics Society of IEEE
Optical Society of America

Optical Society of America
1816 Jefferson Place, N.W.
Washington, D.C. 20036
(202) 223-8130

TABLE OF CONTENTS

PROGRAM v

WA OPTICAL DIAGNOSTICS OF SEMICONDUCTORS AND THIN-FILMS-RAMAN 1

WB OPTICAL IMAGING FOR MATERIAL DIAGNOSTICS 11

WC NONLINEAR PROBES AND INTERACTIONS 23

WD LASER DIAGNOSTICS OF GAS-PHASED PROCESSING: 1 37

WE LASER DIAGNOSTICS OF GAS-PHASED PROCESSING: 2 51

WF OPTICAL DIAGNOSTICS OF SEMICONDUCTOR SURFACES 61

ThA NONRADIATIVE PROBES OF ABSORPTION 71

ThB DIAGNOSTICS OF LASER PROCESSING: 1 87

ThC LASER-DRIVEN MASS SPECTROSCOPY 99

ThD DIAGNOSTICS OF LASER PROCESSING: 2 105

ThE OPTICAL DIAGNOSTICS OF SEMICONDUCTORS-PHOTOLUMINESCENCE 113

KEY TO AUTHORS AND PAPERS 129

Accession For
NTIS GRA&I ☒
DTIC TAB ☐
Unannounced ☐
Justification

By
Distribution/
Availability Codes
Dist | Avail and/or Special
A-1

WEDNESDAY, FEBRUARY 11, 1987

BALLROOM LOBBY

7:30 AM–4:00 PM REGISTRATION

BALLROOM A

8:30 AM–9:45 AM
WA, OPTICAL DIAGNOSTICS OF SEMICONDUCTORS AND THIN-FILMS-RAMAN
J. R. McNeil, *University of New Mexico, Presider*

8:30 AM (Invited Paper)
WA1 Two- and Three-Dimensional Imaging of Thin Films Using the Raman Microprobe, Philippe M. Fauchet, *Princeton U.* Mapping structural properties of thin films, as grown or after processing, has been achieved with a Raman microprobe. The prospects for true 2-D and 3-D imaging are discussed. (p. 2)

9:00 AM
WA2 Picosecond Transient Reflectivity and Raman Gain Spectra of GaAs, John Wessel, Steven Beck, *Aerospace Corporation.* We describe the use of picosecond dye laser probes to measure recombination processes on GaAs surfaces and to study stimulated Raman gain spectroscopy of bulk GaAs. (p. 5)

9:15 AM
WA3 Raman Analysis of Inorganic Thin Films, D. R. Tallant, K. L. Higgins, P. J. Hargis, *Sandia National Laboratories;* A. F. Stewart, *U.S. Air Force Weapons Laboratory.* Techniques for the Raman analysis of plasma-deposited submicrometer silicon films on metallic substrates and dielectric films on Raman-active substrates are described, and typical results are presented. (p. 6)

9:30 AM
WA4 Developments in Raman Spectroscopy for Ion Implant Monitoring, A. C. de Wilton, M. Simard-Normandin, *Northern Telecom Electronics, Ltd., Canada;* P. T. T. Wong, *National Research Council of Canada.* A Raman technique for detector of low dose ($\geq 10^{10}$ ions/cm^2) ion implants in silicon is described. Uses include monitoring of threshold adjust implants for VLSI technology. (p. 7)

BALLROOM LOBBY

9:45 AM–10:15 AM COFFEE BREAK

WEDNESDAY, FEBRUARY 11, 1987—*Continued*

BALLROOM A

10:15 AM–11:15 AM
WB, OPTICAL IMAGING FOR MATERIALS DIAGNOSTICS
James C. Wyant, *University of Arizona, Presider*

10:15 AM (Invited Paper)
WB1 Optical Sensing for Automated Inspection, T. C. Strand, *IBM Almaden Research Center.* Three new types of Pptical tool: laser diode profilometer, phase shifting interferometer, and laser scanning microscope, are described and their uses in automated inspection are discussed. (p. 12)

10:45 AM
WB2 Television-Holography (ESPI) in Materials Diagnostics, Ole J. Lokberg, *Norwegian Institute of Technology;* Jan T. Malmo, *Foundation of Scientific & Industrial Research, Norway.* Electronic speckle pattern interferometry provides instant contour maps of extremely small deformations. Its use for studying very hot objects and detection of defects in various materials is described. (p. 16)

11:00 AM
WB3 Laser Mapping of Al-H^+ Impurity Distribution in Vacuum Swept Crystalline Quartz, J. P. Anthes, P. Garcia, D. R. Koehler, *Sandia National Laboratories.* We have demonstrated that HeNe laser light absorption can be used to map the Al-h^+ impurity concentration distribution in vacuum swept cultured quartz. (p. 20)

BALLROOM A

11:15 AM–12:15 PM
WC, NONLINEAR PROBES AND INTERACTIONS
L. Radziemski, *New Mexico State University, Presider*

11:15 AM
WC1 Surface Second Harmonic Generation Spectroscopy of Oxide Surfaces, W. M. Hetherington III, G. G. Padma Bandu, T. L. Mazely, Z. Z. Ho, W. M. K. P. Wijekoon, *U. Arizona.* Surface SHG theory and spectroscopy have been developed to study molecular adsorption and desorption on oxide surfaces. (p. 24)

11:30 AM
WC2 Surface CARS Spectroscopy with Optical Waveguides, W. M. Hetherington III, Z. Z. Ho, W. M. K. P. Wijekoon, E. W. Koenig, *U. Arizona.* Surface CARS spectroscopy using planar optical waveguide geometry has been developed to study molecular adsorption on oxide surfaces. (p. 26)

11:45 AM
WC3 Analysis of Uranium Solutions Using Laser-Induced Breakdown Spectroscopy, David A. Cremers, Joseph R. Wachter, *Los Alamos National Laboratory.* Uranium solutions were analyzed by laser-induced breakdown spectroscopy. The analytical performance was determined and the effects of some experimental parameters on the analysis was evaluated. (p. 28)

12:00 M
WC4 Optical Methods for the Study of Explosive Chemistry, Wayne M. Trott, Anita M. Renlund, *Sandia National Laboratories.* Emission spectroscopy, time-resolved infrared spectral photography, and single-pulse Raman scattering methods have been used to study chemical reactions in shock-loaded materials and in detonating energetic materials. (p. 32)

BALLROOM A

1:30 PM–2:30 PM
WD, LASER DIAGNOSTICS OF GAS-PHASE PROCESSING: 1
C. B. Hogge, *U.S. Air Force Weapons Laboratory, Presider*

1:30 PM (Invited Paper)
WD1 Laser Spectroscopy of Chemical Vapor Deposition, William G. Breiland, Pauline Ho, Michael E. Coltrin, *Sandia National Laboratories. In situ* laser Raman spectroscopy and laser-excited fluorescence data are compared with a detailed model for chemical vapor deposition. (p. 38)

2:00 PM
WD2 Analysis of the Chemical Vapor Deposition of Silicon by Intracavity Laser Spectroscopy, J. J. O'Brien, G. H. Atkinson, *U. Arizona.* Absorption spectra of SiH_2 and C_2 have been monitored by intracavity laser techniques during the pyrolytic and microwave discharge decomposition of silane and several organosilanes. (p. 42)

2:15 PM
WD3 High Frequency Optical Heterodyne Spectroscopy with Lead Salt Semiconductor Diode Lasers, David E. Cooper, *SRI International.* Optical heterodyne spectroscopy with tunable lead salt diode lasers offers the prospect of infrared absorption measurements at the quantum limit. We discuss the current status of the technique and present some recent experimental results. (p. 46)

BALLROOM LOBBY

2:30 PM–3:00 PM COFFEE BREAK

WEDNESDAY, FEBRUARY 11, 1987 — *Continued*

BALLROOM A

3:00 PM–3:45 PM
WE, LASER DIAGNOSTICS OF GAS-PHASE PROCESSING: 2
Pauline Ho, *Sandia National Laboratories, Presider*

3:00 PM (Invited Paper)
WE1 Laser Diagnostics of Radio Frequency Discharges, Richard A. Gottscho, *AT&T Bell Laboratories.* Recent applications of laser spectroscopy to the study of plasma and plasma-surface processes are reviewed. Using laser-induced fluorescence and optogalvanic spectroscopy, measurements of concentration gradients, reaction probabilites, electric fields, and process end-points have helped to elucidate plasma-chemical mechanisms. (p. 52)

3:30 PM
WE2 Quantum-Resolved Gas-Surface Scattering: NH_3 from Au(111), Bruce D. Kay, T. D. Raymond, Michael E. Coltrin, *Sandia National Laboratories.* Rotationally and vibrationally inelastic scattering of NH_3 from Au(111) is probed using multiphoton ionization. Classical trajectory calculations are employed to theoretically model this system. (p. 56)

BALLROOM A

3:45 PM–4:30 PM
WF, OPTICAL DIAGNOSTICS OF SEMICONDUCTOR SURFACES
J. Gerardo, *Sandia National Laboratories, Presider*

3:45 PM (Invited Paper)
WF1 Characterization of Materials by Visible-Near UV Spectrophotometric and Spectroellipsometric Techniques, D. E. Aspnes, *Bell Communications Research, Inc.* Determination of material characteristics such as microstructures, alloy compositions, densities, film thicknesses, and surface and interface properties are discussed. (p. 62)

4:15 PM
WF2 Spatial Resolution and Defect Contrast of Optical Beam-Induced Reflectance Scans, G. E. Carver, *AT&T Engineering Research Center;* D. C. Joy, *AT&T Bell Laboratories.* Defects in silicon are detected by a new nondestructive technique, OBIR. The spatial resolution and contrast are compared to electron beam-induced current scans. (p. 66)

BALLROOM A

6:30 PM CONFERENCE BANQUET
Colonel Lawrence L. Gooch, *Kirtland Air Force Base, Speaker*

THURSDAY, FEBRUARY 12, 1987

BALLROOM LOBBY

7:30 AM-4:00 PM REGISTRATION

BALLROOM A

8:30 AM-9:45 AM
ThA, NONRADIATIVE PROBES OF ABSORPTION
C. H. Seager, *Sandia National Laboratories, Presider*

8:30 AM (Invited Paper)
ThA1 Laser-Induced Modulated Reflectance in Semiconductor Materials Analysis, Allan Rosencwaig, *Therma-Wave, Inc.* Laser-induced modulated reflectance is a valuable method for studying lattice damage and electronic surface states in semiconductor materials. (p. 72)

9:00 AM
ThA2 Coating Thermal Transport Properties Measurement Using Thermal Diffusion Wave Interferometry, Randall T. Swimm, *U. Southern California.* The present status of a project to measure the thermal transport properties of various optical coating materials in thin-film format is described. (p. 77)

9:15 AM
ThA3 Photothermal Probe-Beam Deflection Measurement of Moisture Adsorption on a Silicon Surface in Atmospheric Conditions, Holger Schroeder, Andrew C. Tam, *IBM Almaden Research Center.* The adsorption of water molecules on a silicon surface in atmospheric conditions is measured by using a pulsed laser to cause desorption nondestructively and probe-beam deflection to detect the pressure pulse caused by the desorption. (p. 79)

9:30 AM
ThA4 Matched Sample Differential Laser Calorimetry, M. Bass, R. T. Swimm, M. E. Innocenzi, *U. Southern California.* A new technique is described for thermocouple laser calorimetry in which matched samples are used, one as the sample under study and one as the reference. In this configuration the signals due to surface absorption, scattering and thermal drifts are balanced out. The result is a means of absolute measurement of optical absorption with minimal errors and extremely high sensitivity. The technique is applicable to both solid and liquid samples. (p. 84)

BALLROOM LOBBY

9:45 AM-10:00 AM COFFEE BREAK

THURSDAY, FEBRUARY 12, 1987—*Continued*

BALLROOM A

10:15 AM-11:15 AM
ThB, DIAGNOSTICS OF LASER PROCESSING: 1
J. Figuera, *Los Alamos National Laboratory, Presider*

10:15 AM (Invited Paper)
ThB1 *In-Situ* Raman Microprobe Analysis of Direct Laser Writing, Irving P. Herman, *Columbia U.* Raman microprobe methods are described that may be used to analyze microstructures fabricated by direct laser writing, either *in-situ* after processing or in real time during processing. (p. 88)

10:45 AM
ThB2 Photodarkening in *In Situ* Textured PbTe Films: Technique for High Contrast Optical Storage in Polycrystalline Thin Films, L. Kameswara Rao, A. Selvarajan, *Indian Institute of Science-Bangalore.* A novel high-contrast optical storage technique based on photodarkening phenomena in polycrystalline films of *in situ* textured PbTe films is demonstrated. Free running Nd:YAG laser pulses are used for irradiating the films. The origin as well as the nature of the photodarkening in these films is investigated using spectrophotometry, transmission electron microscopy, and x-ray photoelectron spectroscopy. It is suggested that the modification of the void network in the film via topological reordering of the atoms by laser heating is responsible for the observed darkening. (p. 92)

11:00 AM (Invited Paper)
ThB3 Characterization of Optically Induced Periodic Structures on Semiconductor Surfaces, Dragan V. Podlesnik, *Columbia U.* High-resolution, spatially periodic structures are produced on semiconductor surfaces by using two interfering beams to initiate localized chemical reactions. This type of processing, which can be monitored in real time, provides insight into many interfacial phenomena. (p. 95)

BALLROOM A

1:30 PM-2:30 PM
ThC, LASER-DRIVEN MASS SPECTROMETRY
R. Keller, *Los Alamos National Laboratory, Presider*

1:30 PM (Invited Paper)
ThC1 Laser Microprobe Mass Spectrometry and its Relationship to Other Microanalytical Techniques, Charles A. Evans, Jr., *Charles Evans & Associates.* There is a variety of techniques employed for the microanalysis of materials, the majority employing focused ions or electron beams to probe the materials. In recent years, laser microprobe mass spectrometry has been developed to provide a unique and complementary characterization capability. This paper deals with the basic phenomena involved, instrumentation, and illustrations of the technique's utility with several applications. (p. 100)

2:00 PM (Invited Paper)
ThC2 Resonance Ionization Mass Spectrometry Using Ion-Beam Sampling, D. E. Goeringer, W. H. Christie, *Oak Ridge National Laboratory*. Resonance ionization mass spectometry has been used to study the effects of surface chemistry on neutral yields from ion-beam sputtered samples. (p. 101)

BALLROOM LOBBY

2:30 PM–3:00 PM COFFEE BREAK

BALLROOM A

3:00 PM–3:45 PM
ThD, DIAGNOSTICS OF LASER PROCESSING: 2
K. E. Greenberg, *Sandia National Laboratories, Presider*

3:00 PM (Invited Paper)
ThD1 Ultraviolet Laser Etching: Diatomic Temperatures by Laser-Induced Fluorescence Measurements, R. W. Dreyfus, R. E. Walkup, Roger Kelly, R. Srinivasan, *IBM T. J. Watson Research Center*. LIF measurements on C_2 radicals produced by excimer etching of graphite surfaces indicate a thermal vaporization mechanism. Conversely, nonthermal energy distributions for diatomics from polymer and sapphire surfaces suggest a photochemical etching process. (p. 106)

3:30 PM
ThD2 Excimer Laser Photochemistry of Al Alkyls Monitored by Dye Laser Mass Spectrometry, Y. Zhang, M. Stuke, *Max-Planck Institute for Biophysical Chemistry, F. R. Germany;* R. Larciprete, E. Borsella, *ENEA, Italy*. Ultraviolet-excimer laser photoproducts of the aluminum alkyls TIBA, TEA, and TMA are identified. Aluminum atoms and AlH molecules are major products (TIBA, TEA at 248 nm). (p. 110)

BALLROOM A

3:45 PM–4:45 PM
ThE, OPTICAL DIAGNOSTICS OF SEMICONDUCTORS-PHOTOLUMINESCENCE
R. C. Hammond, *Los Alamos National Laboratory, Presider*

3:45 PM (Invited Paper)
ThE1 Optical Characterization of III-V Semiconductors, D. C. Reynolds, K. K. Bajaj, *AFWAL/AADR*. High-resolution optical spectroscopy is an important experimental technique that can be used for studying the bulk components, quantum wells, and interfaces of heterostructure systems. (p. 114)

THURSDAY, FEBRUARY 12, 1987—*Continued*

4:15 PM
ThE2 Laser Diagnostics of Cadmium Telluride: Crystal Quality and Exciton Dynamics, Donald E. Cooper, J. Bajaj, P. R. Newman, *Rockwell International Science Center;* P. M. Rentzepis, J. Andrew Hutchinson, *UC-Irvine*. Laser-induced photoluminescence was used to evaluate the crystal quality and purity of CdTe. Photoluminescence decays from polaritons and bound excitons yield information about exciton dynamics. (p. 118)

4:30 PM
ThE3 Picosecond Time-Resolved Emission of Mercury Cadmium Telluride and Related II-VI Semiconductor Crystals, J. Andrew Hutchinson, T. E. Dutton, P. M. Rentzepis, *UC-Irvine;* Donald E. Cooper, J. Bajaj, P. R. Newman, *Rockwell International Science Center*. Picosecond-resolved emission of HgCdTe and CdTe crystals by a IR-visible streak camera shows temperature dependent multiexponential decay kinetics and elucidates the mechanisms of exciton trapping and annihilation. (p. 122)

WEDNESDAY, FEBRUARY 11, 1987

BALLROOM A
8:30 A.M.–9:45 A.M.

WA1–4

OPTICAL DIAGNOSTICS OF SEMICONDUCTORS AND THIN-FILMS-RAMAN

J. R. McNeil, University of New Mexico, *Presider*

TWO AND THREE DIMENSIONAL IMAGING OF THIN FILMS USING THE RAMAN MICROPROBE

Philippe M. Fauchet

Department of Electrical Engineering

Princeton University, Princeton NJ 08544

There is an increasing need for non-destructive characterization techniques that require no special sample preparation, can be used *in-situ*, and provide quantitative information with good spatial resolution. The Raman microprobe fulfills these requirements. We illustrate the capabilities of the Raman microprobe by presenting results obtained on thin films after laser-induced damage, after laser or rapid thermal annealing, and on heteroepitaxial semiconductor layers. The prospects for two and three-dimensional imaging of important properties such as composition, strain, and crystalline quality or orientation are discussed.

The Raman microprobe combines a standard Raman scattering apparatus with an optical microscope. The probe laser beam is focused to a one micron spot on the surface of the sample and the Raman signal from that illuminated area is collected by the same microscope and then analyzed by the monochromator. Microscopy is achieved by translating the sample in the focal plane. Our microprobe is a commercial instrument [1].

Many important properties of solids can be measured by Raman spectroscopy. These include composition, crystallinity, crystal orientation, strain, and

doping level. For example, strain is measured by the shift of the optic phonon frequency [2], the size and shape of very small crystallites are deduced from a complete lineshape analysis [3,4], and the crystal orientation is obtained through polarization studies [5].

The Raman microprobe allows determination of these properties with a spatial resolution comparable to that of good optical microscopes. Furthermore, it does not require any special sample preparation, is non-destructive, can be used *in-situ* [6], and offers the prospect of three-dimensional imaging. This can be achieved by tuning the wavelength of the laser focused through the microscope : in the visible, the penetration depth of light in semiconductors decreases with increasing photon energy. Depth profiling has been used in macro-Raman experiments [7].

We will present results obtained with the Raman microprobe in several situations. Variations in crystallinity and strain have been mapped after pulsed laser-induced damage of optical and semiconductor films [8]; the effects of cw laser and rapid thermal annealing of thin silicon films on insulator have been compared [9]; strain and crystallinity in heteroepitaxial semiconductor structures have been spatially resolved [10]. In all these cases, the Raman microprobe provided information that could not have been gathered with the same accuracy, spatial resolution, or ease.

The next step may now be the development of a true Raman microscope. Several schemes are possible. Presently, switching from a point focus to a line focus appears to be an attractive way to make a practical *scanning Raman micro-*

scope. With the use of a two-dimensional detector array for recording the Raman spectrum, it may be possible to use this new microscope in R and D environments.

This research is supported in part by the National Science Foundation. Thank are due to Ian Campbell who performed most of the work described here.

References

1. Instruments SA, Metuchen NJ

2. E. Anastassakis et al., Solid State Commun. **8**, 133 (1970)

3. I.H. Campbell and P.M. Fauchet, Solid State Commun. **58**, 739 (1986)

4. I.H. Campbell and P.M. Fauchet, to be published in the *Proceedings of the 18th International Conference on the Physics of Semiconductors*, Stockholm, August 1986

5. J.B. Hopkins and L.A. Farrow, J. Appl. Phys. **59**, 1103 (1986)

6. F. Magnotta and I.P. Irving, Appl. Phys. Lett. **48**, 195 (1986)

7. H. Shen and F.H. Pollak, Appl. Phys. Lett **45**, 692 (1984)

8. P.M. Fauchet, I.H. Campbell and F. Adar, Appl. Phys. Lett. **47**, 479 (1985); to be published in the *Proceedings of the 17th Annual Symposium on Optical Materials for High Power Lasers*, Boulder, October 1985; and I.H. Campbell, F. Adar, and P.M. Fauchet, in *Semiconductor-on-Insulator and Thin Film Transistor Technology* , A. Chiang et al. editors, Materials Research Society, 1986, pp 311-316

9. P.M. Fauchet et al., unpublished results

10. P.M. Fauchet et al., unpublished results

Picosecond Transient Reflectivity and Raman Gain Spectra of GaAs

John Wessel and Steven Beck
The Aerospace Corporation, M2-253
P.O. Box 92957, Los Angeles, CA 90009

Recently Woodall and co-workers[1] at IBM reported interesting results from a photowashing procedure applied to (100) GaAs. Unpinned behavior was observed immediately after washing. Photoluminescence yields measured from regions near the surface increased dramatically. The results suggested that the strong surface band bending ordinarily present in GaAs can be essentially eliminated by the photowashing procedure.

We developed a picosecond photoreflectance technique that quantitatively measures surface recombination processes and report the results for photowashed (100) GaAs. The interpretation supports the model suggested by the IBM work. We measured changes in reflectivity of a probe beam induced by an above-bandgap pump pulse. Time delays for the probe beam were scanned over the range 0 to .5 ns. Results obtained before and after photochemical washing were compared for a variety of samples. The unwashed commercial samples displayed complex kinetic behavior that varied appreciably from sample to sample and even for different sides of samples. Typical time scales for the fast decay components ranged from 10 to about 100 ps for these samples. However, the photochemically washed samples yielded uniform results that provide text book examples of diffusion controlled recombination processes. We demonstrate that surface recombination velocities are exceedingly small on photochemically cleaned (100) surfaces of doped and undoped GaAs and that a simple model accurately describes recombination, in terms of a single unknown parameter, the surface recombination velocity. Furthermore, we show that surface recombination processes dominate transient reflectivity results for uncleaned, pinned GaAs samples.

In a separate set of experiments, we employed the tunable picosecond laser system to measure stimulated Raman gain spectra of GaAs samples. Excellent spectra were obtained for below-bandgap scattering from bulk material. We obtained definitive confirmation of GaAs Raman scattering mechanisms by measuring polarization, scattering direction, and wavelength dependence of the scattering processes. The intensity of the important polar LO phonon was shown to be described accurately by contributions from the deformation potential mechanism, the forbidden Frohlich mechanism, and at near-bandgap, from the Gogolin-Rashba mechanism. Theoretical calculations reconciled these results with recent above-bandgap conventional Raman scattering assignments provided by Cardona's group[2]. (1) S. D. Offsey, J. M. Woodall, A. C. Warren, P. D. Kirchner, T. I. Chappell, and G. D. Pettit, Appl. Phys. Lett. 48, 475 (1986). (2) J. Menendez and M. Cardona, Phys. Rev. B31, 3696 (1985).

Raman Analysis of Inorganic Thin Films*

D. R. Tallant, K. L. Higgins, and P. J. Hargis
Sandia National Laboratories
Albuquerque, NM 87185-5800

A. F. Stewart
Air Force Weapons Laboratory
Kirtland AFB, New Mexico 87117

ABSTRACT

Techniques for the Raman analysis of plasma-deposited submicrometer silicon films on metallic substrates and dielectric films on Raman-active substrates will be described and typical results will be presented.

*Work supported in part by the U.S. DOE.

Developments in Raman Spectroscopy for Ion Implant Monitoring

I. C. de Wilton and M. Simard-Normandin

Northern Telecom Electronics Ltd.

Ottawa, Ontario, Canada K1Y 4H7

P.T.T. Wong

National Research Council of Canada

Ottawa, Ontario, Canada K1A 0R6

SUMMARY

As part of a strategy for development of *in situ* process monitoring for VLSI technology we are evaluating a number of optical techniques applicable to implantation and annealing processes. Techniques with potential for non-destructive characterization of patterned production wafers, rather than test wafers, are of primary interest. Consequently, the techniques to be considered must (i) be non-contact and non-contaminating; (ii) have high spatial resolution; (iii) provide rapid real time analysis; and (iv) use equipment that is adaptable for automatic or turn-key operation. Raman spectroscopy meets these criteria and the technique is well suited for studying materials for silicon technology (1). Features in the Raman phonon spectrum of implanted silicon can provide information on ion-damage prior to annealing or on the activation and distribution of dopant after annealing (2). In this paper we investigate the limits to the dose and energy of boron implants which can be detected by Raman spectroscopy.

The Raman phonon spectrum of silicon is sensitive to ion damage caused by both amorphizing and non-amorphizing implants. In order to monitor implant

parameters before annealing, changes in the spectral band intensities can be analyzed to obtain a measure of the extent of ion damage. Raman spectra were recorded for B^+ and BF_2^+ implants in the dose range from 3 x 10^{10} ions/cm^2 to 1 x 10^{16} ions/cm^2. The spectral region which was examined (100-1100 cm^{-1}) included the sharp intense band at 520 cm^{-1}, characteristic of single crystalline silicon, as well as the second order (overtone) band at 980 cm^{-1}. The measured intensity of the optical phonon was observed to decrease with increasing implant dose, but calibration of absolute intensities is difficult. Measurement of implantation dependent changes in the relative intensities of two or more bands within one spectrum was found to be more reliable. When the peak height intensity of the optical phonon was normalized, it was observed that the relative intensities of the band at 980 cm^{-1} and of the disorder induced bands at ~460 cm^{-1} and ~300 cm^{-1} increased with increasing implant dose. In particular, a heavily ion damaged implant (3 x 10^{15} B^+/cm^{-2}) was characterized by a spectrum with broad bands at ~460 cm^{-1} and ~300 cm^{-1}, similar to those of amorphous silicon, as well as the sharp band at 520 cm^{-1}. Although lower dose implants below 10^{13} ions/cm^2 cause correspondingly smaller intensity changes, these small differences can be amplified by taking the ratio of the spectrum of an implanted sample to that of an unimplanted sample. The value of the intensity ratio in the region of one of the damage induced bands, e.g. at ~460 cm^{-1}, can be quantitatively related to the dose and energy of the implant, without necessarily having detailed knowledge of the microstructure of the damaged region.

The ratio technique is shown to be capable of detecting low energy B^+ and BF_2^+ implants at doses as low as 3 x 10^{10} cm^{-2}. Since the method evaluates ion damage, it is equally applicable to P^+, As^+ or other heavy ion implants at

low doses, and to B^+ implants at doses up to ~10^{16} cm^{-2}. Implants which create an amorphous layer thicker than 0.1 μm are beyond the capability of the present technique but can be studied by infrared ellipsometry (3). The samples are evaluated immediately after implantation with no anneal step being necessary and the presence of a surface oxide layer does not interfere with the measurements. A tunable laser can be used to optimize the sensitivity of the method for implants of different energies.

The capability for detection of 20-80 keV B^+ (or equivalent BF_2^+ energies) and 50-120 keV P^+ in the lower dose range is of particular interest. Currently there are few non-contact, non-destructive methods of evaluating implant doses below 10^{13} cm^{-2} in patterned production wafers. Furthermore, the methods commonly used for process monitoring on test wafers require double implants or annealing of the implants before measurement (4). Problems in the anneal cycle may lead to misleading results for the implant parameters unless there is a technique for checking each process independently.

After annealing, a similar Raman technique can be used to determine the distribution of electrically activated boron or to study residual ion-damage. The detection limits for activated boron in annealed implants will be discussed briefly, and some Raman data which compare the electrical activation of boron in B^+ and BF_2^+ implants will be presented. Results will be correlated with secondary ion mass spectrometry (SIMS) and spreading resistance profiles.

Raman spectroscopy is non-destructive and non-contact. Analysis times are typically less than 10 minutes per wafer. A Raman micro-probe system would enable measurements to be made on patterned wafers with spatial resolution of

~1 μm. The technique is therefore a promising optical method with potential capabilities for process monitoring of patterned production wafers for VLSI applications.

REFERENCES

1. F.H. Pollak and R. Tsu, Proceedings of SPIE Vol. 452, eds. F.H. Pollak and R.S. Bauer, pp. 26-43 (SPIE Bellingham 1984).

2. A.C. de Wilton, M. Simard-Normandin and P.T.T. Wong, Proceedings of SPIE, Vol. 623, eds. D.K. Sadana and M.I. Current (SPIE Bellingham 1986).

3. T. Lohner, G. Mezey, E. Kotai, F. Paszti, A. Manuaba and J. Gyulai, Nucl. Instr. Methods 209/210, 615 (1983).

4. W.A. Keenan, W.H. Johnson and A.K. Smith, Solid State Technology 28(6), 143 (1985).

WEDNESDAY, FEBRUARY 11, 1987

BALLROOM A
10:15 A.M.–11:00 A.M.

WB1–3

OPTICAL IMAGING FOR MATERIALS DIAGNOSTICS

James C. Wyant, University of Arizona, *Presider*

Optical Sensing for Automated Inspection

T.C. Strand
IBM Research
Almaden Research Center
650 Harry Road
San Jose, CA 95120

Optics has always played a major role in industrial inspection and measurement applications. However in the past a critical component in such systems has often been the human eye. This aspect is changing rapidly now with the introduction of new technologies and new concepts in optical measurement. We will describe a number of new tools that provide new capabilities in inspection and also can eliminate the human from the measurement process.

Optical inspection can be used in two generic areas: metrology and materials characterization. In metrology one is interested in measuring the dimensional parameters of the parts in question. These applications are conveniently subdivided into measurements of lateral dimensions, e.g. distance between two points on a plane, and longitudinal dimensions, e.g. step heights. New imaging devices such as CCDs and new imaging modalities such as laser scanning systems have brought dramatic changes in the way lateral dimensions of parts are measured. New concepts in stereo methods, heterodyne techniques, and interferometry are having a similar impact on the measurement of longitudinal dimensions. Optics has always been a fundamental tool for materials characterization through such techniques as spectroscopy and ellipsometry. With the advent of new tools these characterization capabilities have been greatly expanded. An area that has seen particularly dramatic rise is high spatial resolution studies of materials. Raman microprobes, laser mass analyzers, and the various capabilities provided by laser scanning microscopes are examples of these new capabilities.

We will describe three specific tools which we have worked on with the goal of extending the capabilities of optics in the types of inspection problems we see in the microelectronics and data storage industries. First we will discuss two metrology tools, a laser diode profilometer and a phase measuring interferometer. Then we will discuss laser scanning microscope systems. We will draw examples from work in our own group and other groups within IBM Research.

In the data storage area there is need to characterize surfaces with nanometer range accuracy. Presently, the main tool for such measurements is a stylus profilometer. These tools have three inherent problems: they are contact measurements which run the risk of damaging the sample; they are relatively slow; they are only practical for one-dimensional measurements. Optical techniques offer means of overcoming these limitations. One device which we have studied as a potential replacement of the stylus profilometer is a laser diode profilometer(1). This device has two main objectives. The first is to provide noncontact measurement. This not only avoids the potential for damage to the sample, it also allows faster scanning, since the desire not to damage the sample or the stylus tip limits the scanning speed of a stylus profilometer. The second objective is to develop a system that provides an output directly related to the surface profile without the need for post-detection processing and without the need to do fringe tracking or phase unwrapping. The system is based on the concept that object to be measured and the front facet of the laser diode form an external cavity whose reflectance is a function of the product of the external cavity length and the laser emission frequency. Thus by monitoring the cavity reflectance, we can learn something about the cavity length. To avoid the need for fringe tracking or phase unwrapping, we use the reflectivity signal as a feedback to the laser diode current. This feedback controls the emission frequency in such a way that as the external cavity length changes as we scan over the object, the frequency is also changed so that the product,and thus the reflectivity, remains a constant. In this situation, the feedback signal is in fact proportional to the cavity length

over a range that is not limited by the laser wavelength. It thus provides us with a direct profile signal which has the basic accuracy of an interferometric system with a range limited by the feedback system. Fig. 1 shows the result of testing this system by monitoring a moving mirror. A linear response was obtained over a range of about 10 microns.

Optics research has also made significant strides in developing interferometric techniques for measuring profiles over two-dimensional surfaces. The major problem in this area has been interferogram interpretation, i.e. how do you go from an image of interference fringes to an image of the surface profile? Phase measuring interferometers represent an advance in data acquisition and processing techniques which greatly simplify the interpretation question(2). Phase measuring interferometers take a series of interference images, each with a different phase shift of the reference beam, and from these calculate the phase at each point. The phase is generally determined modulo 2π To overcome this limitation, the standard procedure is to assume the surface in continuous, and to eliminate the artificial 2π phase jumps in software. Of course this technique fails when the object has a step discontinuity in the surface which is more than half the wavelength of the illumination. We have investigated an extension of the phase measuring interferometer which overcomes this limitation. It is based on using illumination of limited coherence length. This is obtained by taking a white-light source and filtering it to the desired bandwidth. The bandwidth, or equivalently the coherence length, is determined by the measurement range we want. With such a source, the interference fringes have a contrast which decreases as one goes away from the zero path length difference condition. We use this fringe contrast information to remove the ambiguity in a normal, monochromatic interference image. Whereas with a normal phase measuring interferometer, determining the phase at a given point depends upon knowing the phase at at least one neighboring point, with this approach, the phase at each point is determined independently of all other points. We have implemented this in a microscope system shown schematically in Fig. 2. In this drawing, the reference mirror is moved by a piezoelectric crystal to acquire a sequence of images with different phase shifts. Fig. 3 is the result of processing an object with a 1 micron step. Such objects are impossible to measure with normal phase measuring interferometers.

Another recent development in optical techniques for inspection is the emergence of laser scanning microscopes (3). These systems have several unique features which make them useful in inspection applications. Since the image is formed through a scanning process, the optics can be simplified and/or optimized to the problem. Among other things, scanning systems can generally be designed to provide higher contrast than conventional systems. Furthermore, the detector system is simplified since only a single element is required. This for example, permits the use of photomultipliers for situations where light sensitivity is an issue. The high intensity achievable in the scanning beam has several advantages, especially in fluorescence studies or investigations involving nonlinear interactions. One interesting and unique application of the laser scanning microscope technique is for imaging magnetic domains by monitoring Kerr rotation (4). In this system, shown in Fig. 4, the magnetization of the surface under study is modulated. This in turn modulates the polarization rotation of the laser beam. The polarization modulation is detected synchronously. This technique accentuates magnetic domain walls since the motion of the walls causes points along the nominal wall position to see large changes in magnetization. One important modification to the laser scanning microscope is to not only illuminate with a focussed point of light, but also to image the scanning spot onto a pinhole in front of the detector. This is called a confocal arrangement. It has two significant advantages. First it improves the spatial resolution over a normal microscope. Secondly, it provides a sensitive depth discrimination capability since most of the light from an out-of-focus point will be blocked by the pinhole. This contrasts with a conventional microscope where light from out-of-focus planes adds an undesirable background to the image. Confocal systems can be used for profilometry applications and for high resolution imaging of objects with significant surface relief, since only points which are in-focus are imaged. All of these properties of laser scanning systems are well known and have led to commercial products by a number of companies. An area which has received less attention is in laser scanning systems which measure not only the amplitude of the return beam, but also its phase (5-7). These

typically use some form of heterodyne detection which permits very precise phase measurements. When used as profilometers, such systems are capable of measuring sub-angstrom surface variations. Such capabilities of course go beyond the typical industrial inspection requirements, but are useful as an analytic tool in studying surfaces and materials.

In summary, we see the confluence of new concepts in image acquisition, new developments in optical sources, and advances in image detection and image processing helping to give optics an increasingly important role in the industrial inspection arena as well as having an significant impact in a wide variety of research areas.

References

1. T. Yoshino et al., "Self-coupling laser diode interferometry for profilometry applications," Proc. CLEO-86, 56, June, 1986.

2. J.H. Bruning et al., "Digital wavefront measuring interferometer for testing optical surfaces and lenses," Appl. Opt. *13*, 2693 (1974).

3. E.A. Ash, Ed., "Scanned Image Microscopy," (Academic, New York, 1979).

4. P. Kasiraj et al., "Magnetic domain imaging with a scanning Kerr effect microscope," 1986 Intermag Proc., (1986).

5. H.K. Wickramasinghe et al., "Differential phase contrast optical microscope with 1-Å depth resolution," Electron. Lett. *18*, 22 (1982).

6. R.L. Jungerman et al., "Phase sensitive scanning optical microscope," Appl. Phys. Lett. *45*, 846(1984).

7. F. Laeri and T.C. Strand, "Angstrom resolution optical profilometer for microscopic objects," CLEO '86 Proc., 56(1986).

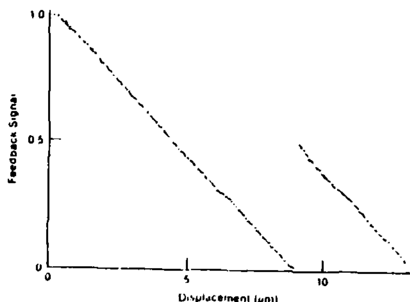

Figure 1. Laser diode interferometer feedback signal as a function of object displacement.

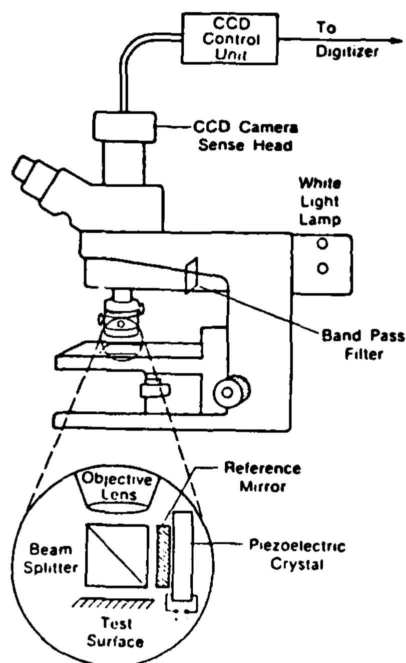

Figure 2. Phase measuring microscope interferometer.

Figure 3. Output from extended range phase measuring interferometer. Measuring test target of 1 mm high bars etched in silicon.

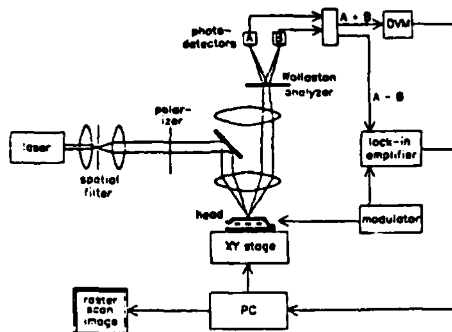

Figure 4. Schematic of laser scanning microscope for measuring Kerr rotation.

TV-HOLOGRAPHY (ESPI) IN MATERIAL DIAGNOSTICS.

OLE J.LOKBERG

Physics Department, The Norwegian Institute of Technology
N-7034 NTH, Trondheim, Norway

JAN T.MALMO

Foundation for Scientific & Industrial Research (SINTEF)
N-7034 NTH, Trondheim, Norway

Introduction

Almost a quarter of a century ago hologram interferometry was hailed as the promising tool for material testing and diagnosis. This prophesy has been partly fulfilled, but mainly within the safe enclosure of the laboratory and for carefully designed experiments. The limitation of the technique has been-and still is,even with the new thermoplastic materials- the time delay between recording and display.

TV-holography or ESPI (Electronic Speckle Pattern Interferometry) is a hologram interferometry technique where the holograms are recorded directly by the video-camera and reconstructed by electronic processing of the video signal. We observe immediately the reconstructed hologram image on the video monitor. This real-time operation has proven beneficiary not only for work under adverse conditions, but also opened up for new techniques for revealing material faults and behaviour.

System description

A detailed description of the ESPI-principle is not possible within the limited space of this paper. Readers interested in the theory behind the technique and the system's practical construction may consult e.g references 1-2, where also some of the applications within material diagnosis are described.

The commercial system used by our group consists of two boxes , each box about the size of a carry on luggage with a total weight of about 20 kg. One box is the optical head and contains laser, video-camera and interferometer components. The other box contains electronic processor, video-monitor and a digital frame store with connected electronics. A video tape recorder is usually used to record the experiments.

In practical use the laser-illumination is directed towards the test - object and a suitable image magnification is chosen. The reconstructed monitor image has interferometric sensitivity regarding the position of the test object. The measurement yardstick is provided by the laser wavelength which in this case is .633 μm. whereby extremely small deformations can be detected and measured.

The ESPI-images look coarse compared to recordings by ordinary holographic interferometry. This is caused by the much lower resolution of the video-system compared to holographic film. However, the speed and ease by which the ESPI-recordings are made amply outweighs the reduced pictorial quality.

Modes of Operation

The ESPI technique is used to visualize and measure small changes of the position of the test-object's surface. The changes are shown as a contour map which is read like an ordinary map except that the contour spacing is given by the laser wavelength. It is natural to divide the measurement modes into vibrations and deformations.

For both modes ESPI works non-destructively and needs no calibration. The test-object is not loaded by e.g strain gages and wires, and its surface does not have to be prepared in any way. ESPI provides immediately a global picture of the surface changes. In this sense the technique works as if 512 * 512 (the number of resolution cells in the video system) individual transducers had been placed across the surface.

Analysis and inspection of vibration resonance patterns are the most common use of the technique. We observe and measure the amplitude- and phase distribution. We determine the direction of the vibration vector and measure the sharpness of resonances. These measurements are possible from almost zero Hz. to the MHz.-region over an amplitude range from 10 pm. to over 10 µm. The technique can be applied on very unstable objects in hostile environments.

Deformation measurements are equally easily performed by use of a digital video-store. A reference position of the object is stored by activating the digital store. The subsequent frames coming from the video-camera are subtracted from this references frame and the resulting images are depicted on the video-monitor. When the object deforms, the video image will be covered with a fringe pattern which shows the relative deformation. Whenever the object deformation becomes too large for the fringes to be resolved by the video-system, a new reference frame is recorded. In this way very large deformations can be monitored and analyzed afterward if the experiment is recorded on a videotape recorder. The deformation testing is more sensible to object instabilities than the vibration analysis. However, successful experiments performed in factory environments have shown that the technique can be used for on - site testing.

Applications in material inspection

We like to stress that the ESPI like hologram interferometry only provide information about the displacement of the surface. Although very tiny displacements can be seen, the main problem will always be to find ways to "excite" the test-object which makes the observed deformation relate to a material or structural defect. This problem is different from applications where we want to find how the object react to a given load.

The optimum excitation will vary with structure and material. Heat, pressure, vibration and mechanical force have all been tried with variable success. The modern materials like honeycombs and laminated structures react surprisingly well to simple heating. This is due to low thermal transfer across the material which (usually) gives the defect time to deform the surface differently. Materials like steel dissipates heat so rapidly that is very hard to bring out for example a crack. Here a mechanical force correctly applied may be the best solution.
Excitation by vibrations may be very effective and simple to use.

The main problem is that high frequencies (and high excitation levels) are needed to bring out the smaller defects.

We have used ESPI for several applications which might be included within material testing and diagnosis. Much work has been on the detection of cracks and their development in different materials. Usually the material is increasingly loaded until failure while we record its surface behaviour. In most cases we have detected cracks and other abnormalities at lower loads than conventional methods.

Samples from such an experiment are shown on figure 1. where a small ceramics plate is deformed by an increasing, symmetrical load. At the lower load, the fringe pattern is regular as expected. The deformation is found by multiplying the number of fringes by the sensitivity factor, for this experiment about 0.3 µm.a fringe. At higher loads, cracks start to develop as seen from the irregularities in the pattern. By analyzing the fringe patterns recorded during the experiment, we find the deformation as function of load. We also can describe and quantify the formations of cracks as they appear and develop during the experiment.

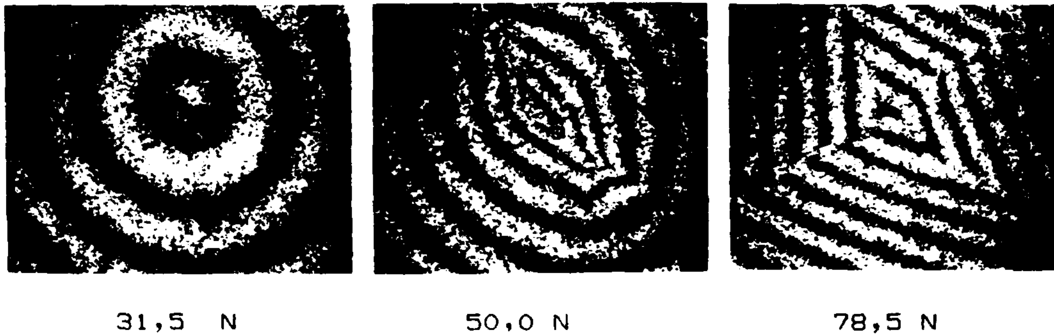

Figure 1. Deformation and crack development in ceramics.

As ceramics is mainly of industrial interest for use at elevated temperatures, we have developed the ESPI-technique to study very hot objects (3). Here the two main experimental problems are micro-structure stability and background radiation. The first problem can be solved by placing the object in an inert atmosphere or vacuum provided the object does not evaporate. Sometimes it might also be of interest to follow and measure the formation of surface shells due to oxidation. The background radiation problem is solved by use of strong lasers and narrow-band filters. Recently we have reached about +3000°C looking at small areas (about 2 * 2 mm^2) on tungsten lamp filaments. ESPI recordings of larger samples, about 1 * 5 cm^2, have been possible to about +2100°C, a limit set mainly by the available laser power (300 mW at 488.0 nm). This opens for interferometric investigations of material behaviour at their working temperature. For example we are able to observe the phase changes taking place in the material as the material is heating up.

"Fabricated" defects in composite materials like honeycomb and laminated structure have been detected as abnormalities in the fringe patterns (4). Sometimes the defect is clearly outlined as in the examples on figure 2. The defect in case a) is letters

inserted in the middle of the laminated structure.(The letters read "god jul" which stands for "merry christmas" in Norwegian). Case b) shows the fringe pattern due a paper clip incorporated in the back plies of the structure. We are here observing and exciting (heating) the 23 plies deep structure from the front side.
For some other "arranged" defects the correlation between defect shape and resulting deformation has been much less obvious if any at all. However, we should not forget that this technique tells us how the surface reacts to a certain load or excitation. This information is clearly related to the strength of the material and might in some cases more important than detecting even smaller defects.

a b

Figure 2. "Defects" in laminated structure.

We stress again that ESPI in principle perform the same measurements as hologram interferometry but at far greater ease and speed. We also point out that the still pictures presented herein are not representative for the technique's potential. The live, real - time observation allows for fringe manipulation which enables finer details to be detected.

Concluding remarks

We have briefly described the principles of ESPI and some of its application for material testing and diagnosis. For certain applications like high temperature measurements, the ESPI offers a new solution. For other applications like defect diagnosis, the technique may provide an interesting supplement to existing techniques like e.g. ultra-sonic diagnosis.

References.

1. Jones,R and Wykes,C. Holographic and Speckle Interferometry. Cambridge U.P. London 1983
2. Lokberg,O.J. and Slettemoen,G.A., Electronic Speckle Pattern Interferometry (To be published in Applied Optics and Optical Engineering, Vol. IX) (primo 1987 ?).
3. Lokberg,O.J., Malmo,J.T. and Slettemoen,G.A.,Interferometric Measurement of High Temperature Objects by Electronic Speckle Pattern Interferometry. Applied Optics,Vol.24,pp.3167-72.1985
4. Lokberg,O.J., On-Site Inspection by Compact TV-Holography. Proc.First International Conference on Post Failure Analysis for Fiber Reinforced Composites. pp.13.1-13.9. Dayton.Ohio.1985

LASER MAPPING OF Al-h$^+$ IMPURITY DISTRIBUTION IN VACUUM SWEPT CRYSTALLINE QUARTZ

J.P. Anthes, P. Garcia, and D.R. Koehler
Sandia National Laboratories
P.O. Box 5800 Albuquerque NM, 87185.

We have used HeNe laser light absorption to perform 2-D spatial mapping of hole-compensated aluminum (Al-h$^+$) impurity sites produced during vacuum sweeping of crystalline quartz. Application of an electric field parallel to the optic axis can produce a hole[1] trapped at a non-bonding oxygen ion $(AlO_4)^0$ site. These hole-compensated Al-h$^+$ sites introduce color center absorption. The electro-diffusion process (sweeping) is performed under elevated temperature and vacuum conditions. The diffusion process produces a time-dependent spatial distribution of the Al-h$^+$ centers and associated A_1-band optical absorption which is coincident with the 633-nm-HeNe laser wavelength. Spatial variations in the A_1-band absorption for swept quartz and for quartz subjected to ionizing radiation are correlated with the observed[1] coloration. Devices fabricated from crystalline quartz with hole-compensated aluminum impurity sites are resistant to the effects of ionizing radiation. The 2-D mapping of optical absorption is compared to electron spin resonance (ESR) measurements of aluminum impurity concentration in samples of vacuum swept cultured quartz.

<u>EXPERIMENTAL PROCEDURES</u>: The laser mapping of the swept quartz bar, shown in Fig.1, utilized a stabilized single longitudinal mode HeNe laser to minimize intensity variations during the measurement. A cube beam splitter divided incident laser light, I, into two beams, I_R and I_0, of approximately equal intensity. The reference laser beam intensity, I_R, was detected by a Si-PIN diode which had an integral signal preamplifier. The laser beam, I_0, was then directed onto the quartz sample at near-normal incidence to define the polarization dependent[1] interaction of the laser light with the quartz sample. The laser intensity transmitted by the sample, I_T, was detected by a second identical Si-PIN diode detector. Laser beam intensities, I_R and I_T, were alternately recorded at 1/10 second intervals.

Note that polarization of the laser light was parallel to the quartz X-Y plane and that the sample was translated in 1-mm-increments in the Z-direction (along the optic axis) by the motorized translation stage. When a single Z-scan was completed, the sample was then translated 2-mm in the Y-direction for the next Z-scan. The unfocussed laser beam diameter was ~1 mm and limited the spatial resolution to ~0.5 mm (one beam radius). During the sweeping process the E-field is normally applied parallel to the optic axis and directed toward the location of the seed in the as-grown crystal.

Values of the optical absorption coefficient, $\alpha(X)$, are compared to ESR measurements taken for the swept quartz samples. One sample was originally purchased from Bliley Electric Co. and the other samples were all Premium-Q grade quartz originally purchased from Sawyer Research Corp. ESR measurements determined the hole-compensated aluminum concentration at five Z-

positions for the Bliley sample. The Al-impurity levels in the Bliley sample varied from ~6-26 ppm. ESR measurements for the Sawyer samples indicated that the aluminum impurity concentration levels varied from ~0.5-0.8 ppm.

The optical absorption coefficient, $\alpha(X)$, can be determined from the experimental data using,

$$I_T = I_0 \times (1-R)^2 \times e^{-\alpha T}$$

where R is the calculated reflection loss for each air/quartz interface and T≃1.7 cm is the sample thickness. To experimentally determine $\alpha(X)$ in terms of the signals recorded, we only require that the recorded signals V_R and V_T must be linearly proportional to laser intensities I_R and I_T, respectively. Furthermore, if we define a normalization constant $K(t=0)=V_T/V_R$ with the sample removed (before the start of each experimental run) and recognize that the external transmission, Tx, can be found at each beam position from the signal ratio $Tx=V_T/(K \times V_R)$, then $\alpha(X)$ can be determined at the ith position using,

$$\alpha(X)_i = (-1/T) \times \ln[Tx_i/(1-R)^2] \quad (\text{in cm}^{-1})$$

where the experimental accuracy of Tx was estimated to be ±0.5%.

EXPERIMENTAL RESULTS: A Y-Z mapping of absorption coefficient $\alpha(X)$ is shown in Fig.2 for the Bliley swept quartz sample. Absorption varied between an average low value of ~0.01 cm^{-1} and an average peak value of ~0.22 cm^{-1}. Darker striations, associated with absorption values exceeding the average peak value, were clearly visible to the unaided eye. If the sweeping process had been allowed to continue, the darkened region would have completed the entire distance to the Z=14-mm position.

Values of Tx for two samples of swept Premium-Q quartz were approximately twice that of a reference sample that was still in the as-grown (unswept) condition. Absorption values for the swept Premium-Q quartz were much lower (~0.015 cm^{-1}) than the Bliley quartz absorption values.

Hole-compensated aluminum impurity concentration from the ESR measurements and $\alpha(X)_i$ are compared in Fig.3 for the Bliley sample. The average value for $\alpha(X)_i$ at Z=10 mm was normalized to the peak ESR value. Fig. 2 absorption coefficient data were multiplied by 19.55 at each Z-position in the figure to provide a clearer comparison. The dashed line connecting average $\alpha(X)$ values guides the eye only.

CONCLUSIONS: We have demonstrated that HeNe laser light absorption can be used to map the $Al\text{-}h^+$ impurity concentration distribution in vacuum swept cultured quartz. Observation of peak A_1-band color center formation spatially corresponded with the peak concentration in aluminum-hole centers and may be useful to perform real-time monitoring of sweeping. In a similar way, we speculate that a second laser-based light source near 3-μm could be used to monitor an intermediate step in the sweeping process; OH^- compensation of the Al^{3+} impurity.

The present experimental sensitivity was limited to $Al\text{-}h^+$ levels of ≃0.1 ppm (corresponding to $\alpha(X)$≃0.01 cm^{-1}). Future experiments, including possible

insitu measurements during sweeping of low impurity quartz, may require improved sensitivity. Experimental methods that offer improved absorption sensitivity include multiple-pass cells[2], photothermal[3] response to absorbed laser light, and synchronous detection techniques.

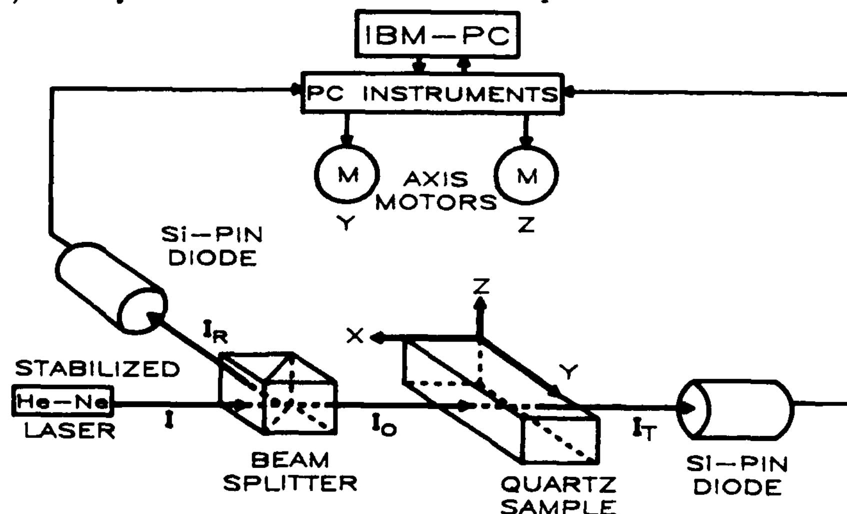

Fig.1 Experimental Setup

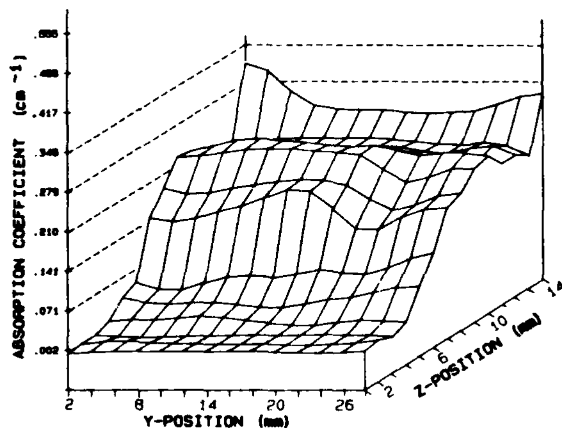

Fig.2 2-D Laser mapping of Absorption Coefficient

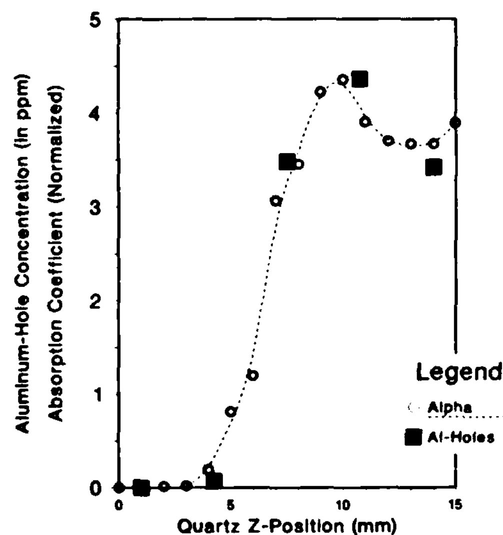

Fig.3 Al-h^+ concentration compared to $\alpha(X)$ (normalized)

1) Gerda B. Krefft "Effects of High-Temperature Electrolysis On The Coloration Characteristics and OH-Absorption Bands in Alpha-Quartz," Radiation Effects, 26, 249, 1975.

2) R.A. Hill and D.L. Hartley "Focused, Multiple-pass Cell for Raman Scattering," Appl. Optics, 13, 186, 1974.

3) Joel M. Harris "Photothermal Methods for Detection of Molecules in Liquids," Optics News, 12, 8, Oct. 1986.

WEDNESDAY, FEBRUARY 11, 1987

BALLROOM A
11:15 A.M.–12:15 M

WC1–4

NONLINEAR PROBES AND INTERACTIONS

L. Radziemski, New Mexico State, *Presider*

Surface Second Harmonic Generation Spectroscopy of Oxide Surfaces

W. M. Hetherington III, G. G. Padma Bandu, T. L. Mazely, Z. Z. Ho and W. M. K. P. Wijekoon
Department of Chemistry, University of Arizona, Tucson, AZ 85721

Second harmonic generation has been established recently as a specific probe of interfacial species. On dielectric surfaces, it has been used to detect the presence, the electronic states and the average orientation of interfacial species.

We have performed a detailed analysis of the effects of the orientation distribution of a surface species upon the pattern of the macroscopic second order susceptibility tensor. Variation of the polarizations of the input and output beams and of the angle of incidence in the reflection geometry can provide useful data for the determination of the orientation distribution of interfacial species if the molecular tensor is known. Also, semi-empirical calculations have been performed to estimate the pattern of molecular tensors near two photon resonances

On materials such as TiO_2 and oxide-coated silicon under vacuum conditions, the SH signal decreases significantly as desorption of surface species occurs at elevated temperatures. The adsorption of water and a variety of other molecular species has been detected as a function of the pressure and the temperature of the surface. The applicability of this method to the detection of adsorbates on crystalline and amorphous surfaces will be discussed.

The two photon resonance enhanced SHG spectrum of cinnamic acid on SiO_2 surfaces has been obtained at 300, 77 and 4 K. For low exposure times, only a few adsorption sites are apparent in the spectrum, and the resonance of one isolated species exhibits vibrational structure at 4 K. For long exposure times, broad features appear in the spectrum and are associated with aggregate formation. Two photon absorption leads to desorption of the more weakly bound molecules, and the relative rates of desorption for two such species have been measured.

Surface CARS Spectroscopy with Optical Waveguides

W. M. Hetherington III, Z. Z. Ho, W. M. K. P. Wijekoon
and E. W. Koenig
Department of Chemistry, University of Arizona, Tucson, AZ 85721

Using the planar optical waveguide geometry, coherent anti-Stokes Raman scattering becomes a very sensitive type of vibrational spectroscopy for the study of surface structure and chemistry. The waveguide structure consists of a film (about one micron thick) of a material such as ZnO on a fused silica substrate. Laser fields can be constrained by total internal reflection such that they propagate through the film as guided waves. The concept is to perform CARS using the evanescent fields extending above the waveguide surface. The key to making this a very attractive form of surface spectroscopy is the establishment of an interference condition within the film, thereby eliminating the contribution from the vibrationally resonant or nonresonant third order susceptibility of the film itself. The remaining signal consists mainly of the signal from the surface and any surface adsorbates. With this technique, the Raman spectrum of interfacial species can be observed over the 0 to 4000 cm^{-1} range under environments ranging from UHV to condensed phases.

The surfaces that can be studied with this CARS technique can be crystalline (ZnO) or amorphous (Nb_2O_5), and they can be readily characterized by a number of standard methods. In the work to be discussed, ZnO waveguides were placed in a high vacuum chamber, heated and then exposed to various molecular species. Beams from two synchronously-pumped dye lasers were coupled into the

waveguides through $SrTiO_3$ prisms in optical contact with the film. The field at the output frequency grew as a guided wave and was coupled out through another prism. Under non-phase-matched conditions, the output was easily detectable.

The CARS spectrum of pyridine on ZnO has been interpreted in terms of sites for physisorption, hydrogen bonding and protonation. Physisorbed and three types of chemisorbed ethylene also have been detected on ZnO. Physisorbed molecular oxygen was detected at a pressure of 1 atm of O_2. The adsorption and desorption kinetics have been studied for the case of ethylene on ZnO. On hydroxylated ZnO surfaces, diffusion of ethylene among some of the adsorption sites has been seen.

In general, this type of spectroscopy is applicable to studies of dielectric, semiconductor and metallic surfaces. There are also possibilities for investigations of surface relaxation and photochemical processes.

ANALYSIS OF URANIUM SOLUTIONS USING LASER-INDUCED BREAKDOWN SPECTROSCOPY

by

David A. Cremers
Chemistry and Laser Sciences Division

Joseph R. Wachter
Energy Division

Los Alamos National Laboratory
Los Alamos, NM 87545

SUMMARY

Measurement of the uranium content in liquid streams is important for criticality safety, process and quality control, and nuclear material accountability in nuclear fuel cycle facilities. Conventional analytical techniques such as spectrophotometry, passive gamma-ray spectroscopy, x-ray fluorescence, and densitometry are frequently unsuitable because they may be slow, require sample handling, or be subject to interference by high concentrations of fission products or neutron emitters in the solutions to be analyzed.

At Los Alamos National Laboratory, the application of laser-induced breakdown spectroscopy (LIBS) to the measurement of the uranium content in solutions is under investigation. This method utilizes a focused laser pulse to produce a hot spark that vaporizes the solution and generates a plasma of electrons and excited ions and neutral atoms. Spectral and temporal resolution of the plasma light permits identification of the atomic constituents.

The LIBS technique has several potential advantages compared to the conventional methods listed above. No sample handling or preparation is needed because only optical access is required to produce and observe the plasma. The

technique is fast because the laser spark simultaneously vaporizes and excites the sample. In addition, LIBS is unaffected by gamma-ray signals from high concentrations of fission products. This report presents the results of an investigation of the suitability of LIBS for analysis of uranium solutions. Topics discussed include dynamic range, precision, detection limit, and the effects of some experimental parameters on the analysis.

Powerful Nd:YAG laser pulses (15 ns, 250 mJ/pulse, 10 Hz) were focused on the surfaces of uranium solutions to create the spark plasmas. The resulting emissions were spectrally resolved with a 1/2-m grating spectrograph and detected with a time-gated photodiode array. Time resolution of the plasma signal was employed to minimize detection of the strong continuum radiation at early times after spark formation. Line strengths were measured by averaging the spectra from multiple laser sparks. Solutions of depleted uranium in 4-M nitric acid at concentrations from 0.1 to 300 g/ℓ, a range useful for process control and monitoring were used. The spectral region from 350 to 700 nm was examined to find the most suitable emission lines for uranium determination. The strongest uranium emission free from spectral interference, the U II line at 409.0 nm, was used for most measurements.

With the laser spark formed below the surface of the solutions, no uranium signal was detected at concentrations up to 300 g/ℓ. Formation of the spark at the liquid surface, however, resulted in a considerable improvement in detection sensitivity because of the higher temperature of the spark formed in air compared to a spark formed in the bulk solution.[1,2] The lower spark temperature for bulk excitation probably comes about because a large fraction of the laser energy goes into vaporization of the liquid leaving a smaller fraction for plasma formation.[1]

Surface excitation requires that part of the plasma be formed in the liquid and part in the atmosphere above it. For this reason, the signal strength was sensitive to the distance between the surface and the lens focusing the laser pulses. This sensitivity increased as the focal length of the lens decreased. For a 50-mm focal length lens, the distance over which the net uranium signal remained at one-half or more of its maximum value was 2.3 mm.

The net signal increased by a factor of 23 and measurement precision increased by a factor of 3.5 as the laser repetition rate was increased from 1 to 15 Hz. The increased intensity and reproducibility at 15 Hz probably results from an increase in the concentration of aerosols in the spark volume above the surface which is averaged over many sparks at the higher repetition rates.

A calibration curve of the intensity of the net 409.0-nm signal versus uranium concentration exhibits good sensitivity over the range 0.1 to 300 g/ℓ. The detection limit for uranium was established as 0.1 g/ℓ. The precision of the measurements, determined as the %RSD of 10 replicate measurements of the net uranium signal strength, was calculated to be 1.8% for analysis times of about three minutes (1600 sparks). Ratioing the net uranium signal to a background region adjacent to the uranium line improved the precision to 1.0% for the same measurement time.

The use of LIBS to analyze static uranium solutions at concentrations useful for process stream analysis has been demonstrated. Experiments are under way to study spectral interferences due to other materials in the stream (e.g. zirconium), the effects of industrial environment on analytical performance, and calibration methods suitable for in situ analysis.

REFERENCES

1. L. J. Radziemski, T. R. Loree, D. A. Cremers, and N. M. Hoffman, Anal. Chem. 55, 1246 (1983).

2. D. A. Cremers, L. J. Radziemski, and T. R. Loree, Appl. Spectrosc. 38, 721 (1984).

OPTICAL METHODS FOR THE STUDY OF EXPLOSIVE CHEMISTRY

Wayne M. Trott and Anita M. Renlund
Sandia National Laboratories
Albuquerque, New Mexico 87185

SUMMARY

An understanding of the reaction zone in a detonating high explosive (HE) requires characterization of both the mechanical response of the material and the chemical reaction mechanisms that control the rate at which the HE is consumed. Moreover, the detailed chemistry is clearly a contributing factor in the shock-initiation of energetic materials. Although a considerable body of empirical knowledge on shock sensitivity and explosive performance is presently available, practically no information exists regarding the important microscopic physical and chemical processes. Much additional insight into these processes is needed for the development of predictive capabilities in the areas of initiation and performance. In this paper, we discuss the application of several optical diagnostic methods for the study of explosive chemistry. We have emphasized techniques which provide good spatial and temporal resolution and are applicable to "single-shot" measurements on pressed, polycrystalline samples of widely used HEs. These techniques include electronic fast-framing photography, time-resolved emission spectroscopy, single-pulse Raman scattering and time-resolved infrared spectral photography (TRISP).

We have observed significant differences in the characteristic visible emission between oxygen-balanced and fuel-rich explosives. The emission from propagating detonation waves in fuel-rich explosives (e.g., hexanitroazobenzene, HNAB, and hexanitrostilbene, HNS) contains band structure attributable to CN(B), C_2(d) and probably NO_2(A). For HNS, the CN(B-X) system near 388 nm has been studied at a wavelength resolution of 0.05 nm. We have observed band intensities indicative of substantially incomplete equilibration of vibrational and rotational modes of the emitting CN for light generated before (i.e., scattered out of the pressed granular material) and light coincident with detonation wave arrival at the free surface. Emission in this temporal region appears to be associated with void collapse in the compressed material. At slightly later times, CN(B-X) band intensities consistent with a single rotational and vibrational temperature are observed. Boltzmann temperatures have been calculated by comparing the experimental data with computer-simulated spectra. Best fits to the observed spectra indicate temperatures of the emitting CN(B) at 5000 $\pm$ 200 K and 6500 $\pm$ 400 K from detonating HNS at densities of 1.70 g cm^{-3} and 1.50 g cm^{-3}, respectively. Data from HNS pressed to two intermediate densities gave temperatures between these values, following a trend of increasing temperature with decreasing initial charge density.

In previous studies, we have shown[1,2] that excellent single-pulse spontaneous Raman spectra can be obtained from the

surface of many unshocked explosive samples and that Raman scattering methods can be used to monitor the depletion rate of the parent molecule in a detonating explosive. In the case of pentaerythritol tetranitrate (PETN), the observed monotonic attenuation of parent molecule Raman scattering intensity over a 100 ns interval is consistent with previously obtained experimental and theoretical determinations of global reaction times for high-density PETN and other explosives.[3-5] In more recent studies, we have observed Raman scattering from a common transient chemical species in detonating 1,3,5,7-tetranitro-1,3,5,7-tetraazacyclooctane (HMX) and 1,3,5-trinitro-1,3,5-triazacyclohexane (RDX). The measured Raman shift (near 2100 cm^{-1}) for this transient feature is consistent with formation of a nitrile species.

TRISP allows the acquisition of "single-shot" infrared absorption spectra over a 1000 cm^{-1} spectral region with temporal resolution of <5 ns. Hence, this technique provides excellent sensitivity for real-time detection of transient species and reaction products in low concentration. We have used TRISP to examine early gas-phase products of detonation. In the case of detonating RDX, we have observed transient absorption in the OH-stretching region (likely due to rapid formation of H_2O). Ongoing experiments using TRISP to study chemical changes in shock-loaded liquid nitromethane will also be discussed.

REFERENCES

1. W. M. Trott and A. M. Renlund, Appl. Optics 24, 1520 (1985).

2. W. M. Trott and A. M. Renlund, "Time-resolved Spectroscopic Studies of Detonating Heterogeneous Explosives," in Proceedings of the Eighth Symposium (International) on Detonation, in press.

3. A. N. Dremin, S. D. Savrov, V. S. Trofimov and K. K. Shvedov, Detonation Waves in Condensed Media, edited translation, AD-751 417, Wright-Patterson Air Force Base, Ohio, August 1972, p. 133.

4. E. L. Lee and C. M. Tarver, Phys. Fluids 23, 2362 (1980).

5. S. A. Sheffield, D. D. Bloomquist and C. M. Tarver, J. Chem. Phys. 80, 3831 (1984).

NOTES

WEDNESDAY, FEBRUARY 11, 1987

BALLROOM A
1:30 P.M.–2:30 P.M.

WD1–3

LASER DIAGNOSTICS OF GAS-PHASE PROCESSING: 1

C. B. Hogge, U.S. Air Force Weapons Laboratory, *Presider*

Laser Spectroscopy of Chemical Vapor Deposition

William G. Breiland, Pauline Ho, and Michael E. Coltrin
Sandia National Laboratories
Albuquerque, NM 87185

Summary

Chemical vapor deposition (CVD) is an important industrial process used to deposit solid films for protective coatings and microelectronic applications. The CVD processes used in the fabrication of microelectronic devices are becoming more complex, and higher demands are being made on the resulting films. A fundamental understanding of the chemistry and physics of CVD may help meet future process control requirements, and could lead to novel deposition methods.

We are pursuing a coordinated experimental and theoretical program to investigate the fundamental mechanisms of CVD. The experimental part of our program involves the use of laser spectroscopic techniques for *in situ* measurements of the gas phase in a research CVD reactor. The theoretical part of the program consists of modeling of the coupled fluid mechanics and the gas-phase chemical kinetics of silane decomposition and subsequent reactions of intermediate species. We have initially chosen to concentrate on the silane CVD system, although the techniques and principles involved are applicable to more complex systems. This paper summarizes our experimental and theoretical research

on silane CVD.

For making measurements during deposition, an ideal diagnostic technique would be non-intrusive, selective, sensitive enough to measure species present at sub-Torr partial pressures, general, and quantitative. Good spatial resolution is also necessary for measurements in the strong temperature and chemical species gradients present in CVD environments. Although no single technique meets all of these requirements, optical techniques satisfy many of these criteria. We have used a variety of laser spectroscopic techniques to measure gas temperatures [2] and velocities [3], densities of reactant [1,2,3] and chemical intermediate species [2,4-6], and to monitor particulates in the gas phase [3].

Laser Raman spectroscopy provides quantitative density measurements for species present at relatively high concentrations (fractions of a Torr), as well as the determination of local gas temperatures. This technique is general, selective, and reasonably sensitive. The spatial resolution is determined by the size of the focused laser beam and the light-collection optics. We have used Raman spectroscopy to obtain profiles of the gas temperature [2,3] and silane density [1,2,3] as a function of position in our CVD cell.

Laser-excited fluorescence (LEF) is an extremely sensitive technique that allows the detection of gas-phase species present in low concentrations, such as highly-reactive chemical intermediates. This spectroscopic technique provides an unequivocal identification of a gas-phase species, but generally yields only relative (rather than absolute) measurements of species density. We have used this technique to monitor Si atoms [6], HSiCl [4] and Si_2 [2,5] molecules during deposition.

The theoretical part of the program consists of detailed computer modeling [7-9] of the coupled fluid mechanics and the gas-phase chemical kinetics in a CVD reactor. The

model solves the boundary layer equations coupled to chemical species continuity equations describing chemical reactions and transport.

The chemical kinetics portion of the model consists of 27 reversible elementary reactions that describe the gas-phase decomposition of silane and subsequent reactions of intermediate species [8]. A single set of transport data and rate constants are used for all conditions.

We have made many comparisons between predictions of the model and our laser-based measurements [2,6]. In general, the agreement between the predictions of our model and our experimental results over a wide variety of conditions is very good. This indicates that fluid mechanics and gas-phase chemical kinetics are important to a fundamental understanding of silicon CVD. Laser diagnostic techniques provide valuable characterization of the gas-phase chemistry and fluid flow in a CVD reactor. In addition, our model supplies a theoretical framework for explaining the chemical origins that give rise to the experimental observations.

References

1. "Pulsed UV laser Raman spectroscopy of silane in a linear-flow chemical vapor deposition reactor", W.G. Breiland and M.J. Kushner, Appl. Phys. Lett. **42**, 395 (1983).

2. "Comparisons between a gas-phase model of silane CVD and laser-diagnostic measurements", W.G. Breiland, M.E. Coltrin and P. Ho, J. Appl. Phys. **59**, 3267 (1986).

3. "In-situ laser measurements of silicon CVD", W.G. Breiland and P. Ho, in *Proceedings*

of the Ninth International Conference on CVD, edited by McD. Robinson, C.H.J. van den Brekel, G.W. Cullen and J.M. Blocher, Jr., (Electrochemical Society, Pennington, NJ, 1984) p. 44.

4. "Observation of HSiCl in a chemical vapor deposition reactor by laser-excited fluorescence", P. Ho and W. G. Breiland, Appl. Phys. Lett. **43**, 125 (1983).

5. "Observation of Si_2 in a chemical vapor deposition reactor by laser-excited fluorescence", P. Ho and W.G. Breiland, Appl. Phys. Lett. **44**, 51 (1984).

6. "Gas-phase silicon atoms in silane chemical vapor deposition: laser-excited fluorescence measurements and comparisons with model predictions" W.G. Breiland, P. Ho and M.E. Coltrin, J. Appl. Phys. **60**, 1505 (1986).

7. "A mathematical model of the coupled fluid mechanics and chemical kinetics in a chemical vapor deposition reactor", M.E. Coltrin, R.J. Kee and J.A. Miller, J. Electrochem. Soc. **131**, 425 (1984).

8. "A mathematical model of silicon chemical vapor deposition: further refinements and the effects of thermal diffusion", M.E. Coltrin, R.J. Kee and J.A. Miller, J. Electrochem. Soc. **133**, 1206 (1986).

9. "A mathematical model of silicon chemical vapor deposition", M.E. Coltrin, R.J. Kee and J.A. Miller, in *Proceedings of the Ninth International Conference on CVD,* edited by McD. Robinson, C.H.J. van den Brekel, G.W. Cullen and J.M. Blocher, Jr., (Electrochemical Society, Pennington, NJ, 1984) p. 31.

Analysis of the Chemical Vapor Deposition of silicon by Intracavity Laser Spectroscopy

J.J. O'Brien and G.H. Atkinson
Department of Chemistry and Optical Sciences Center
University of Arizona, Tucson, Arizona 85721

Introduction

Both the analysis and control of chemical vapor deposition (CVD) processes, are greatly aided by the availability of experimental methods for monitoring the gas phase precursors of the depositing material. The real time, in situ detection of intermediate reaction species is an almost essential element in studies directed at understanding the fundamental chemistry and physics of CVD processes. Such studies also can have a major impact on CVD processing practices.

Laser induced fluorescence (LIF) has been the technique of choice for the detection of transient reaction intermediates because of its significantly greater sensitivity than conventional absorption spectroscopy. Since many species do not emit in all environments, however, absorption spectroscopy can be more effective in providing information on the quantitive concentrations of and energy distribution within transient species if its detection sensitivity is significantly enhanced.

Techniques based on intracavity laser spectroscopy (ILS) which increase the detection sensitivity of absorption by as much as six orders of magnitude over conventional absorption spectrometry have been developed by Atkinson and others [1]. The enhanced sensitivity derives from the competition between the gain in the laser medium and the wavelength-dependent losses within the laser resonator. By placing the species of interest inside the optical resonator cavity of a longitudinally multimode laser, the absorption spectrum of the intracavity atomic or molecular species is superimposed on the wavelength-dispersed spectrum of the laser output.

Experimental

The ILS laser system is shown schematically in Figure 1. A modified dye laser (Coherent 590) is pumped by an argon ion laser (Coherent I-53-8). The pumping radiation is attenuated as a function of time (33 Hz) by passing it through an acousto-optic modulator (AOM1). AOM1 diverts enough pump power to prevent the dye laser from reaching threshold conditions. When AOM1 is switched off, the pump laser brings the dye laser rapidly above threshold ($\sim$0.15 μs). The dye laser output passes through a second acousto-optic modulator (AOM2) which, on operation, ($\sim$0.15 μs) deflects part of the dye laser output to the spectrometer. The wavelength-dispersed radiation exiting the spectrometer is focused onto the face of an intensified vidicon camera. Such multichannel detection makes it feasible to monitor substantial portions of the rovibronic absorption spectrum of the intracavity species in real time.

The period of time during which the dye laser operates above threshold and AOM2 remains open determines the generation time, t_g, of the ILS laser system [2]. It has been shown that the intracavity absorption obeys a Beer-Lambert relationship with the equivalent pathlength of absorption, L_{eq}, given by $L_{eq} = R.t_g.c$ where R is the ratio of the pathlength of the laser through the intracavity absorber to the length of the laser resonator cavity and c is

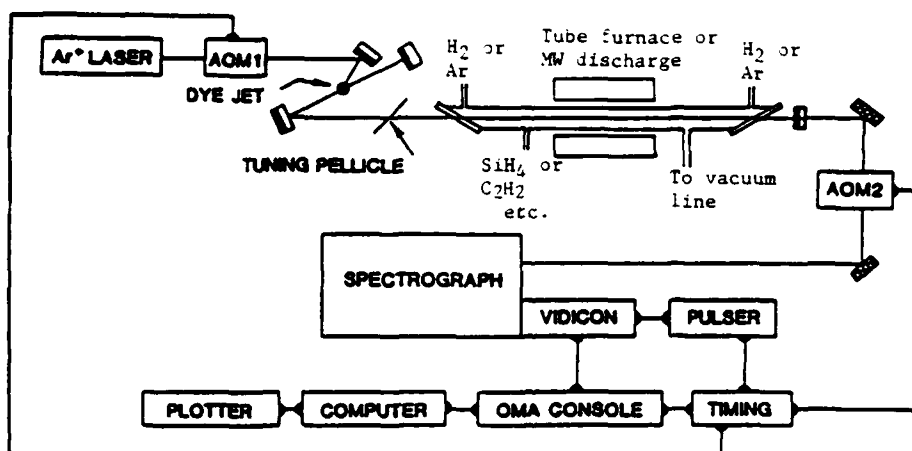

Figure 1: Instrumentation used for intracavity laser spectroscopy of gaseous species produced in the pyrolytic and/or microwave discharge decomposition of silane, organosilanes and acetylene. See text for details.

the velocity of light. For the results presented here, L_{eq} was in the range of 3-8 km.

The wavelength of the ILS dye laser is controlled by angle tuning an intracavity pellicle. The spectral bandwidth of the dye laser is 0.8 nm (22 cm^{-1}) and the overall spectral resolution of the detection system is about 95000 (0.18 cm^{-1}). The spectra presented here are a composite of a number of individual spectra obtained from overlapping wavelength regions.

Contained within the 1 m long cavity of the dye laser is the sample cell. It is equipped with 0.5 inch thick, fused-silica windows positioned at Brewster's angle. During the CVD process, these windows are continuously flushed with hydrogen or argon to prevent contamination by any particulate products of the decomposition which would render the cell windows opaque to the transmission of the laser radiation. The sample cell is modular in design consisting of sections of quartz tubing joined together using stainless steel fittings (Cajon Ultra-Torr). Decomposition of the silane or organosilane source material in the intracavity cell is accomplished by (1) a microwave discharge in an Evenson-Broida cavity operated at ∿100 W and in a geometry concentric with the laser axis or (2) pyrolysis in an 1500 W tube furnace surrounding the central 6" section of the cell. The various silanes and the other gases used are introduced into the cell by stainless steel handling systems which include flowmeters and mass flow controllers.

In order to examine resulting deposited films, 1/4" x 1/2" sections of oxidized (∿1 μm thick) silicon wafer are placed inside the decomposition zone of the intracavity CVD cell. The surface composition of the films resulting from the various silane and organosilane decomposition processes are examined by XPS analysis.

Results and Discussion

We have previously reported the ILS detection of silylene (SiH_2) in the microwave discharge decomposition of silane in argon [3]. Electronically excited argon and H_2 species are observed also under these conditions. Different concentrations of SiH_2 are observed by ILS in the microwave discharge decomposition of phenylsilane, ethylsilane and ethyltrichlorosilane

under similar experimental conditions. Since several studies [4] have indicated that SiH_2 is a dominant precursor to Si and α-Si-H deposition, its detection is of special importance in examining source materials for the preparation of silicon.

Figure 2 shows a section of the ILS spectrum observed during the pyrolysis of silane at 750° and with a total pressure of 6.2 Torr in a 1:1 mix with H_2. The wavelength region is within the (0,2,0)-(0,0,0) vibronic band in the A←X transition of SiH_2. Almost all the absorption features in this spectrum are due to known transitions of SiH_2. Spectra in this wavelength region also have been obtained during the pyrolysis of a number of organosilanes. Different relative intensities of SiH_2 absorption transitions are observed under similar pyrolysis conditions. For example, more intense SiH_2 absorptions can be observed in the pyrolysis of ethylsilane than in the pyrolysis of silane.

ILS spectrum of silane pyrolysis

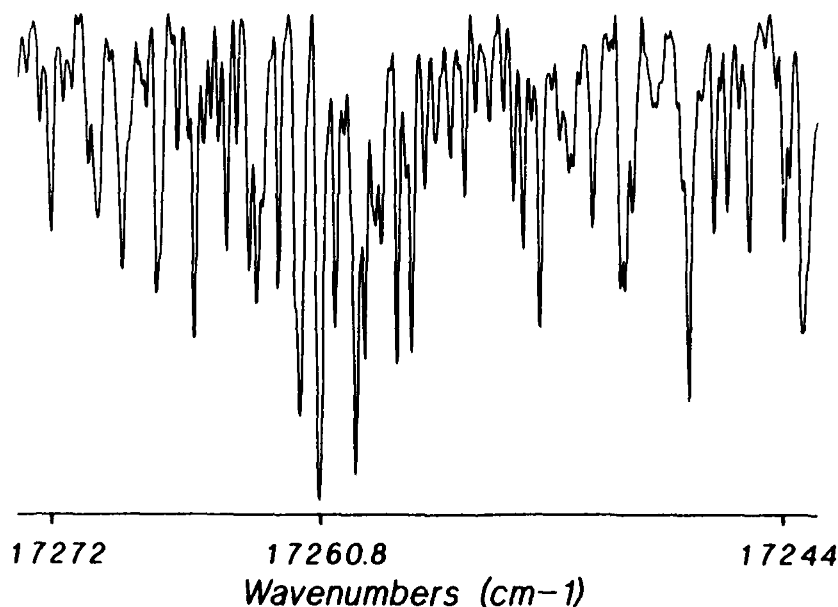

Figure 2: ILS spectrum of a silane pyrolysis at 750°C in the region of the (020)'-(000)" vibronic band of SiH_2 near 579 nm. See text for details.

A primary obstacle to the use of organosilanes for the CVD of silicon is the seemingly inevitable incorporation of carbon in the resulting silicon films. It is thought that carbon deposition under these conditions occurs via a polymeric process [5]. As a consequence, the radical C_2 is a possible gas phase precursor to carbon incorporation in the films. Figure 3 shows a section of the ILS spectrum obtained of the microwave discharge decomposition of 0.1 Torr of acetylene in 0.8 Torr of argon in the region of the 3-5 band head of the C_2 Swan system [6]. Transitions due to electronically excited H_2 [7] and argon are also observed. A very similar spectrum is observed from the microwave discharge decomposition of ethylsilane. This wavelength region (∿600 nm) also is the region of some of the rotational lines of the (0,1,0)-(0,0,0) vibronic band in the A←X transition of SiH_2. Many lines in the 600 nm region that can be attributed to SiH_2 [8] are observed in the pyrolysis of ethylsilane whereas only the strongest SiH_2 lines of this region are clearly

evident in the ILS spectra obtained during silane pyrolyses. There are many potential spectral overlaps of C_2 and SiH_2 transitions in the 600 nm region, however, and currently it remains difficult to determine if C_2 transitions also are contributing to the spectra observed during the pyrolysis of ethylsilane.

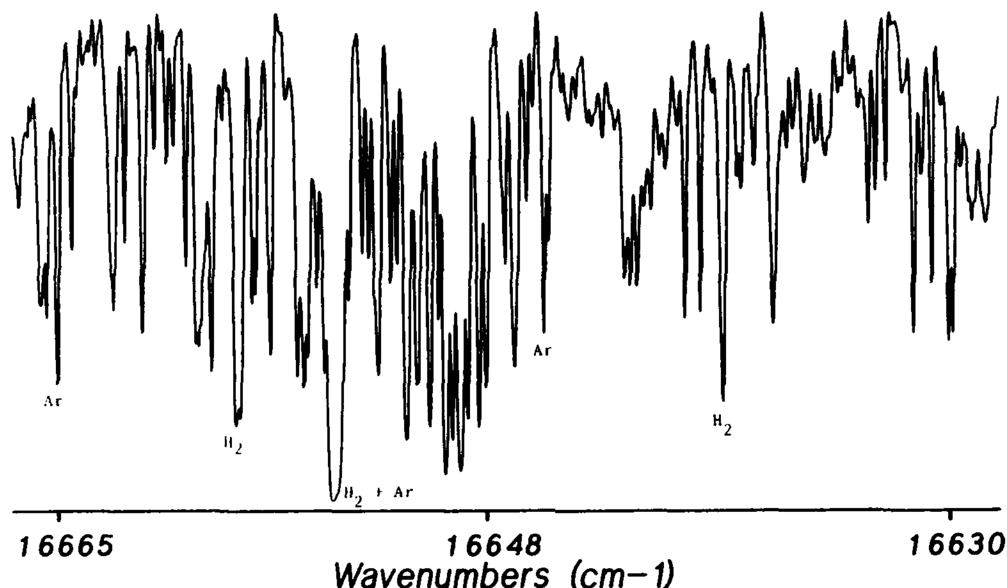

Figure 3: ILS spectrum of an acetylene microwave discharge in the region of the 3-5 band head of the C_2 Swan system. Strong transitions due to presence of excited state H_2 and Ar are indicated. See text for details.

The XPS analyses of silicon films produced in this work indicate that, while films grown from the pyrolysis of silane are essentially pure crystalline silicon, those films grown from organosilanes such as ethylsilane contain carbon. The ILS technique is being used as a method for the real-time, in situ monitoring of SiH_2 concentrations. This serves as a guide to the selection of processing conditions that minimize the carbon content of the deposited silicon films.

References

1. G.H. Atkinson, Proceedings of the NATO Advanced Study Institute on Advances in Chemical Reaction Dynamics (P.M. Rentzepis and C. Capellos, eds.)(1986) 207.
2. F. Stoeckel, M.A. Melieres and M. Chenevier, J. Chem. Phys. 76 (1982) 2191.
3. J.J. O'Brien and G.H. Atkinson, Chem. Phys. Letters, in press.
4. For example, B.A. Scott, R.M. Plecenik and E.E. Simonyi, Appl. Phys. Letters 39 (1981) 73.
5. J.S. Francisco, S.A. Joyce, J.I. Steinfeld and F. Walsh, J. Phys. Chem. 88 (1984) 3098.
6. J.G. Phillips, Ap. J. 108 (1948) 434.
7. The Hydrogen Molecule Wavelength Tables of Gerhard Heinrick Dieke (H.M. Crosswhite, ed.) Wiley Interscience (1972).
8. I. Dubois, Depository for Unpublished Data, National Science Library, Ottawa, Canada.

HIGH FREQUENCY OPTICAL HETERODYNE SPECTROSCOPY WITH LEAD-SALT SEMICONDUCTOR DIODE LASERS

David E. Cooper
SRI International
333 Ravenswood Avenue
Menlo Park, California 94025
(415) 859-3742

Absorption spectroscopy with lasers has traditionally been limited in sensitivity by noise intrinsic to the laser source. Numerous methods of surmounting this limitation using various forms of sample and source modulation have been proposed and demonstrated. One technique in particular, familiar to most users of lead-salt diode lasers, incorporates low-frequency wavelength modulation of the laser source and detection at either the first or second harmonics of the modulating waveform. Although this technique has been used successfully to measure weak absorptions, it remains fundamentally limited by diode laser amplitude fluctuations because the signal is detected in a frequency regime where the lasers exhibit considerable excess noise. Although the high frequency noise characteristics of lead-salt diode lasers are complex,[1,2] one expects their excess noise power to drop considerably at frequencies larger than the intrinsic laser linewidth. Hence, diode laser frequency modulation at radio-frequencies should offer greater immunity to laser noise and consequently a higher sensitivity to absorption than can be obtained with conventional low frequency techniques.

Optical heterodyne or frequency modulation (FM) spectroscopy with radio-frequency (rf) modulated laser light was first reported in 1980 and demonstrated using single-mode organic dye lasers.[3] Since this technique is insensitive to laser excess noise, it is in principle limited only by the quantum-noise in the laser carrier and sidebands. In the years since this initial demonstration, much of the work in FM spectroscopy has been concentrated in the visible spectral region, where much progress has been made. However it is clear that the main application of these techniques is in the infrared spectral region where absorption is essentially the only spectroscopic method and where most neutral molecules, molecular ions, and radicals exhibit strong and characteristic rotation-vibration spectra. Indeed, FM spectroscopy has recently been demonstrated in the IR using both carbon-dioxide lasers[4] and semiconductor lead-salt diode lasers.[5] The implementation of these techniques with lead-salt diode lasers is particularly interesting because they are a standard IR spectroscopic source and they can be directly modulated at high frequency.

Absorption spectroscopy with frequency modulated diode laser light can be implemented in several ways. In one scheme the laser is modulated at a single frequency and both in-phase and quadrature signals

are recovered at either the first or second harmonics[6] of the modulation frequency. This, however, requires a photodetector of relatively broad-bandwidth which may pose a significant problem in the IR, especially if one must use modulation frequencies of several hundred MHz to several GHz. An alternative scheme that relaxes the constraints on the detector bandwidth is to use two-tone modulation[7] of the diode laser. In this method the laser is modulated simultaneously at two arbitrary but closely spaced frequencies, and the beat tone between these two frequencies is monitored as the laser carrier and associated sidebands are tuned through an absorption line. The two-tone beat frequency is chosen for convenience to lie within the passband of the available detector, but it must remain high enough to lie in the low-noise region of the laser.

Two-tone frequency modulation spectroscopy with a tunable lead-salt diode laser has recently been demonstrated at high sensitivity using the experimental arrangement illustrated schematically in Figure 1.[8] We report here the results of subsequent experiments performed at higher modulation frequencies. The diode was driven by two distinct but closely spaced rf components, $\nu_m \pm 1/2\ \Omega$. In these experiments, ν_m typically ranged from 110 MHz to 1.1 GHz with Ω fixed at 1.4 MHz. The rf modulated light was directed through an absorption cell containing NH_3 gas and then onto a HgCdTe photoconductor. The detector photocurrent Fourier component at the two-tone beat frequency Ω was monitored as the laser carrier and sidebands were tuned through a pair of NH_3 absorption lines in the 930 cm^{-1} region. The signals typically recovered are illustrated in Figure 2 for various modulation frequencies ν_m. Notice that for modulation frequencies comparable to the Doppler width of the NH_3 line (83 MHz FWHM) the two-tone signals resemble a second derivative of the absorption line. However as the modulation frequency is increased the negative peaks begin to separate from the central positive peak, becoming quite distinct at the highest frequencies. Also note the signal baseline curvature increases with modulation frequency. This results from an etalon formed by the salt windows of the gas absorption cell.

A prominent feature of the two-tone spectra in Figure 2 is the asymmetry of the negative peaks. This is a manifestation of the modulation characteristics of diode lasers. Specifically, rf modulation of diode lasers results in a light beam that is simultaneously frequency and amplitude modulated.[9] The FM and AM are each characterized by modulation indices β and M respectively. The mesa-stripe lead-salt lasers that we have examined to date operate with $\beta/M \approx 10$ to 20 for radio frequency modulation. This nonzero AM index M gives rise to the asymmetry observed in the two-tone spectra. Unfortunately, it also gives rise to a non-zero background signal that fluctuates with the full amplitude noise spectrum of the diode laser and consequently limits the ultimate sensitivity of the technique. Figure 3 plots the results of a recent analysis[10] that shows how the minimum detectable absorption in two-tone FM spectroscopy varies with FM index β for several values of the AM index. Note that the ultimate detection sensitivity decreases

strongly with increasing M. Also, highest sensitivities are obtained for values of β approximately equal to 1.15.

To date, the highest sensitivity obtained using two-tone FM spectroscopy with lead-salt laser diodes is an absorption of 10^{-5} with a 1 sec averaging time. This result was limited by the detector quantum efficiency at 1.4 MHz and the preamplifier noise level. Higher sensitivities will require improved detectors, preamplifiers, and laser structures that yield a low AM index for radio frequency modulation. This latter point is an important consideration in view of the results plotted in Figure 3 and the fact that the high frequency modulation characteristics of AlGaAs diode lasers are known to depend on device structure.[9] Specifically it has been found that certain device structures favor a low AM index. The extent to which some of these advanced laser structures can be incorporated into lead-salt laser technology is currently an open question. However the fact that cleave-coupled-cavity lead-salt diodes have been successfully fabricated[11] and that single-quantum-well devices are on the horizon leave one optimistic about the future.

REFERENCES

1. C. Freed and J. Bielinski, MIT Report prepared for NASA under Contract NAG-1-164, 1982.
2. R. T. Ku and D. L. Spears, Optics Letters 1, 84, 1977.
3. G. C. Bjorklund, Optics Letters 5, 15, 1980.
4. D. E. Cooper and T. F. Gallagher, Applied Optics, 24, 710, 1985.
5. M. Gehrtz, W. Lenth, A. T. Young, and H. S. Johnston, Optics Letters, 11, 132, 1986.
6. G. Janik, C. Carlisle, and T. F. Gallagher, Applied Optics, 24, 3318, 1985.
7. G. Janik, C. B. Carlisle, and T. F. Gallagher, JOSA B 3, 1070, 1986.
8. D. E. Cooper and J. P. Watjen, Optics Letters, 11, 606, 1986.
9. S. Kobayashi, Y. Yamamoto, M. Ito, and T. Kimura, IEEE J. Quant. Elect., QE-18, 582, 1982.
10. D. E. Cooper and R. E. Warren , Unpublished Manuscript.
11. K. J. Linden and R. E. Reeder, Appl. Phys. Lett., 44, 377, 1984.

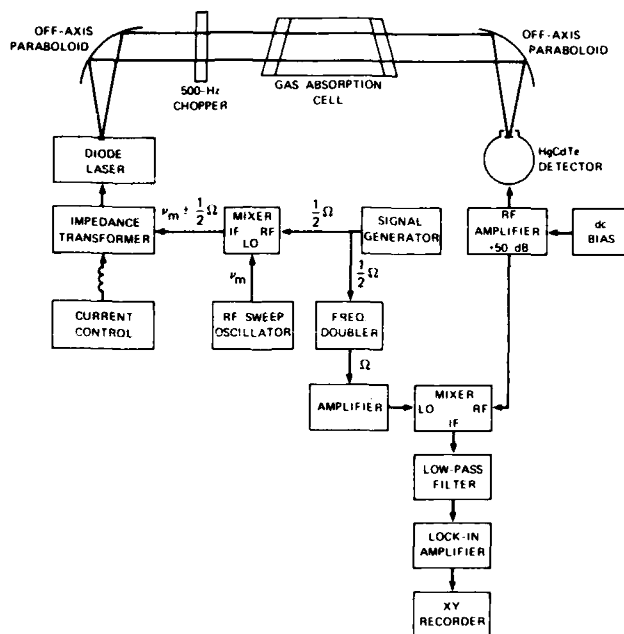

Figure 1 Experimental Arrangement for Two-Tone Optical Heterodyne Spectroscopy with Tunable Lead-Salt Diode Lasers.

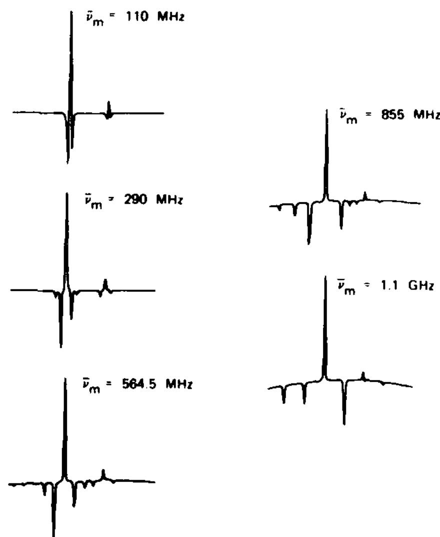

Figure 2 Experimental Two-Tone Spectra from a Pair of Doppler-Broadened NH_3 Lines.

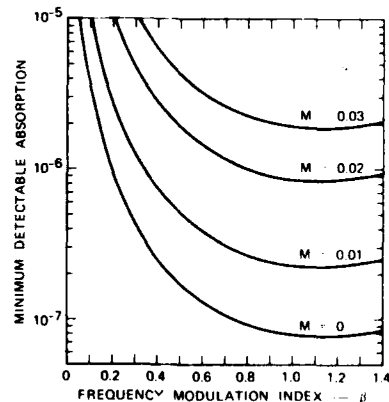

Figure 3 Dependance of Minimum Detectable Absorption on FM Index for Various Values of AM Index.

NOTES

WEDNESDAY, FEBRUARY 11, 1987

BALLROOM A
3:00 P.M.–3:45 P.M.

WE1–2

LASER DIAGNOSTICS OF GAS-PHASE PROCESSING: 2

Pauline Ho, Sandia National Laboratories, *Presider*

Laser Diagnostics of Radio Frequency Discharges

Richard A. Gottscho

AT&T Bell Laboratories
Murray Hill, New Jersey 07974

I. Abstract

Recent applications of laser spectroscopy to the study of plasma and plasma-surface processes are reviewed. Using laser-induced fluorescence and optogalvanic spectroscopy, measurements of concentration gradients, reaction probabilities, electric fields, and process end-points have helped to elucidate plasma-chemical mechanisms.

II. Introduction

Radio frequency plasmas are used throughout the microelectronics industry to etch and deposit thin films in very large scale integrated circuit fabrication.[1] For this reason, it is desirable to develop new diagnostic methods that provide additional insight into and control of the myriad of non-equilibrium processes that occur in a plasma reactor.

In this talk, recent applications of laser spectroscopy to the monitoring of rf discharge processes will be discussed.[2] Laser-induced fluorescence has been shown to be a useful means for monitoring reactive neutral and ion densities,[3–13] electric field magnitudes,[14–19] and process end-points.[20] Optogalvanic spectroscopy has been useful in the detection of positive[21] and negative ions,[22–27] metastable states,[28–30] and electric fields.[31–34]

III. Concentration Measurements

Utilizing the inherently high spatial resolution of one and two photon laser-induced fluorescence spectroscopy, concentration gradients have been measured for ions at the plasma-sheath boundary[3,4] and for neutrals at reactive surfaces.[10,11,20] The former measurement provides information on the mechanisms for extraction of ions from the plasma and is important for understanding ion-modified surface reactions. The latter measurement provides information on the surface loss rate of reactant atoms and molecules and is important for understanding neutral surface chemistry.

Complementary information can be obtained by making time-resolved concentration measurements.[3,35] Because the applied field in an rf discharge is time-varying, the formation rates for ions and neutrals can also be time-varying. By synchronously firing a dye laser and detecting laser-induced fluorescence, effective lifetimes can be determined from the density modulation and phase shift. Different lifetimes can be expected for ions and reactants in different portions of the discharge. For example, an ion accelerated by the large sheath field will have a different reaction or charge exchange probability than the same ion in the weak field plasma. Similarly, neutrals will exhibit a shorter lifetime near a reactive surface than in the homogeneous plasma.

IV. Electric Field Measurements

Recently, optogalvanic and laser-induced fluorescence detection schemes have been employed in determining the magnitude of sheath electric fields.[14-19,31-35] These measurements are perhaps the most important for understanding the discharge structure and charged particle transport. They also permit detailed comparisons with self-consistent plasma theories. The fields in electropositive dc discharges have been found to vary linearly with position.[31-34] However, the fields in electronegative dc and rf discharges depart substantially from a linear form and, because of the presence of negative ions, occasionally exhibit maxima and minima (*i.e.* double layers).[27,36]

V. Negative Ion Measurements

Negative ion densities can be measured by photodetachment of electrons.[22-27] The transient increase in electron density can be monitored using microwave interferometry, electrostatic probes, or optogalvanic detection. Recently, laser-induced fluorescence from the neutral created by photodetachment has also been reported.[20] These experiments have led to greater understanding of the formation and loss mechansims of negative ions in glow discharges and the effects that negative ions have on plasma and sheath electrodynamics. From the sign of the optogalvanic signal resulting from photodetachment, the direction of the electric field can be deduced.[27] In low frequency plasmas, the field is sometimes directed away from the electrode so that negative ions and electrons bombard device surfaces.

VI. Diagnostic Wish List

Despite recent advances in understanding there are many technological problems remaining to be addressed. Foremost among these is *in situ* surface analysis to evaluate the extent of surface damage and contamination. Another area for future development is improving sensitivity and resolution so that concentration and field gradients can be measured near or inside sub-micron surface features. These and other needs will be discussed briefly.

REFERENCES

[1] N.G. Einspruch and D.M. Brown, VLSI Electronics **8**, Academic Press (Orlando, Fla. 1984).

[2] L. Luessen and J. Proud, Proceedings of NATO Advanced Study Institute on Radiative Processes in Glow Discharges, Pitlochry, Scotland (June 1985).

[3] R. A. Gottscho, R. H. Burton, D. L. Flamm, V. M. Donnelly, and G. P. Davis, J. Appl. Phys. **55**, 2707 (1984).

[4] V. M. Donnelly, D. L. Flamm, and G. Collins, J. Vac. Sci. Technol. **21**, 817 (1982).

[5] R. A. Gottscho and T. A. Miller, Pure and Appl. Chem. **56**, 189 (1984).

[6] P. J. Hargis and M. J. Kushner, Appl. Phys. Lett. **40**, 779 (1982).

[7] R. A. Gottscho, G. Smolinsky, and R. H. Burton, J. Appl. Phys. **53**, 5908 (1982).

[8] S. Pang and S. R. Brueck, "Laser Induced Fluorescence Diagnostics of $CF_4/O_2/H_2$ Plasma Etching", in *Laser Diagnostics and Photochemical Processing for Semiconductor Devices*, edited by R. M. Osgood, S. R. J. Brueck, and H. R. Schlossberg, North Holland (New York, 1983), p. 161.

[9] R. Walkup, K. Saenger, and G.S. Selwyn, Mat. Res. Soc. Symp. Proc. Vol. **38**, 69 (1985).

[10] G. Selwyn, J. Appl. Phys. **60**, 2771 (1986).

[11] J.W. Thoman, K. Suzuki, S.H. Kable, and J.I. Steinfeld, J. Appl. Phys. **60**, 2775 (1986).

[12] M. Kitamura, H. Akiya, and T. Urisu, Dry Process Symposium, Tokyo, Japan, November 1986, Abstract I-2.

[13] L. F. DiMauro, R. A. Gottscho, and T. A. Miller, J. Appl. Phys. **56**, 2007 (1984).

[14] C. A. Moore, G. P. Davis, and R. A. Gottscho, Phys. Rev. Lett. **52**, 538 (1984).

[15] M. L. Mandich, C. E. Gaebe, and R. A. Gottscho, J. Chem. Phys. **83**, 3349 (1985).

[16] T. Oda and K. Kawasaki, Jap. J. Appl. Phys. **20**, L761 (1981).

[17] K. Kawasaki, T. Usui, and T. Oda, J. Phys. Soc. Jap. **51**, 3666 (1982).

[18] T. Oda, T. Usui, K. Takiyama, T. Fujita, and Y. Kamiura, Proc. US-Japan Workshop on Tokamak Diagnostics by X-Ray, VUV, and Optical Radiations, Nagoya University 1984, p. 78.

[19] J. Derouard and N. Sadeghi, Opt. Comm.**57**, 239 (1986).

[20] G. Selwyn, Sixth Symposium on Plasma Processing, The Electrochemical Society, San Diego, CA, October 1986, Abstract 296.

[21] R. Walkup, R. W. Dreyfus, and Ph. Avouris, Phys. Rev. Lett. **50**, 1846 (1983).

[22] J. Taillet, C. R. Acad. Sc. Paris **269**, 52 (1969).

[23] M. Bacal, G. W. Hamilton, A. M. Bruneteau, H. J. Doucet, and J. Taillet, J. de Physique **40**, C7-791 (1979).

[24] K. E. Greenberg, G. A. Hebner, and J. T. Verdeyen, Appl. Phys. Lett. **44**, 299 (1984).

[25] R. Klein, R. P. McGinnis, and S. R. Leone, Chem. Phys. Lett. **100**, 475 (1983).

[26] C. R. Webster, I. S. McDermid, and C. T. Rettner, J. Chem. Phys. **78**, 646 (1983).

[27] R. A. Gottscho and C. E. Gaebe, IEEE Trans. Plasma Science **14**, 92 (1986); J. Vac. Sci. Technol. A **4**, 1795 (1986).

[28] D. K. Doughty and J. E. Lawler, Appl. Phys. Lett. **42**, 234 (1983).

[29] B.N. Ganguly and A. Garscadden, Appl. Phys. Lett. **46**, 540 (1985).

[30] R.A. Gottscho, Sixth Symposium on Plasma Processing, The Electrochemical Society, San Diego, CA, October 1986, Abstract 294.

[31] D. K. Doughty and J. E. Lawler, Appl. Phys. Lett. **45**, 611 (1984).

[32] D. K. Doughty, S. Salih, and J. E. Lawler, Phys. Lett. **103A**, 41 (1984).

[33] B.N. Ganguly and A. Garscadden, Phys. Rev. A **32**, 2544 (1985).

[34] B.N. Ganguly, J. Appl. Phys. **60**, 571 (1986).

[35] R. A. Gottscho and M. L. Mandich, J. Vac. Sci. Technol. **A 3**, 617 (1985).

[36] R. A. Gottscho, Phys. Rev. A. submitted.

Quantum-Resolved Gas-Surface Scattering: NH_3 from Au (111)

Bruce D. Kay, T. D. Raymond, and Michael E. Coltrin
Sandia National Laboratories
Albuquerque, NM 87185

Summary

We have measured angular, velocity, and quantum-state distributions for ammonia molecules scattered from a gold (111) single crystal for a number of surface temperatures and incident beam energies. A molecular beam source produces a well-collimated, rotationally cold (~15 K) beam of NH_3 molecules with a narrow dispersion of translational energy (~10%). The molecular beam impinges on an atomically clean, single crystal of gold (111) and the scattered NH_3 is detected in a quantum-resolved manner using two-photon resonant, three-photon ionization [1].

The scattered angular distribututions are sharply peaked about the specular angle, in constrast to the broad distributions observed in our earlier studies of NH_3 scattering from NH_3-saturated W (100) [2]. The final velocity distributions indicate a non-equilibrated mean translational energy, which is highly dependent on the incident beam kinetic energy. The mean scattered energy is up to five times that expected if this degree of freedom were fully accommodated with the surface. These observations are indicative of a direct-inelastic

scattering mechanism in which the molecules do not reside on the surface long enough to become equilibrated with it.

Further information about the ammonia-gold interaction is contained in the internal state distributions of the scattered molecules. The rotational state distributions of the scattered molecules were found to be strongly dependent on beam kinetic energy. These distributions are markedly non-Boltzmann and indicate that the population in the ground state is preferentially scattered into the lowest K states; these are states in which the molecule is tumbling normal to the symmetry axis as opposed to spinning about it. Since ammonia is an oblate symmetric top, these states are the energetically least favored for a given angular momentum. The observed rotational state distribution is thus indicative of a dynamical rather that a thermal effect. Such an anomalous rotational distribution suggests the importance of the long-range dipole-image dipole and dispersion interactions and/or the short range chemical attraction which have strong polar dependences but little or no azimuthal dependence.

We have observed up to three quanta of vibrational excitation in the umbrella mode of the scattered ammonia molecule. The degree of vibrational excitation scales strongly with the normal component of incident beam kinetic energy and is insensitive to surface temperature. At the highest incident beam energy employed (0.4 eV), roughly 3% of the scattered NH_3 has three quanta of vibrational excitation. This degree of excitation is roughly 1000 times greater than expected if the NH_3 were thermally equilibrated with the surface.

In order to explain the experimental observations, we have developed a classical trajectory code for the scattering of a rigid, nonlinear molecule from a rigid, flat gold surface. Our classical trajectory calculations predict the propensity for tumbling vs. spinning seen

experimentally. The distribution of scattered molecules is markedly non-Boltzman, with the low-K states preferentially populated.

The trajectory calculations also predict that if the molecule is initially rotationless the long-range potential causes the molecule to re-orient as it approaches the surface. This causes the molecule to preferentially strike the surface with the symmetry axis perpendicular to the surface, giving rise to rotationally elastic collisions. Thus, in the collision either the nitrogen atom alone or all three hydrogen atoms hit the surface. In either case no torque is exerted about the molecule's center of mass, and thus no rotational energy is transferred to the molecule. Thus, the long-range term in the potential serves to suppress rather than enhance the rotational energy transfer.

In an attempt to explain the large degree of vibrational excitation seen experimentally, we have extended our classical trajectory model to include the "umbrella" vibrational motion in NH_3. The model predicts very efficient transfer of translational energy to the umbrella vibrational mode. The vibrational excitation is predicted to scale with the normal component of incident kinetic energy, in agreement with the experimental observation.

ACKNOWLEDGEMENTS

This work performed at Sandia National Laboratories and supported by the U.S. Department of Energy under contract No.DE-AC0476DP00789.

References

1. "MPI spectroscopy of NH_3: application to rotational energy accomadation on surfaces", B. D. Kay, A. J. Grimley, and T. D. Raymond, SPIE Southwest Conference on Optics **50**, 330 (1985).

2. "Rotationally inelastic gas-surface scattering: NH_3 from NH_3-saturated W(100)", B. D. Kay and T. D. Raymond, J. Chem. Phys. **85**, 4140 (1986).

NOTES

WEDNESDAY, FEBRUARY 11, 1987

BALLROOM A
3:45 P.M.–4:30 P.M.

WF1–2

OPTICAL DIAGNOSTICS OF SEMICONDUCTOR SURFACES

J. Gerardo, Sandia National Laboratories, *Presider*

SUMMARY

I. Advantages and limitations of optical characterization.

The primary advantages of optical measurements are that they are general, convenient, nondestructive, and can yield information about dynamic systems or processes in real time and in any transparent ambient. No special sample requirements are needed other than a reflecting surface, and measurements can be made with the sample in air or in atmospheric-pressure ambients. Nondestructiveness is obviously important for the analysis of unstable materials systems such as interfaces buried under oxide overlayers, while real-time capabilities suggest useful applications in process control. A final advantage is that optical probes offer unsurpassed energy resolution, important for accurately determining compositions of semiconductor alloys.

The optical data themselves are characterized by high sensitivities to both microstructure and interface conditions. (Microstructure is used here in the usual materials science sense of spatial inhomogeneities on the length scale of 1-100 nm.) Ellipsometry in particular can easily detect submonolayer changes in layers of foreign material at surfaces and interfaces.

On the other hand, visible-near uv optical probes have a relatively small accessible wavelength range, of the order of 200 to 800 nm. As a result, compared to particle (electron and ion) spectroscopies, optical probes are very nonspecific, generally not capable of identifying individual atomic species. Lateral resolution fundamentally limited by the wavelength of light restricts many potential applications, particularly as technology moves into the submicron range. Third, optical probes do not directly measure compositions, densities, film thicknesses, or other material properties of interest: they measure optical responses such as transmittances, reflectances, etc., which must be connected to material properties by model calculations. Models introduce uncertainties by separating the investigator from the information. In addition, the construction of suitable models may require additional knowledge and/or good physical insight, and because every part of the sample to which light penetrates contributes to the measured optical response the modeling and analysis of graded or complex multilayered systems may be difficult or impossible. Finally, the evaluation of models requires a computer, good software, and an accurate database.

In short, if time and sample destruction are not considerations, there usually are better approaches to determining any specific material characteristic. But for many applications the convenience, nondestructiveness, and generality of optical analysis offers clear advantages.

II. General remarks concerning optical characterization.

Optical characterization is a very old field that has recently undergone considerable growth primarily because of the development and fairly widespread implementation of automatic spectroellipsometers. These computer-based instruments, which bear the same relationship to spectrophotometers that impedance-measuring instruments do to wattmeters, are fast, accurate, and able to return spectral information over the entire quartz-optics range. They have not only greatly increased the available database but also our understanding of the role of microstructure in determining optical properties.

To make the optical characterization topic more understandable, particularly with respect to what optical analysis can and cannot do, it is useful to keep two elementary points in mind. The first, as mentioned above, is that optical measurements directly determine only optical properties such as reflectances, transmittances, complex reflectance ratios, etc., not the sample properties or material characteristics of interest. As this gap can only be bridged by model calculations, models are unavoidable. (We define a model as an idealized mathematical representation of an actual physical sample.) At the first level, modeling is phenomenological: the Fresnel equations are used to parameterize the measured optical properties of the sample in terms of its physical properties such as layer thicknesses and the dielectric functions of the separate layers.

The second elementary point is that the measured optical properties are macroscopic or average quantities that directly give only macroscopic or average information, even though the microstructural characteristics -- compositions, grain sizes, densities, etc. -- actually determine the macroscopic response. For materials analysis, this creates a second gap that must also be bridged by model calculations. At this level the model must specify how the microstructural parameters determine the wavelength-dependent complex dielectric function, ϵ, that represents the material in the Fresnel expressions. While ϵ can be calculated from first principles if we are given the detailed atomic or microstructure of a material, this presupposes the very information that we seek to obtain. Consequently, we typically assume that the sample has some simple microstructure for which the ϵ-microstructure connection has already been established in analytic form, then use the ϵ data to determine the parameters of the effective medium model as an approximation to the actual parameters of the material.

From the above discussion it may seem like the determination of material characteristics from optical analysis is a task restricted to the wildly optimistic, but in fact recently developed limit theorems have established rigorous, and fairly narrow, bounds on the dielectric properties of microscopically inhomogeneous materials -- even if nothing at all is known about compositions or microstructures. These

theorems are extremely useful not only for assessing the fundamental limits to what we can and cannot know about microstructure from ε, but also for determining which effective medium model may best represent a given sample.

In short, the determination of material characteristics from optical data is a procedure of the inverse type, which loosely means a situation where one is given the answer and asked to find the problem. From this perspective, it is clear that the real goal of optical analysis is not to devise models that represent a given sample or to determine the parameters of a given model from optical data, but rather to demonstrate that a proposed model accurately represents a given sample to the desired level of accuracy. To achieve this goal, it is necessary to assess the capability of the model to represent data over as many different experimental conditions as possible. In practice, this is accomplished by obtaining spectral data over a wide range of wavelengths. In the same vein, one reason why ellipsometry replaced photometry as the dominant optical characterization technique (after the technology advanced to the point where spectroellipsometric measurements could be made routinely) is that ellipsometers return two pieces of information per measurement instead of one, providing further overdetermination.

While information obtained in this way is less definitive than that obtained by direct microstructural probes such as transmission electron microscopes, nevertheless the representation of microscopically complex physical systems in terms of a few macroscopic parameters is often more useful in practice. The description of a gas by the positions and velocities of its individual molecules vs. its pressure and temperature is a parallel situation to consider.

III. REPRESENTATIVE EXAMPLES.

A. Alloy compositions and carrier concentrations. Analysis of $Hg_{1-x}Cd_xTe$: F. H. Pollak, C. E. Okeke, P. E. Vanier, and P. M. Raccah, J. Appl. Phys. 49, 4216 (1978).

B. Film thickness measurements by spectroreflectometry. Determination of thicknesses of SiO_2 and polycrystalline Si films on crystalline Si substrates: P. S. Hauge, J. Opt. Soc. Am. 69, 1143 (1979).

C. Thicknesses, damage assessment, and states of crystallinity in ion-implanted materials by spectroellipsometry. Multilayer analysis of ion-implanted crystalline silicon: K. Vedam, P. J. McMarr, and J. Narayan, Appl. Phys. Lett. 47, 339 (1985).

D. Real-time assessments of cleaning procedures and the removal of residual overlayers. Cleaning of crystalline Si: D. E. Aspnes and A. A. Studna, SPIE Proceedings 276, 227 (1981).

E. Determination of thicknesses and microstructural parameters of deposited metal films by various spectrophotometric and spectroellipsometric probes; application of limit theorems to materials analysis. Combined analysis of deposited Rh films: D. P. Arndt et. al. (20 authors), Appl. Opt. 23, 3571 (1984); D. E. Aspnes and H. G. Craighead, Appl. Opt. 25, 1299 (1986).

IV. Bibliography.

This lecture was drawn primarily from a set of notes prepared for a short course on materials characterization given for SPIE; the notes are available on request. The following published works provide more detail on specific topics:

R. M. A. Azzam and N. M. Bashara, Ellipsometry and Polarized Light (North-Holland, Amsterdam, 1977).

Optical Characterization Techniques in Semiconductor Technology, SPIE vol. 276, edited by D. E. Aspnes, S. So, and R. F. Potter (1981).

Spectroscopic Characterization Techniques for Semiconductor Technology, SPIE vol. 476, edited by F. H. Pollak and R. S. Bauer (1983).

Proceedings of the International Conference on Ellipsometry and Other Optical Methods for Surface and Thin Film Analysis, J. Phys. Colloque C10, edited by F. Abeles (1983).

Thin film reviews:

F. Abeles, in Physics of Thin Films 6, edited by G. Hass and R. E. Thun (Academic, New York, 1971), pp. 151-204.

P. Rouard and P. Bosquet, Progr. Opt. 4, 145 (1965).

W. R. Hunter, Appl. Opt. 21, 2103 (1982).

S. P. F. Humphreys-Owen, Proc. Phys. Soc. (London) 77, 949 (1961).

Optical modeling, effective medium theory, and related topics:

D. E. Aspnes, Am. J. Phys. 50, 704 (1982).

D. E. Aspnes, J. Mater. Education 7, 849 (1985).

The Spatial Resolution and Defect Contrast of Optical Beam Induced Reflectance (OBIR) Scans

G. E. Carver

AT&T - Engineering Research Center
Princeton, New Jersey, 08540

D. C. Joy

AT&T - Bell Labs
Murray Hill, New Jersey, 07974

There is substantial current interest in developing non-contact, non-destructive probes of semiconductor surfaces.[1] [2] [3] [4] [5] A major reason for this activity is that micro-stuctural flaws near the surface of silicon wafers generally impair the successful manufacture of integrated circuits.[6] Detrimental defects such as stacking faults, dislocations, and metallic precipitates are often 1 to 2 microns in size. Thus, a probing system would need to exhibit both high spatial resolution and contrast at defective sites.

A pump-probe laser system to satisfy these requirements has been developed. The system, named OBIR for optical beam induced reflectance, is non-destructive and operates at 20C in air. A schematic of OBIR is shown in figure 1. The wafer surface is excited by a focused pumping laser. Holes and electrons generated by the pump significantly alter the optical constants of silicon in the infrared. A second laser then probes the infrared reflectance of the photo-excited area. Recombination within electrically active defects reduces carrier concentration from levels in non-defective material. The resulting changes in infrared reflectance are then observed as dark spots on a two dimensional display as the beams are rastered over the sample.

The OBIR system combines the high sensitivity of far infrared reflectance to plasma density with a spatial resolution typical of visible light, (about 1 micron). The resolution is obtained by modulating the pump, running the probe cw, and detecting only that portion of the reflected probing beam that becomes modulated at the chopping rate of the pumping beam. In addition, the probe is incident near the Brewster angle of the un-excited wafer. This allows use of a high intensity probe without detector damage, and enhances the fraction of the reflected probe that is photo-modulated. Further, as diffusion drives carriers away from the pumping spot, the ensuing falloff in carrier density ensures that only carriers near the pumping spot contribute to the infrared signal. In summary, OBIR's sensitivity to plasma density allows for a spatially resolved 2-D mapping of carrier lifetime.

To date, the OBIR system has observed metallic precipitates, epitaxial stacking faults, oxygen precipitates, and fine surface scratches in silicon wafers. Some oxygen precipitates appear as features 0.75 micron in size. OBIR is not capable of observing photo-modulation on fine polycrystalline silicon, or on un-annealled implanted layers. This implies a higher sensitivity to damage than is possible with thermal-wave systems that monitor implant damage distributions.[2] The Drude model, with an inter-valence band contribution, can be used to calculate the optical constants of the photo-excited wafer.[7] [8] The model, coupled

with the temperature dependence of the index of refraction,[9] clearly shows that OBIR depends on plasma, not thermal effects, at 10.6 microns. Further, sensitivity to plasma density, and therefore to recombination centers, falls off rapidly as the probing wavelength is decreased. Sensitivity to defects should therefore be considerably less if one probes in the visible, although spatial resolution is easy to obtain with visible probes.[10] [11]

Figure 2 shows the results of an OBIR scan on a MOS wafer. The defects exhibited in part b) include metallic precipitates and a fine scratch. Part a) shows that the defects were not observable with conventional microscopy before etching, and part c) demonstrates a one-to-one correlation between etch pits and the defects revealed by OBIR. Figure 3 shows two EBIC[12] scans of an adjacent piece of the same wafer from figure 2. The EBIC measurements were done with an accelerating voltage of 15-20 kv, a beam current of 10^{-10} amps, and a spatial resolution of 1 micron. EBIC parameters indicate that the defects were 1/2 to 1 micron deep. Parts a) and b) of figure 3 show that OBIR and EBIC contrast profiles of prominent defects are comparable.

REFERENCES

1. A. Rosencwaig, J. Opsal, W. L. Smith, D. L. Willenborg App. Phys. Lett., 46, p.1013, 1985
2. W. L. Smith, A. Rosencwaig, D. L. Willenborg App. Phys. Lett., 47, p.584, 1985
3. H. Hasegawa, H. Ohno, H. Shimizu, S. Seki, J. Electronic Materials, 13, p.931, 1984
4. S. R. J. Brueck, " Optical Microanalysis of Device Materials and Structures", in: Proceedings of International Conference on Laser Processing and Diagnostics, D. Bauerle, editor, Springer-Verlag, p.447. 1984
5. R. M. Silva, F. D. Orazio Jr., J. M. Bennet, Optics News, 12, p.14, 1986
6. H. R. Huff, Solid State Technology, p.89, 1983
7. E. Barta, Infrared Physics, 17, p.319, 1977
8. E. Barta, Infrared Physics, 17, p.111, 1977
9. H. H. Li, J. Phys. Chem. Ref. Data, 9, p.561, 1980
10. D. Guidotti, H. van Driel, App. Phys. Lett., 47, p.1336, 1985
11. A. Rosencwaig, J. Opsal, W. L. Smith, D. L. Willenborg, App. Phys. Lett., 49, p.301, 1986
12. H. J. Leamy, J. App. Phys., 53, p.R51, 1982

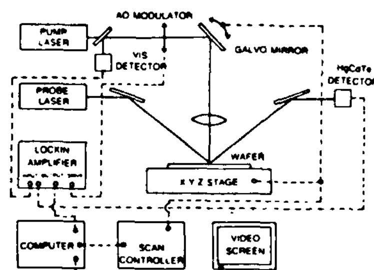

Figure 1

Optical Beam Induced Reflectance (OBIR) MOS Silicon Wafer

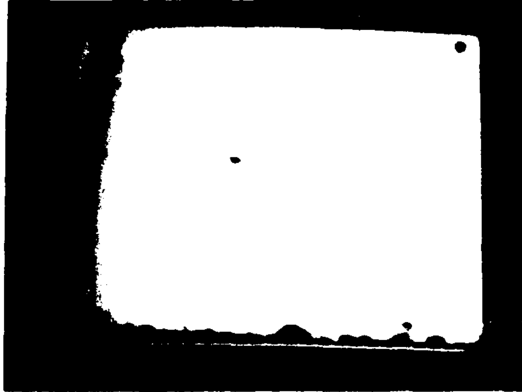

OPTICAL MICROSCOPY PRE-ETCH a)

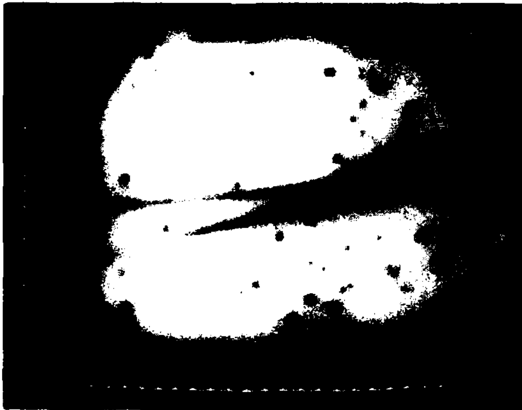

OBIR b)

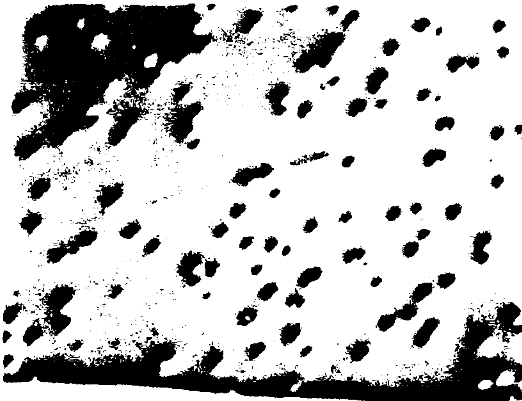

OPTICAL MICROSCOPY POST-ETCH c)

Figure 2

EBIC Scan and Contrast Profiles

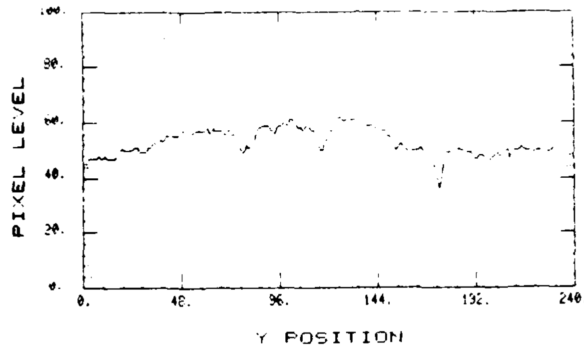

a) OBIR Contrast Profile

Line Scan Position

b) EBIC Scan Including Contrast Profile

Signal

Zero

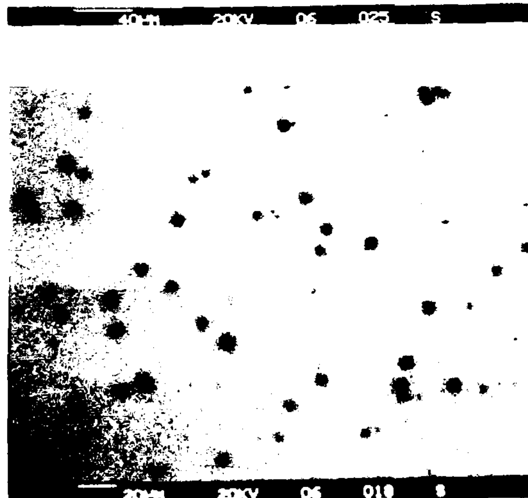

c) Higher Magnification EBIC Scan

Figure 3

NOTES

THURSDAY, FEBRUARY 12, 1987

BALLROOM A
8:30 A.M.–9:45 A.M.

ThA1–4

NONRADIATIVE PROBES OF ABSORPTION

C. H. Seager, Sandia National Laboratories, *Presider*

During the past few years, thermal wave physics has been successfully applied to studies of semiconductor materials and microelectronic devices. Previously, we described how these materials and devices might be examined with thermal wave imaging.[1] This imaging is performed in a scanning electron microscope with a thermoelastic technique for thermal wave detection. Although this technique is a very sensitive detection method for thermal waves,[2] it has limited applicability for integrated circuit process control and inspection because it requires contact to a transducer and thus is potentially contaminating. Furthermore the results are often strongly dependent on difficult to control acoustic variables such as sample geometry and sample/detector coupling. To overcome these problems we have developed a noncontact thermal wave technique that can be used at the high modulation frequencies required for micron-scale resolution.[3-5]

When a material is excited with an intensity-modulated energy source, or pump, its optical properties can be altered by the absorption of the incident energy. This results in the sample's complex refractive index undergoing periodic variations at the modulation frequency of the pump intensity excitation. The induced changes in the sample's optical refractive index can be detected by measuring the modulated reflectance of an optical probe from the sample surface. By the use of phase-sensitive detection methods, probe beam modulated reflectances, $\Delta R/R$, as low as 10^{-7} can be measured.[3]

This phenomenon, called modulated photoreflectance, was

first observed nearly thirty years ago and developed into a useful spectroscopic technique for investigating the optical properties of various materials.[6] These spectroscopic studies employ low intensity pump ($< 1W/cm^2$) and probe ($< 1mW/cm^2$) optical beams and operate at low pump intensity modulation frequencies (typically $< 1kHz$). The wavelength of the probe beam is scanned and its modulated reflectance is recorded as a function of its wavelength. In most materials the modulated photoreflectance signal arises from a purely thermoreflectance effect.[7] That is, since the optical properties of most materials are dependent to some extent on the sample temperature, and since the temperature of the sample surface undergoes a periodic variation from the heat produced by the absorbed intensity-modulated pump beam, the reflectance of the probe beam experiences a corresponding modulation. In semiconductors, however, there are often more significant contributions to the photoreflectance signal from the free carriers that are generated by the pump beam. These contributions arise from thermal effects associated with free carrier recombination, from a free carrier Drude effect on the optical refractive index, and also from an electroreflectance effect whereby the photogenerated carriers modulate the amount of surface band bending, or surface electric field, in the semiconductor. Under the experimental conditions used for conventional photoreflectance, it has been found that the electroreflectance term is the dominant effect on the recorded signal.[8]

We have developed a somewhat different modulated

reflectance technique.[3] In this method we employ a highly focused (~ 1 μm spot size) laser beam as the pump with a typical intensity in the 10^4-10^5 W/cm^2 range, and we intensity-modulate the pump laser in the MHz range. In addition, the probe beam is a laser at a fixed wavelength that is usually far removed from any critical points in the sample's band structure. Our interest is not to perform optical spectroscopy as in the conventional photoreflectance method, and thus the probe wavelength is not scanned. Instead we are interested in characterizing the spatial and frequency dependence of the photogenerated thermal waves in non-semiconductors and of the photogenerated thermal and electron-hole plasma waves[4] in semiconductors. Our different experimental conditions produce modulated reflectance signals that, unlike conventional photoreflectance, are primarily due to the Drude effect. Using this signal we are able to detect and quantify those intrinsic and defect characteristics in the near-surface region of the sample that affect the local thermal and electrical transport properies. In particular, we have used this laser-induced modulated reflectance method for monitoring the dose and uniformity of ion implantation in Si and GaAs wafers,[5] for detecting and quantifying the residual damage in silicon wafers that results from chemopolishing and scrubbing processes,[9] and for detecting and characterizing radiation damage and contamination in silicon from reactive ion and plasma etch processes.[10]

In addition we have observed an interesting temporal

behavior of our modulated reflectance signal in silicon; a phenomenon that has apparently not been detected in the conventional photoreflectance experiments. We have found that this temporal behavior appears to be very useful for detecting and studying the electronic surface states in silicon that are defect or damage related.

REFERENCES

1. A. Rosencwaig, in VLSI Electronics: Microstructure Science, Vol. 9, ed. Einspruch, (Academic, Orlando, 1985), p. 227.

2. A. Rosencwaig and J. Opsal, IEEE Trans. Ultrasonics, Ferroelectrics and Frequency Control, UFFC-33, 516 (1986).

3. A. Rosencwaig, J. Opsal, W.L. Smith, and D.L. Willenborg, Appl. Phys. Lett. 46, 1013 (1985).

4. J. Opsal and A. Rosencwaig, Appl. Phys. Lett. 47, 498 (1985).

5. W.L. Smith, A. Rosencwaig, and D.L. Willenborg, Appl. Phys. Lett. 47, 584 (1985).

6. E.Y. Wang, W.A. Albers, and C.E. Bleil, in II-VI Semi-Conducting Compounds, ed. Thomas (Benjamin, New York, 1967) p. 136.

7. B. Batz, in Semiconductors and Semimetals, ed. Willardson and Beer, (Academic, New York, 1972), p. 315.

8. B.O. Seraphin, in Semiconductors and Semimetals, ed. Willardson and Beer, (Academic, New York, 1972), p. 1.

9. W.L. Smith, S. Hahn, and M. Arst, in Proc. Fifth Intl. Symp. of Silicon Mat. Sci. and Tech. Semiconductor Silicon 1986, eds. Huff, Abe, Kolbesen, (Electrochemical Society, Pennington, NJ, 1986), p. 206.

10. P. Geraghty and W.L. Smith, Mat. Res. Soc. Symp. Proc. 68, 387 (1986).

Coating Thermal Transport Properties Measurement Using Thermal Diffusion Wave Interferometry

Randall T. Swimm
Center for Laser Studies
University of Southern California
Los Angeles, CA 90089-1112

Recently there has been an upsurge of interest in measuring the thermal transport properties of optical coating materials in thin-film format in order to determine by what amount, if any, the coating properties differ from the bulk properties. The motivation for this interest is the possibility that thermal properties may be as important as optical properties in influencing the laser-induced damage threshold.

The present work is an effort to measure the thermal conductivity and thermal diffusivity of several dielectric coating materials grown by various coating deposition techniques, under various growth conditions. In addition, the determination of the thermal properties of thin metal coatings is also required because of the special sample configuration being used. Finally, the influence of the coating interfaces upon the thermal properties measurement must be determined.

The experimental approach being used is that of thermal diffusion wave interferometry. This method was employed in a feasibility study published by Swimm[1], and the present implementation of that technique is based on a different photothermal detection scheme designed to allow an improvement of the system figure of merit by a factor of 40. (The figure of merit is the maximum permissible coating critical frequency, defined as the coating thermal diffusivity divided by the square of the coating thickness. This is the frequency above which thermal diffusion wave interference effects are essentially absent.)

The sample consists of a thin metal overlayer deposited on the dielectric coating under study, which is deposited on a substrate. The purpose of the metal overlayer is twofold. It forces the boundary conditions into an asymptotic limit that allows simplified theoretical analysis. This occurs because the optical depth in the metal is less than all other characteristic lengths. Secondly, the metal coating acts as a thermometer, as will be explained shortly. Operation is best understood in two stages: the generation of a thermal diffusion wave, and the detection of the resultant surface temperature variation.

The thermal diffusion wave is produced by an intensity-modulated argon-ion laser beam focused onto the metal coating. The spot size is chosen large enough to permit a one-dimensional approximation to the solution to the heat diffusion equation to be applied. The thermal diffusion wave

probes the coating, and is reflected at the coating/substrate interface if there is a discontinuity in the thermal effusivity (defined as the thermal conductivity divided by the square root of the thermal diffusivity). The sample acts as a thermal diffusion wave Fabry-Perot interferometer, where instead of the usual bright or dark spot at the center of the interference pattern, there is a hot or cold spot at the sample surface.

The temperature of the surface is monitored by means of a HeNe laser beam, using the fact that the metal coating reflectivity is temperature dependent[2]. Thus, the coating temperature modulation induces an intensity modulation on the probe beam. Synchronous detection provides adequate sensitivity. Signal strength of several microvolts are seen using 100 mW of pump power, at 1 kHz modulation frequency, with a 140 μm pump beam diameter (@ $1/e^2$).

The phase shift between the pump beam and probe beam modulation as a function of the modulation frequency constitutes the desired raw data. This data may be analyzed by adjusting two parameters in the theoretical model (the dielectric coating thermal conductivity and thermal diffusivity) provided that all layer thicknesses are known, and the metal coating thermal properties have been previously characterized by identical methods. Analysis methods are a generalization of those published by Swimm[1], taking account of the multiple-layer structure of the sample.

The present status of the research is that the measurement system has been assembled, and initial system calibration is in progress at the time of abstract submission. Progress achieved by the time of the conference will be reported at that time.

1 R.T. Swimm, Appl. Phys. Lett. 42,955(1983)

2 A. Rosencwaig, J. Opsal, W.L. Smith, and D.L. Willenborg, Appl. Phys. Lett. 46,1013(1985)

PHOTOTHERMAL PROBE-BEAM DEFLECTION MEASUREMENT OF MOISTURE ADSORPTION ON A SILICON SURFACE UNDER ATMOSPHERIC CONDITIONS

Holger Schroeder and Andrew C. Tam,

IBM Almaden Research Center, K07-803,

San Jose, CA 95120-6099.

Although there is much work done on thermal desorption of molecules on a solid surface /1/, most previous work was performed in vacuum or low-pressure conditions and utilized direct particle detectors (e.g. mass spectrometer). The present work examines photo-thermal desorption from a surface in atmospheric conditions utilizing a probe-beam deflection /2/ technique. This is demonstrated for an important case of adsorbed water on a silicon wafer with normal surface oxide.

The experimental arrangement is shown in Fig. 1 /2/. A nitrogen laser pulse, of pulse duration 8 nsec and pulse energy adjustable (by attenuation) up to 1 mJ, is directed onto a polished Si surface situated in a glass chamber. A gas, e.g. dry nitrogen, or nitrogen with high relative humidity at room temperature is passed into the chamber to produce a "dry" silicon surface, or a silicon surface with adsorbed water molecules respectivley. A probe beam that is focussed vertically above the pulsed laser spot is used to detect the shape of the pressure pulse produced at the Si surface. The separation between the probe beam and the Si surface is small (typically 1 mm). The observed probe-beam deflection signal is basically proportional to the spatial derivative of the pressure pulse produced at the Si surface and arriving at the probe beam location /2/.

The observed deflection signal for the cases of a Si surface that has been in a dry nitrogen atmosphere and in a moist nitrogen atmosphere (with 20 Torr water partial pressure) for more than 1 second are shown in Figs. 2 (a) and (b) respectively. We see that the signal for the "dry" case is simple and bipolar; since this is a derivative of the pressure pulse, which should thus be simply a compression pulse due to the "thermal piston" produced by photo-thermal heating of the nitrogen near the Si surface by the pulsed laser. However, the signal for the "moist" case in Fig. 2 (b) is more complicated, broader, and much larger in amplitude; this derivative signal suggests that the pressure pulse produced at the Si surface is composed of three components: (1) "thermal piston of the nitrogen gas adjacent to the Si

surface, (2) desorption of the water molecules originally on the Si surface, and (3) re-adsorption of water molecules onto the Si surface after the pulsed heating is dissipated. It is the re-adsorption of water molecules that is expected to cause the delayed positive peak in Fig. 2(b), whose magnitude is a measure of amount of adsorbed molecules, and whose delay from the earlier positive peak is a measure of the "re-adsorption time" of water molecules onto the Si surface in atmospheric conditions.

Fig. 3 shows the magnitude of the observed first peak in the deflection signal for the "dry" Si surface, and of the later peak for the "moist" Si surface for various pulsed laser energy ranging from 0.01 to 0.1 mJ. We found that in the "dry" case, the signal magnitude is linear to the laser energy, and the signal shape is constant in this photo-thermal heating range showing that the "thermal piston" effect is linear to the pulsed heating over this range. However, in the "moist" case, the delayed positive peak does not show up until beyond a certain "threshold" laser power, corresponding to the threshold energy needed for desorbing the surface water molecules. Similar effects are observed if nitrogen is replaced by argon or freon.

The magnitude of the delayed deflection signal peak in Fig. 2(b) corresponds to a beam deflection of about 1.5 E(-5) radian; using ray optics and the refractive index of nitrogen and water, we estimate that the delayed peak corresponds to the adsorption of approximately a monolayer of water molecules on the Si surface. The delayed time interval between the two peaks suggests an "adsorption time" of several hundred nsec.

In summary, we have made a first demonstration of probe-beam deflection measurement of adsorbed water molecules on a Si surface in one atmosphere of nitrogen mixed with 20 Torr of water vapor. Tne desorption of water molecules by pulsed photo-thermal heating produced a characteristic delayed peak in the signal, which can be used to estimate the amount of desorbed molecules and the re-adsorption time. The behavior is observed to be very similar when the nitrogen atmosphere is replaced by oxygen, argon, helium, or freon gases at one atmosphere.

This work is supported in part by the Office of Naval Research.

/1/ T. J. Chuang, J. Va. Sci. Technol. Vol B3, 1408 (1985).

/2/ A. C. Tam and W. P. Leung, Phys. Rev. Lett., Vol. 53, 560 (1984).

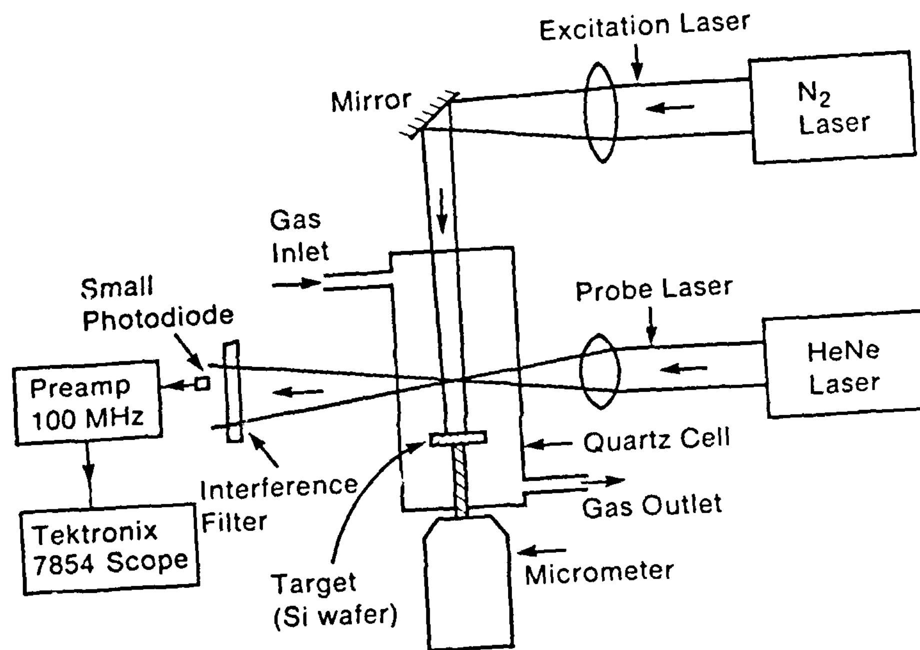

Fig. 1

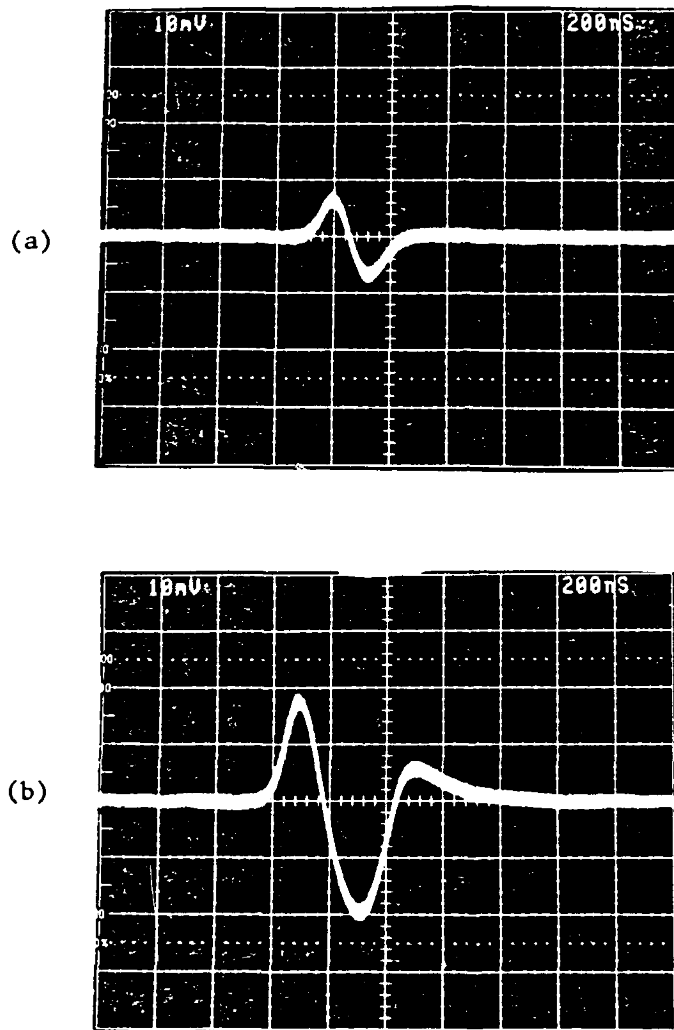

Fig. 2

Observed probe-beam deflection signal for photothermal heating of Si exposed to dry nitrogen in (a), and to nitrogen mixed with 20 Torr of water vapor in (b) in standard temperature and pressure.

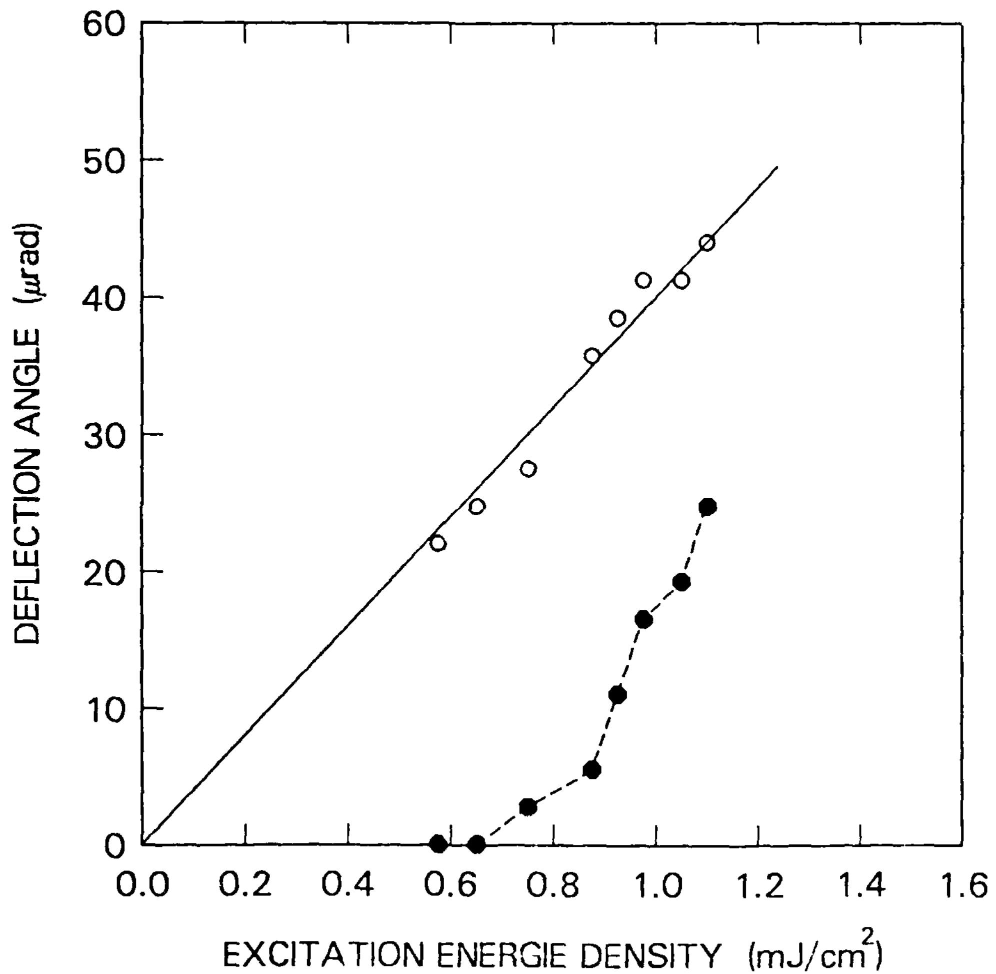

Fig. 3

Magnitude of the deflection signal for the "dry" Si surface (open circle), and the magnitude of the delayed peak in the deflection signal for the "moist" Si surface (closed circle) for various excitation pulse energy.

MATCHED SAMPLE DIFFERENTIAL LASER CALORIMETRY

M. Bass, R. T. Swimm and M. E. Innocenzi
Center for Laser Studies
and
Electrical Engineering - Electrophysics
University of Southern California
Los Angeles, CA 90089-0271

EXTENDED ABSTRACT

Thermocouple laser calorimetry was developed to allow absolute measurement of very small optical absorptions in materials to be used for high power laser optics. The technique involves sending a beam of light through the sample to be studied and, by means of an attached temperature sensor, measuring its change in temperature due to light energy absorption. The temperature change is measured relative to a reference object which is not exposed to the light. Sensitivities to absorptions as small as 10^{-5} cm^{-1} are possible. Photoacoustic detection of the absorbed energy allows relative measurements of absorption and when calibrated against thermocouple measurements yeilds similar absolute sensitivities.

Differential absorption measurements are common in commercial spectrophotometry and have been described in certain photoacoustic studies. By studying the sample relative to a reference sample it is possible to balance out undesired effects and enable measurement of the desired quantity. In the present work we describe the adoption of a new differential technique to thermocouple laser calorimetry.

When performing standard laser calorimetry measurements with either thermocouple or photoacoustic sensing there are three crucial sources of additional signals that require attention. They are, surface absorption, direct scattering of light onto the sensor and temperature drifts between the sample and the reference due to different thermal environments. By using properly shaped, oriented and located matched samples as both the object of study and the reference it is possible to balance out all three of these problems.

Two samples , in the form of prisms (see Fig. 1) with the laser beam entering and exiting at Brewster's angle, are oriented so that the beam traverses different lengths in each sample. One thermocouple of a differential pair is attached to each sample in the same position along the sample's base or on one of its trianglular sides. If the entrance and exit surfaces in both samples are identically polished any heating of the samples due to surface absorption is exactly balanced. The choice of Brewster's angle for the orientation of these surfaces also assures a minimum of reflection losses at the surfaces and, except for differences in absorption due to the different optical paths in the samples. assures that both samples see nearly the same laser power.

Scattering of light onto the temperature sensors is dominated by surface imperfections. However, this is also balanced using the matched samples. Very small scattering due to bulk imperfections can not be balanced completely because of the different path lengths within the samples.

Both samples are located close to each other and mounted identically inside the calorimeter so that they are both in the same thermal environment. This eliminates errors due to drift in the sample or reference temperature unrelated to light energy absorption.

Initial experiments using this technique are reported. Comments are made concerning its applicability to absolute absorption measurement and to the determination of trace contaminant concentrations in solids and liquids.

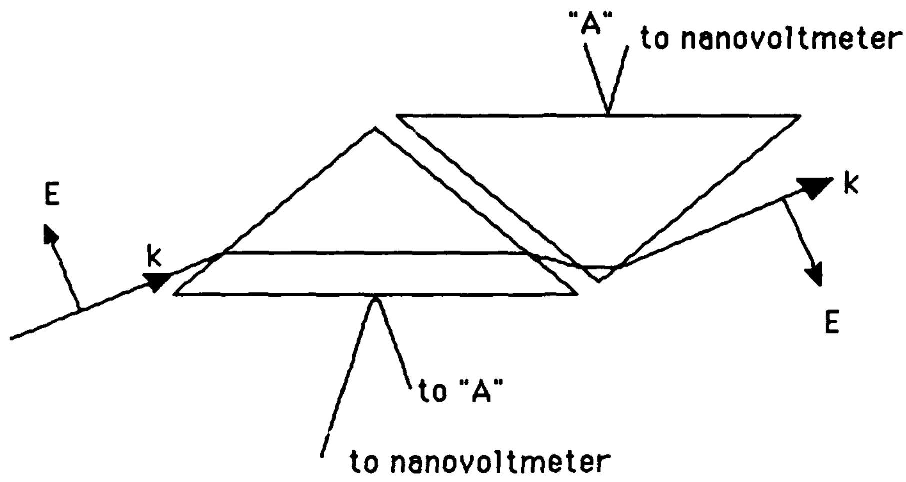

Figure 1. Schematic diagram of the configuration of matched sample differential thermocouple laser calorimetry.

THURSDAY, FEBRUARY 12, 1987

BALLROOM A
10:15 A.M.–11:15 A.M.

ThB1–3

DIAGNOSTICS OF LASER PROCESSING: 1

J. Figuera, Los Alamos National Laboratory,
Presider

In-Situ Raman Microprobe Analysis of Direct Laser Writing

Irving P. Herman
Department of Applied Physics
Columbia University
New York, N.Y. 10027

Summary

Raman scattering is a versatile, non-destructive diagnostic of semiconductors and other materials, which can be used either in-situ after processing has occurred or, in many circumstances, in real-time during processing. By proper selection of lasers and optical design, Raman microprobe methods may be used to investigate sample stoichiometry, doping, crystallinity, stress, and temperature with micron or sub-micron lateral and depth resolution. The use of Raman microprobe techniques to analyze microstructures made by direct laser writing and to analyze microstructures heated by localized laser irradiation is described here.

Polysilicon microstructures can be deposited on absorbing substrates by localized heating induced by a laser focused on the substrate in the presence of silane[1]. With appropriate lateral motion of the laser or the substrate, arbitrary microstructure configurations can be written using this method. Raman scattering has been used to monitor this example of direct laser writing in real

time. In these experiments[1], 5145 Å argon-ion laser radiation was focused on the chosen substrate to induce the surface pyrolytic reaction and also to serve simultaneously as a source of photons for Raman scattering. In addition to these real-time measurements, these same polysilicon microstructures were then re-examined in-situ after deposition, with no reactive gas present. Since the Stokes shift of Si decreases with increasing temperature (520 cm^{-1} at 300 K) while the width of the scattered line increases with increasing temperature (3.4 cm^{-1} at 300 K), the Raman spectra of these inhomogeneously laser-heated microstructures provide information regarding microstructure temperature profile, which also depends on substrate thermal conductivity[1,2]. Stress information is also available from these measurements. Comparison of the real-time and post-processing data of laser-written polysilicon, suggests that during direct laser writing the silicon reaction front is at temperatures near melting.

Other demonstrations of Raman microprobe analysis in direct laser writing have illustrated the ability to determine material composition in-situ. For example, in one preliminary study the level of p-type doping in boron-doped polysilicon deposited by direct laser writing employing $B_2H_6/SiH_4/Si_2H_6$ reactant mixtures was analyzed using these techniques [2]. In another experiment[3], Ge-Si alloy microstructures were formed by pyrolytic, direct laser writing using 5145 Å argon-ion laser radiation focused to about 2 microns, in either of two ways: by co-deposition from GeH_4/SiH_4 mixtures on substrates that absorb visible radiation or by Si deposition from SiH_4 on locally,

laser-melted Ge substrates. The relative strengths and frequencies of the characteristic three-peak Raman spectrum of Ge-Si alloys, consisting of peaks near 300, 400, and 500 cm^{-1} due to Ge-Ge, Ge-Si, and Si-Si local modes, respectively, were used to determine deposit stoichiometry in-situ[3]. Furthermore, using Raman microprobe analysis these codeposited Ge-Si alloys were observed to be either polycrystalline or amorphous depending on the substrate characteristics.

The use of these techniques to determine precisely the stresses of microstructures[4] and grain boundary locations in polycrystalline materials[5] prepared by direct laser writing represents a straightforward extension of the procedures employed in low-laser power Raman analysis of silicon thin films prepared by optical lithography and other means[4,5].

Submicron lateral resolution is easily obtainable in Raman microprobe analysis by using visible or ultraviolet probe lasers and large numerical aperture focusing optics. Proper choice of laser wavelength and substrate temperature can alter the effective depth of the Raman probe, which is ≈ ½ the absorption depth. For most semiconductors, sub-micron and even sub-1000 Å surface probe depths are easily achievable.

The versatility of the techniques described here for real-time Raman diagnostics of direct laser writing can easily be expanded by use of a second laser in either of two ways. In one variation the second probe laser is used to trail the reaction-inducing laser during a scan in order to examine the cooled deposit, while in the other mode it is used to probe regimes near the scanning reaction zone by

choosing the probe laser at a wavelength different from that of the heating laser.

Analogous photoluminescence techniques can be used to probe the properties of direct-band gap semiconductors during laser modification of surfaces. Furthermore, these optical diagnostic procedures can be applied to large-area laser processing, photolytic (non-thermal) laser modification, and to conventional thin film processes, as well as to the pyrolytic direct laser writing procedures described here.

(1) F. Magnotta and I. P. Herman, Appl. Phys. Lett. 48, 195 (1986).

(2) I. P. Herman, F. Magnotta, and D. E. Kotecki, J. Vac. Sci. Technol. A4, 659 (1986).

(3) I. P. Herman and F. Magnotta, submitted for publication.

(4) For example, see S. R. J. Brueck, B-Y. Tsaur, J. C. C. Fan, D. V. Murphy, T. F. Deutsch, and D. J. Silversmith, Appl. Phys. Lett. 40, 895 (1982).

(5) For example, see J. B. Hopkins, L. A. Farrow, and G. J. Fisanik, Appl. Phys. Lett. 44, 535 (1984).

PHOTODARKENING IN insitu TEXTURED PbTe FILMS – A NOVEL TECHNIQUE FOR HIGH CONTRAST OPTICAL STORAGE IN POLYCRYSTALLINE THIN FILMS

L. KAMESWARA RAO
Instrumentation and Services Unit
Indian Institute of Science, Bangalore, India

A. SELVARAJAN
Department of Electrical Communication Engineering
Indian Institute of Science, Bangalore, India

Introduction

Recent studies (1,2) have shown that textured films are ideally suited for optical storage as they exhibit appreciable optical contrast upon laser irradiation. Craighead et al (1) demonstrated that relatively thick films of various materials exhibit good reflectance contrast due to a mechanism of columnar collapse, when the films are prepared by sputter-etch technique. Kameswara Rao et al (2) observed that thin films of Ge, prepared by oblique angle deposition technique, exhibit good transmittance contrast due to chemical modification of the irradiated region to a selective oxide phase. It thus appears that the origin as well as the nature of the optical contrast in textured films critically vary with method of preparation as well as the thickness of the film. In the present study we report the observation of optical contrast of thin polycrystalline films of PbTe, via darkening of irradiated region. The observed darkening is found to be similar to the photodarkening widely known in amorphous materials.

Experimental Observations and Results

Thin films of PbTe of thickness 3000 Å were deposited on clean microscopic glass slides in a vacuum of 10^{-6} Torr at 80° angle of deposition. A pulsed free running Nd:YAG laser with a pulse width of 300 micro-seconds is used for irradiating the films. The films showed darkening effects at nearly 7 KW/cm^2 power density, giving rise to good optical contrast via reduced transmittance in the irradiated region. Fig.1 shows the transmission optical micrograph of the image of a 200 mesh TEM grid pattern on a 80° deposited PbTe film, immediately after irradiation. Fig.2 and Fig.3 show the TEM micrographs of the sample, both before and after the irradiation respectively. The observation of the associated electron

diffraction patterns showed characteristic ring structures indicating that the films are polycrystalline, both before and after irradiation. The micrographs clearly indicate appreciable microstructural reordering, upon irradiation. The films have been subjected to XPS studies to probe into the chemical modifications upon irradiation and their contribution for the darkening. The films are found to compose of PbTe, PbO and TeO_2. It is found that at the irradiation level where darkening is found, no change has been observed in the relative percentage of the above species. This indicates that chemical reactions are not responsible for the observed darkening.

The transmittance characteristics of the film both before and after irradiation are recorded using a double beam spectrophotometer. A 15% relative transmittance difference between irradiated and unirradiated regions is measured, which can easily be measured by conventional techniques. A visual observation of the transmittance characteristics both before and after irradiation indicate that there is a shift in the absorption edge towards the longer wavelength. This indicates that the observed darkening is similar to the photodarkening phenomena widely known in the amorphous materials. However there is a small difference; the darkening in the present study can not be reversed by heat treatment, unlike in amorphous materials. The specular reflectance of the film as well as the transmittance variation of the film for polarised light (He-Ne laser output) as a function of angle of incidence, clearly indicated that the overall textural features of the film still remain unaltered even after irradiation. This suggests that the columnar collapse mechanism originally suggested by Craighead et al can not explain the observed darkening, in the present case. Based on the above observations, it is proposed that the observed darkening in the insitu textured films of PbTe is mainly due to microstructural topological reordering of atoms in the film, wherein the overall surface features remain nearly unaltered. The above observation is expected to broaden the scope of the polycrystalline materials in thin film form as well as the range of useful materials for optical storage for read/write applications.

References

1. H.G. Craighead and R.E. Howard. Appl. Phys. Lett. 39, 532 (1981).
2. L. Kameswara Rao, K. Solomon Harshavardhan, A. Selvarajan and M.S. Hegde. (To appear – Appl. Phys. Lett. Sept. 1986).

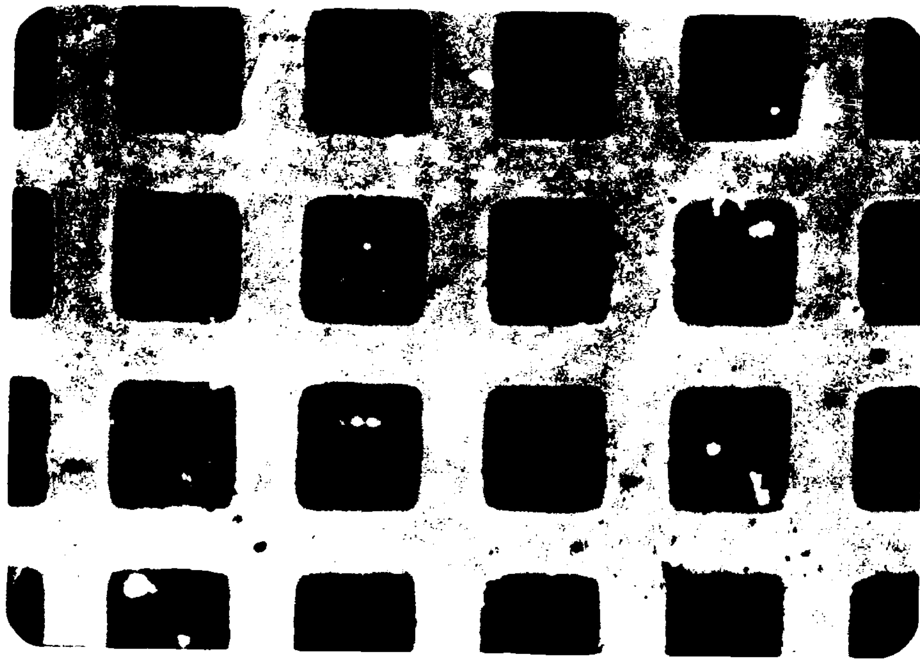

Fig. 1

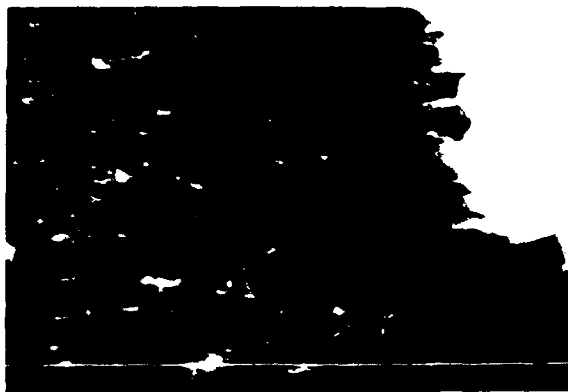

Fig. 2

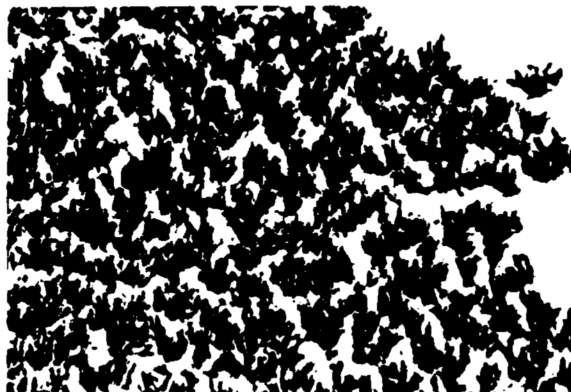

Fig. 3

ThB3-1

Characterization of Optically Induced Periodic Structures on Semiconductor Surfaces

Dragan V. Podlesnik
Microelectronics Sciences Laboratories and Center for Telecommunications Research, Columbia University
New York, New York 10027-6699

Increasing applications are being found for laser and optical techniques in the fabrication of semiconductor devices and in the diagnostics of processing steps such as etching or metal deposition. For example, by using two interfering laser beams to initiate localized chemical reactions, spatially periodic structures can be produced on semiconductor surfaces. Practically, such structures are of interest because of the potential for utility in a variety of electrooptical and electronic applications.[1] An important aspect of this processing is that the structure growth can be monitored in real time by observing the diffraction of the writing beams, thus allowing a precise control over the feature depth. In addition, because the structures can have a high spatial frequency, the process of their fabrication becomes a method of studying the wavelength-scale physical processes which influence the structure growth. These processes may involve, for example, the diffusion of photoexcited species or the magnification of the optical fields at the illuminated surfaces.

In this talk, the above aspects of laser processing will be illustrated by describing two experiments in this area: light-controlled etching of compound semiconductors and photodeposition of metals from surface layers. In both cases high-resolution diffraction gratings have been fabricated and basic physical phenomena observed. Finally, spontaneous ripple formation on semiconductor surfaces via photogeneration of electron-hole pairs will be discussed.

In most of the laser chemical processing of materials, the temporal coherence of the laser source has not played an important role in the processing results or physics. For example, in many photon-assisted processes, the monochromatic nature of the laser is important only in so far as it is necessary to drive a specific chemical channel. In this talk a laser chemical processing technique which requires that the light source have a high degree of temporal coherence will be described. In this technique, two parts of a laser beam are interfered to produce a coherent light pattern across a substrate surface.

A study of laser holographic processing provides information on both the fabrication of device structures for specific near-term applications and the basic physical phenomena occurring in interfacial chemical reactions. In particular, most of the initial work on holographic semiconductor etching has emphasized high-resolution diffraction gratings. These gratings are potentially important for single-wavelength distributed feedback lasers, for optical

couplers, and as wavelength filters for a variety of passive electrooptical devices. For example, for the fabrication of distributed feedback lasers, optical gratings with periods between 100 and 300 nm are required. Currently, gratings are typically produced by holographic or electron beam exposure of a photoresist mask followed by ion milling or wet chemical etching of the semiconductor surface. More recently, several direct writing techniques have been investigated. Light-sensitive chemical or electrochemical etching of semiconductors in conjunction with coherent laser radiation provides a simple method for recording the gratings.[2,3] In general, light from a laser source is split into two nearly equal intensity beams which then intersect at the sample surface. The resulting interference fringe pattern creates a sinusoidal spatial intensity variation on the sample surface. Selective etching results since photogenerated minority carriers in the semiconductor accelerate or induce the etching.

A schematic of the laser interferometer arrangement used to produce the gratings is shown in Fig. 1(a). A laser beam passes through a spatial filter and a wide-beam collimator before impinging on the right-angle corner. The corner, on which a mirror and the semiconductor sample are mounted, is inside an optical cell containing an etching solution. An interference pattern is produced by the superposition of the direct and the reflected beams (Lloyd's mirror arrangement) inside the solution, which has an index of refraction, n, greater than one (approximately 1.33). A wide range of grating spacings can be obtained by simple rotation of the right-angle corner. The grating period, s, is then given by

$$s = \lambda/(2n \sin\theta_i) \quad (1)$$

where λ is the free-space wavelength of incident light and θ_i is the incident angle on the sample surface. The incident, s-polarized laser beams had an approximately flat intensity distribution across the sample.

An important feature of the direct etching process is that the parameters of the gratings can be monitored during fabrication. The processing laser beam, reflected from the etched corrugation, produces a diffraction pattern that characterizes the depth and the shape of the grating profile at any given moment. The general form of the grating equation is

$$\sin\theta_r - \sin\theta_i = m\,(\lambda/sn) \quad (2)$$

where m is the order of diffraction, n is the refractive index of the outer medium, s the groove spacing, θ_i the angle of incidence, and θ_r the angle of diffraction (θ_i and θ_r will have the same sign on the same side of the grating normal.)

In order to perform in situ monitoring, a beam splitter is periodically inserted in the main beam to reflect the diffracted minus first order beam, as shown in Fig. 1(b). In this special case where $\theta_i = -\theta_r$, the grating is said to

be positioned in "autocollimation" (Littrow) and the grating equation, Eq. (2), is reduced to Eq. (1).

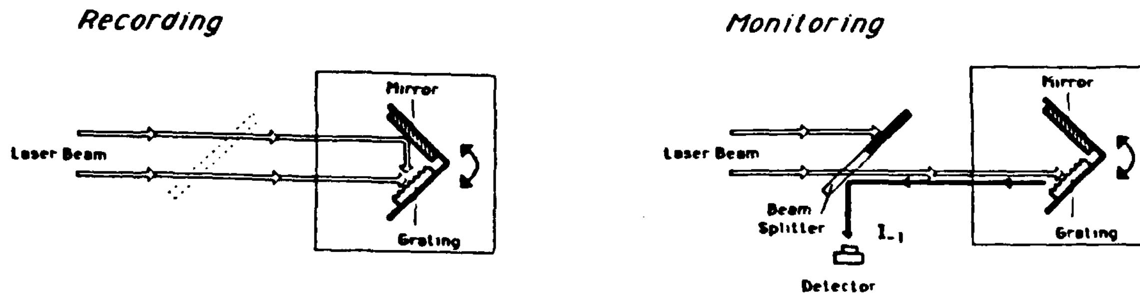

Figure 1. Photochemical recording and monitoring of diffraction gratings etched in semiconductors.

The measured diffracted light intensity can be related to the groove depth and profile. Theoretical treatments of a simple sinusoidal grating have shown that the ratio of the minus first order diffracted and the initially reflected I_0 (taken as 100%) beams is given by[4]

$$I_{-1}/I_0 = J_1^2[2\pi nd\ (1+\cos\theta_{-1})/\ \lambda] \qquad (3)$$

where d is the depth of the grating grooves. For shallow gratings, the grating growth rate can be determined to within an accuracy better then 10% from the position of the first maximum of the Bessel function. Detailed groove profiles were measured with a scanning electron microscope (SEM) and compared with the optical measurements.

In separate experiments, arrays of deep submicrometer size grooves were etched in GaAs crystals with a projected ultraviolet light pattern. Two writing laser beams were symetrically incident onto the sample surface where they intersect at a small angle. The interference fringe pattern produced by the intersecting beams results in a sinusoidal variation in the irradince at the sample surface with the fringe spacing of ~ 1.4 µm. In contrast to the results described previously, the long-exposure etching, typically 30 to 40 minutes, results in deep, vertical features. A scanning electron micrograph of the cross-sectional profile of 20-µm-deep grooves is shown in Fig. 2.

Figure 2. SEM micrographs of the cross-sectional profile of 20-μ-deep grooves etched in GaAs.

The entrance edge of the etched structure is tapered for a short distance into the sample, i.e. < 1 μm, corresponding to the incident, sinusoidal laser intensity pattern. However, for deeper etching, the grooves assume a characteristic tubular shape as the feature sidewalls become vertical. The etched width, ~0.5 μm, remains then constant, independent of the etched depth. The etched structure acts now as a self-propagating, hollow waveguide which confines and efficiently transmits the processing laser light.

Acknowledgments

I would like to acknowledge the contributions by Heinz Gilgen, Alan Willner, Ray Beach, and Richard Osgood. This work was supported in part by the National Science Foundation, the Defense Advanced Research Projects Agency and the Air Force Office of Scientific Research.

References

1. A. Yariv and Nakamura, IEEE J.Quantum Electron. QE-13, 233 (1977).
2. R.M. Osgood, A. Sanchez-Rubio, D.J. Ehrlich, and V. Daneu, Appl. Phys. Lett. 40, 391 (1982).
3. R.M. Lum, A.M. Glass, F.W. Ostermayer, Jr., P.A. Kohl, A.A. Ballman, and R.A. Logan, J. Appl. Phys. 57, 39 (1985).
4. I. Pockrand and H. Roethen, Opt. Commun. 18, 395 (1976).

THURSDAY, FEBRUARY 12, 1987

BALLROOM A
1:30 P.M.–2:30 P.M.

ThC1–2

LASER-DRIVEN MASS SPECTROSCOPY

R. Keller, Los Alamos National Laboratory, *Presider*

LASER MICROPROBE MASS SPECTROMETRY AND ITS RELATIONSHIP TO OTHER MICROANALYTICAL TECHNIQUES

by

Charles A. Evans, Jr.

CHARLES EVANS & ASSOCIATES
301 Chesapeake Drive
Redwood City, California 94063

There are a variety of techniques employed for the microanalysis of materials. The majority of these techniques employ focused ions or electron beams to probe the materials. In recent years, a technique called Laser Microprobe Mass Spectrometry has been developed to provide a unique and complementary characterization capability. This paper will deal with the basic phenomena involved, instrumentation and illustrations of the technique's utility with a variety of applications.

Resonance Ionization Mass Spectrometry Using Ion-Beam Sampling

D.E. Goeringer and W.H. Christie
Analytical Chemistry Division
P.O. Box Y; Bldg. 9735
Oak Ridge National Laboratory
Oak Ridge, TN 37831

1. Introduction

Sputter atomization/resonance ionization mass spectrometry (SA/RIMS) is a highly sensitive technique for materials analysis which combines ion beam sputtering, resonance ionization, and mass spectrometry. A pulsed beam of high-energy primary ions bombards the sample producing a plume of neutral atoms. The cloud of sputtered neutrals is intersected and ionized by a synchronized, pulsed laser beam tuned to a resonant transition for specific sample atoms. Laser-generated ions are then extracted into a mass spectrometer for mass analysis. Ion beam sputtering allows the sampling process to be highly controlled by varying the energy, current density, and composition of the primary beam; the pulsed nature of the beam results in efficient sample utilization. Use of a micro-focused beam permits imaging of small areas and particles. The pulsed dye laser generates the high optical power necessary to efficiently ionize the sputtered atoms. Mass analysis of the laser-generated ions provides the capability for isotope ratio measurements.

2. Experimental

The instrument used in this work was a modified ion microprobe mass analyzer (IMMA) manufactured by Applied Research Laboratories (Sunland, CA) and is based on the design of Liebl (Liebl 1967). In essence, the instrument is two mass spectrometers. In the primary spectrometer, a beam of ions is generated, mass analyzed, and focused (2 µm diameter) onto the sample of interest. Secondary ions sputtered from the sample are directed into a double-focusing mass spectrometer where mass analysis is accomplished. Modifications to the ion extraction lens system, which allow discrimination against sputtered ions while allowing efficient collection of laser-generated ions have been described in another publication (Donohue et al 1985). The IMMA instrument also has complete sample manipulation and viewing capability.

2.1 Laser Source and Light Optics

The laser system used in this study was a tunable dye laser (Quanta Ray PDL-2) pumped by a pulsed Nd:YAG laser (Quanta Ray DCR-2A). The dye laser was operated in fifth order resulting in a bandwidth of approximately 0.3 cm^{-1} as determined by a 1 cm^{-1} Fabry-Perot etalon. Rhodamine 610 dye used in our experiments gave a useful tuning range from about 582-598 nm. Dye

laser wavelength scans were performed under computer control via a programmable motor controller (Quanta Ray MCI-1). Wavelength calibration was confirmed by recording the optogalvanic spectrum of a Ne-filled U hollow cathode lamp.

2.2 Signal Processing/Control Electronics

The signal from the Daly detector's photomultiplier was simultaneously processed by both analog and digital electronic systems. The analog system consisted of a fast current amplifier and gated integrator (Stanford Research Systems SR250). The signal produced by a packet of ions generated from a single laser shot was integrated by the current amplifier into a single pulse approximately 15 µs wide. This pulse was sampled by a gated integrator triggered by the laser and delayed for the flight time of the ion packet through the mass spectrometer. The resultant DC signal was further processed by the data system. The analog signal from the current amplifier was also used to drive video amplifiers in the standard ARL video display system. The digital system was composed of the standard ARL preamp/discriminator, pre-scaler, and fast pulse counting (30 ns pulse-pair resolution) system. The digital system was mainly used to determine relative signal strengths for SIMS signals.

The primary ion beam was pulsed by applying a ±450V pulse to opposing alignment plates located at the top of the primary lens column. The ion beam gate width and delay were set by gate/delay generators triggered by the laser flashlamp sync pulse.

2.3 Data System

Data acquisition and control for the experiments were performed by a microcomputer system (MDB Micro-11) based on the LSI-11/23-Plus (Digital Equipment Corp.) central processing unit. The system contained an analog-to-digital converter (ADC)/digital-to-analog converter (DAC) interface board; the ADC was used to convert the DC output of the gated integrator, and the DAC was used to control the secondary magnet. Amplified signals from a second DAC were used to position the primary ion beam via the standard primary beam sweep plates. Another direct memory access DAC was used to drive an x-y scope for real-time signal display. A parallel interface was used to control the dye laser motor controller (see above). Spectra could also be sent to a digital plotter (Hewlett-Packard 7475A) for hard copy output.

3. Results and Discussion

Earlier studies in our laboratory demonstrated that Ar^+ sputtering of uranium metal in the presence of residual oxygen produced both SIMS and SA/RIMS spectra rich in UO^+ and UO_2^+ as compared to the atomic ion (Donohue et al 1985). The present study shows that for U metal samples the molecular species are

essentially eliminated if the partial pressure of oxygen and oxygen-containing species (e.g. H_2O) is sufficiently reduced. To accomplish this in our instrument the existing 400 l/s ion pump was replaced with a 1200 l/s cryosorption unit.

3.1 RIMS Sensitivity Improvement for U Metal Samples

For maximum sensitivity in the SIMS analysis of electropositive metals O_2^+ bombardment or oxygen flooding of the sputtering region is commonly used to maximize secondary ion yields. Table 1 presents a comparison of laser-generated U^+ signals using Ar^+ and O_2^+ sputter atomization of U metal with a time normalized SIMS U^+ signal generated by an O_2^+ primary beam on the same sample. The time normalization for the SIMS signal was done by using the gated integrator/ADC electronics and a gate width (6 µs) identical to that for the SA/RIMS signals rather than the pulse counting system. The primary beams were also run in cw mode for these experiments. As expected, a given flux of Ar^+ primary ions was significantly more effective at generating sputtered neutral U atoms from a U metal target than O_2^+ primary ions were.

Table 1

	SA/RIMS		SIMS
Primary Beam (10 nA)	Ar^+	O_2^+	O_2^+
Net Signal (V-s x 10^{-6})	19.3	0.09	0.06
Relative Strength	320	1.5	1.0

3.2 Pulsed Primary Ion Beam Experiments

We have found that for highly oxidizable metal samples such as U that the duration of the SA/RIMS sputter pulse must be long enough to remove adsorbed impurities that accumulate on the sample surface while the primary beam is not on the sample. A set of experiments which demonstrated the effect was performed. The region of the U metal surface being pulse-sputtered was initially sputter-cleaned with a cw Ar^+ beam, then the primary beam was switched to pulsed operation and the detected resonance U^+ signal allowed to stabilize as equilibrium was achieved between arrival rate of chemisorbed species from the vacuum system and Ar^+ from the pulsed sputtering beam. The Ar^+ sputtering beam was then switched to cw mode and the time response of the U^+ signal monitored. The primary beam pulse width was varied from 5 to 150 µs. For all pulse widths there was an immediate increase in laser-generated U^+ signal upon switching to cw mode; in each case the signal was also observed to decay after switching to pulsed mode as the surface was again recovered with chemisorbed impurities. The equilibrium signal after switching to pulsed mode was seen to increase with primary beam pulse width. For the particular Ar^+

current density being used we found that it took a pulse width of 120 µs or longer to provide enough presputtering to restore the maximum neutral uranium population that can be sputtered from the surface under those conditions. Sm is considerably more resistant to oxidation than U. In another experiment the same Ar+ beam current was used to sputter a Sm target, but the beam diameter was increased to 60 µm so that the current density was reduced to about 20% of that used in the U experiment. Even with the lowered current density which should enhance surface coverage effects and with only a 5 µs sputter pulse the fall off in Sm^+ resonant ion signal was much less severe than for U. The results of these experiments reflect the fact that oxide formation on U is considerably faster than on Sm.

3.3 SIMS and SA/RIMS Comparisons

Table 2 compares the SIMS signals determined under similar conditions for U metal, UO_2, and U_3O_8 samples and also compares the SA/RIMS ion signals measured under similar conditions for U and UO_2 samples. No data for SA/RIMS ion formation on the U_3O_8 sample is shown because no laser-generated ion signal was obtained under the conditions used for these comparisons. UO^+ and UO_2^+ signals seen in the SA/RIMS experiments were found to be broadband photoionization effects. The U^+ SA/RIMS signal on the other hand was always sharply tunable with wavelength. The case of U_3O_8 is interesting in that despite the highly oxidized state of the U, it is the U^+ ion that appears in greatest abundance in the SIMS spectra. Viewed in terms of the SA/RIMS results for U_3O_8, it would appear that relatively few neutral U atoms are sputtered from this sample, and for that matter little UO^o and UO_2^o. These experiments also suggest that conventional SIMS offers more sensitivity for the analysis of this material.

Table 2

	SIMS counts/s x 10^3			SA/RIMS V-s x 10^{-6}	
Ion	U metal	UO_2 crystal	U_3O_8	U metal	UO_2 crystal
U^+	93	102	750	17.0	0.39
UO^+	6	575	90	0.21	6.3
UO_2^+	2	895	52	---	0.57
UO_3^+	--	---	0.5	---	---

References

Donohue D L, Christie W H, Goeringer D E and McKown H S 1985 Anal. Chem. 57 pp 1193-1197
Liebl H J 1967 J. Appl. Phys. 38 pp 5277-5283

THURSDAY, FEBRUARY 12, 1987

BALLROOM A
3:00 P.M.–3:45 P.M.

ThD1–2

DIAGNOSTICS OF LASER PROCESSING: 2

K. E. Greenberg, Sandia National Laboratories,
Presider

Laser-induced etching is receiving significant attention, motivated by applications in microelectronics and medicine and by long standing concern about optical damage phenomena. In the present experiments, we emphasize etching with pulsed UV (excimer) lasers in the low fluence, i.e. near threshold, region. Under these conditions etching has been attributed to a variety of phenomena, among them thermally activated vaporization and photochemical bond breaking processes. The present work is aimed at distinguishing between the thermal and electronic processes for several materials. According to the thermal model, one requires a sufficiently high peak temperature that vaporization is the primary source of surface etching.

To distinguish between the above two mechanisms we use laser-induced fluorescence (LIF) to probe species in the etch plume as they expand away from the surface, see Fig. 1. This technique measures particle densities, and it is particularly useful for monitoring the population of translational and rotational/vibrational states; thus LIF provides a "thermometer."

Materials that have been investigated are graphite, sapphire, oxidized aluminum surfaces ($Al{:}O_2$), and polymers. These materials etch are studied with excimer fluences $\lesssim 1$ J/cm^2 so that plasma formation and gas-phase collisions are minimized. Also these materials span a wide range of properties: graphite is metallic-like and can be anticipated to exhibit rapid electronic energy dispersal, while sapphire and polymers should have long-lived electronic (excitation) states. Based on this, graphite is anticipated to etch by a thermal process, i. e. after degradation of the original excitation into heat, whereas the insulators sapphire and polymers may show photochemical etching mechanisms.

A. Graphite: The graphite samples were highly oriented pyrolytic (HOPG) graphite mounted with the c-axis parallel both to the surface normal and to the etch-laser beam. This means that the low thermal conductivity direction is also perpendicular to the surface and the depth heated during a pulse was effectively within $\lesssim$200nm of the surface; such a shallow depth contributes to a high peak temperature. Estimates of the peak surface temperature, $\hat{T}_s$, are obtained by the following approaches. Samples receiving only ~ 0.5 J/cm^2 showed surface morphology which precluded extensive melting; the melt temperature is ~4100K at atmospheric pressure. Second, a temperature estimate of 4000±300K is derived from the rate of material removal. The conclusion is that $\hat{T}_s$ is near 4000K when one monolayer of graphite is removed per excimer pulse.

Figure 2 illustrates a section of the Mulliken bands of C_2 obtained by LIF. This section covers only ~3% of the observable spectrum, as rotational lines out to J=92 have been recorded in both the P and R branches of $v'' = 0$ and 1. Figure 3 shows the LIF signal (corrected for degeneracy) plotted as a function of J(J+1), i.e. the rotational energy. The observation that the data in Fig. 3 fit a straight line means that the energy follows a Boltzmann distribution (with average temperature of ~3800K).

The C_2 signal as a function of velocity has been determined by time-of-flight. The resultant curves fit a Boltzmann distribution with $T_{trans.}$ = 4500K when $<<1$ monolayer is removed per pulse; $T_{trans.}$ doubles when $\gtrsim 1$ monolayer is removed. Although these values are greater than the deduced surface temperature, gas dynamic corrections play an important role in translational motion. As detailed in Ref. 1, laser vaporization is in general *not a simple single step of solid→gas transition.* Instead, it is more like a three-step process in

that vaporization (solid→gas) occurs first into a dense, possibly 50 to 100 μm thick Knudsen layer, and when $\gtrsim 1$ monolayer is removed there are initially some 5 to 20 collisions before the gas gradually expands to infinity. While undergoing these collisions, the $\cos\theta$ dependence of normal vaporization is partially converted into directed motion perpendicular to the solid surface. There is some similarity between this process and the collimation and cooling present in a supersonic expansion from a nozzle.

In conclusion, the results for C_2 kinetic and internal energies are seen to be in good agreement with expectations for a simple thermal evaporation.

B. Al_2O_3: The LIF results for excimer etching of sapphire and $Al:O_2$ have been recently discussed in detail.[2] In order to compare these results to the results for graphite above, we shall summarize them here.

The Al atom density in the etch plume above the target was determined by exciting ground-state atoms at 394.4 nm and observing the fluorescence at 396.1 nm. The AlO molecule densities, as well as the kinetic and internal energies, were measured using $(v')B^2\Sigma^+ \leftrightarrow (v'')X^2\Sigma^+$ electronic transitions. The velocity distributions for Al are significantly broader than is appropriate for a Maxwell-Boltzmann form and there exists marked differences in both the velocity and the kinetic energy between the Al and AlO. These disparities increase rapidly with fluence: the Al energy increased from ~3.8 eV near threshold to ~17 eV at 3.2 J/cm^2. In contrast to this *increase*, the AlO energy started at ~1.2 eV near threshold and monotonically *decreased* with increasing fluence to ~0.3 eV at 3.2 J/cm^2.

Internal energies for AlO are again obtainable from the LIF spectra since a large number of rotational transitions are resolved within the first two vibrational bands (Fig. 4). With the rotational distributions, no deviation from Boltzmann form was observed. Low populations in $v'' \geq 2$ indicate that the AlO left the surface as a diatomic, because AlO formed by recombination in free space has extensive vibrational excitation. The present AlO rotational and vibrational energies are low, i.e. only 200-600K above ambient, and are similar for the two types of aluminum oxide targets.

For Al and AlO, the very high kinetic energies and low internal energies clearly indicate non-thermal behavior. In order for a thermal mechanism to account for the etch rate, peak temperatures of~ 4800K would be required. Such temperatures are much larger that the rotational and vibrational temperatures observed. It is difficult to calculate the temperature rise of bulk Al_2O_3 because of uncertainty about its electronic condition; however, this same limitation does not apply to $Al:O_2$. In this case one can use the bulk constants of Al metal, as a thin (0.3 to 3 nm) layer of oxide changes neither the optical properties at 248 nm nor the thermal properties, and thereby deduce ~500K to result from 1 J/cm.[2] For $Al:O_2$ the surface temperature remains too low for thermal vaporization to account for the etching; and similar energy distributions are obtained for this material and sapphire.

C. Polymers: The LIF technique has also been used to determine energies of the diatomics C_2 and CN ablated from polyimide and C_2 ablated from polymethylmethacrylate. While the investigation is continuing, several conclusions are currently possible. First, the kinetic energies of the diatomics are quite high, being greater than the values found for AlO from sapphire. After including the gas dynamical correction discussed above, one still concludes that the translation energies are >1.3 eV. Note that this value is much greater than the

kinetic energies found for the (thermal) etching of graphite. In the case of polymers, as in the case of graphite, the present excimer etch fluences are too low to produce significant plasma density, so plasma formation is not the source of high kinetic energies.

The establishment of internal energies by LIF is more complicated. The population of the various states is non-Boltzmann, with the high energy states indicating a high (~2500K) "temperature" and the low lying states indicating a lower temperature T~1000K. At this point, we cannot rule out the possibility that gas phase collisions are influencing the populations. There is a profusion of larger polyatomics in the plume and hence collisions are statistically more common than with the other solids. Measurements are underway to find the source of the non-Boltzmann like distributions. It is already clear, however, that interpreting laser ablation of polymers as simply thermal vaporization does not fit the present results.

In summary, laser induced fluorescence provides detailed, reliable information about internal energies (temperatures) of diatomics including AlO, CN and C_2. In particular, laser impact on *graphite* produces C_2 with essentially the *energies* expected for *thermally activated vaporization*. The elevated C_2 kinetic energy is in principle understood on the basis of vaporization occurring as a three-step process, first as a dense collisional medium and only later in a supersonic, then freely expanding state. In contrast, laser impact on Al_2O_3 or polyimide leads to the sputtering of diatomics (AlO, CN, C_2) which have very low rotational energies and, at the same time, kinetic energies so high that they cannot be thermal. This contrast thus permits one to separate thermal from photochemical etching on the basis of diatomic particle energies within the plume while supporting the earlier conclusions about *photochemical* effects with the *insulating materials*.

References

1. Roger Kelly, R. W. Dreyfus and R. E. Walkup, work in progress.
2. R. W. Dreyfus, Roger Kelly and R. E. Walkup, Appl. Phys. Lett., in press.

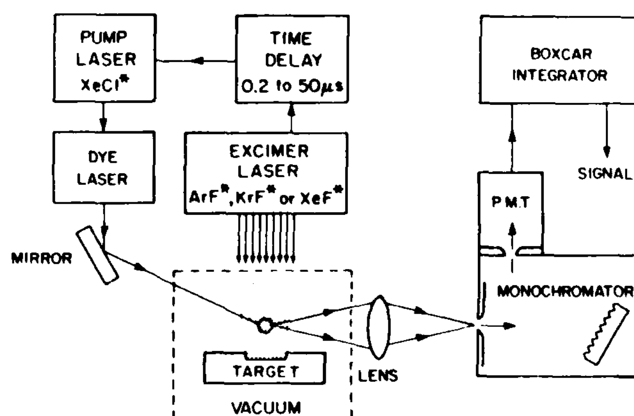

Fig. 1: Schematic of equipment for LIF measurements in the etch plume above excimer etched surfaces. A frequency doubler is inserted after the dye laser for the C_2 Mulliken band measurements.

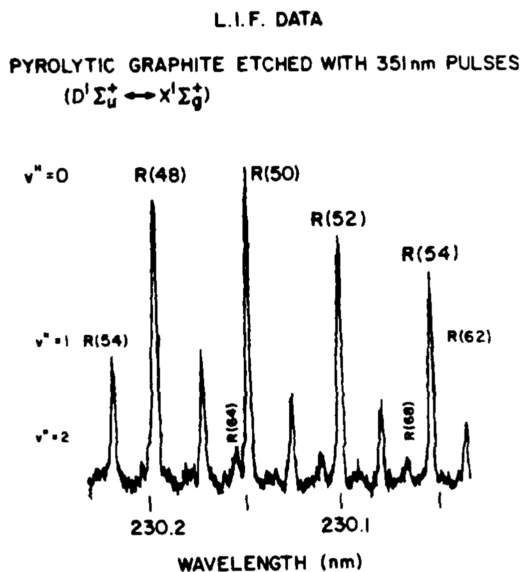

Fig. 2: A section of the LIF spectrum of C_2 diatomics from excimer etched graphite.

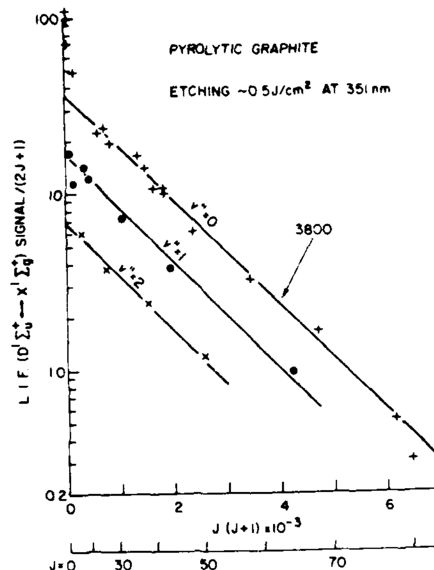

Fig. 3: (Normalized) LIF signal vs. rotational energy for three vibrational bands taken from data such as Fig. 2.

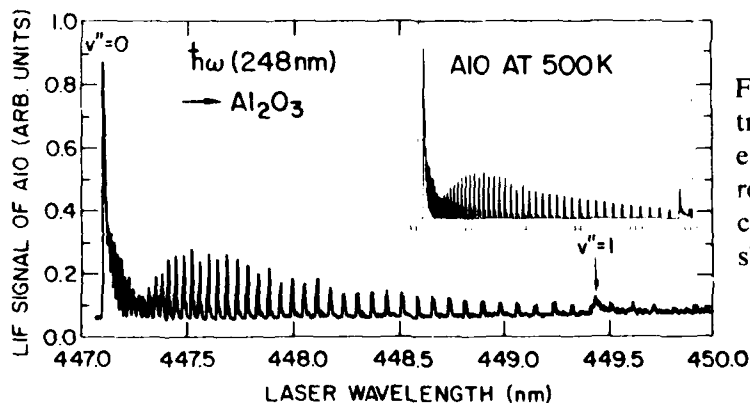

Fig. 4: LIF rotational spectrums of AlO from excimer etched sapphire. Note the reasonable agreement with the calculated 500K spectrum shown in the insert.

Excimer laser photochemistry of Al-alkyls monitored by dye laser mass spectroscopy.

Y. Zhang, M. Stuke
Max-Planck-Institut für biophysikalische Chemie,
Dept. Laserphysik,
D-3400 Göttingen, F. R. Germany

R. Larciprete*, E. Borsella
ENEA, Dept. TIB,
Frascati (Roma), Italy

Metal Organic Chemical Vapor Deposition (MOCVD) is a powerful technique for the generation of well-defined layers of metals and semiconductors [1]. Extending MOCVD by the use of lasers to Laser-MOCVD, selective area growth can be obtained ([2] and references therein). Laser induced deposition of structured aluminum films can be achieved using UV lasers and Al-alkyls *like triisobutylaluminum (TIBA) as gaseous organometallic* precursor [3, 4].

The use of multiphoton ionization for the detection of gallium atoms, formed by visible multiphoton dissociation of trimethylgallium, was demonstrated by Mitchell and Hackett [5].

We studied the UV excimer laser induced photochemistry of the Al-alkyls TIBA, triethylaluminum (TEA) and trimethylaluminum (TMA) using tunable dye laser time-of-flight mass spectroscopy [6, 7, 1].

The experimental setup is shown schematically in Fig. 1. Excimer laser induced neutral photoproducts of the aluminum alkyls (TIBA, TEA, TMA) are detected after a suitable delay (100 ... 500 ns) by the tunable dye laser.

In the following, the results obtained for TIBA and a photolysis wavelength of λ = 248 nm (KrF-Excimer laser) are presented. Major photoproducts are free aluminum atoms Al and aluminum-hydride molecules AlH. This is shown in Fig. 2. The probing dye laser was scanned in the 459 - 428 nm range, the delay after the excimer photolysis laser was set to Δ t= 100 ns in this case. Fig. 2 shows the dye laser reference energy (top trace), the Al^+ signal (middle trace) and the AlH^+ signal (lower trace). The sharp resonances observed in the Al^+ spectrum are well known and due to atomic resonances of the free Al atoms. Fig. 3 shows on an expanded wavelength scale the AlH^+ spectrum. These molecular bands can be assigned to two-photon transitions in the AlH molecules (X-C), and information on the rovibronic internal

*ENEA guest

energy of the AlH photoproducts can be obtained. Bands corresponding to two-photon X-D transitions were also observed. Very similar results were obtained for TEA, whereas in the case of TMA AlH is no major photoproduct at 248 nm. Results for TEA and TMA will be presented, as well as data obtained at other photolysis laser wavelengths. Picosecond UV-laser mass spectra of TMA, TEA and TIBA show in the case of TMA mass peaks, which can be attributed to the TMA dimer, whereas for TEA and TIBA dimer peaks were not identified.

[1] "Metalorganic Vapor Phase Epitaxy 1986", G. B. Stringfellow Ed., North-Holland: Amsterdam 1986
[2] "Laser Chemical Processing of Semiconductor Devices", F. A. Houle, T. F. Deutsch, R. M. Osgood, Eds.; Material Research Society: Pittsburg, PA 1984
[3] J. Y. Tsao, D. J. Ehrlich, Appl. Phys. Lett. 45, 617 (1984)
[4] G. S. Higashi, C. G. Fleming, Appl. Phys. Lett. 48, 1051 (1986)
[5] S. A. Mitchell, P. A. Hackett, Chem. Phys. Lett. 107, 508 (1984)
[6] M. Stuke, Appl. Phys. Lett. 45, 1175 (1984)
[7] R. Larciprete, M. Stuke, J. Phys. Chem. 90, 4568 (1986)

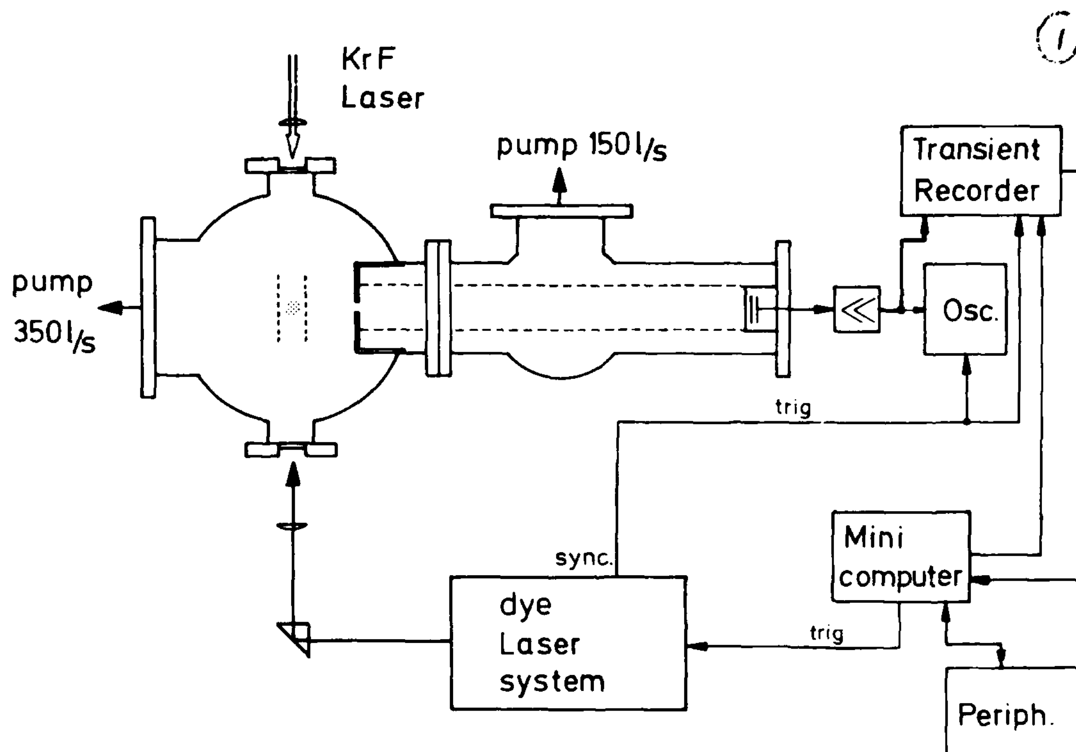

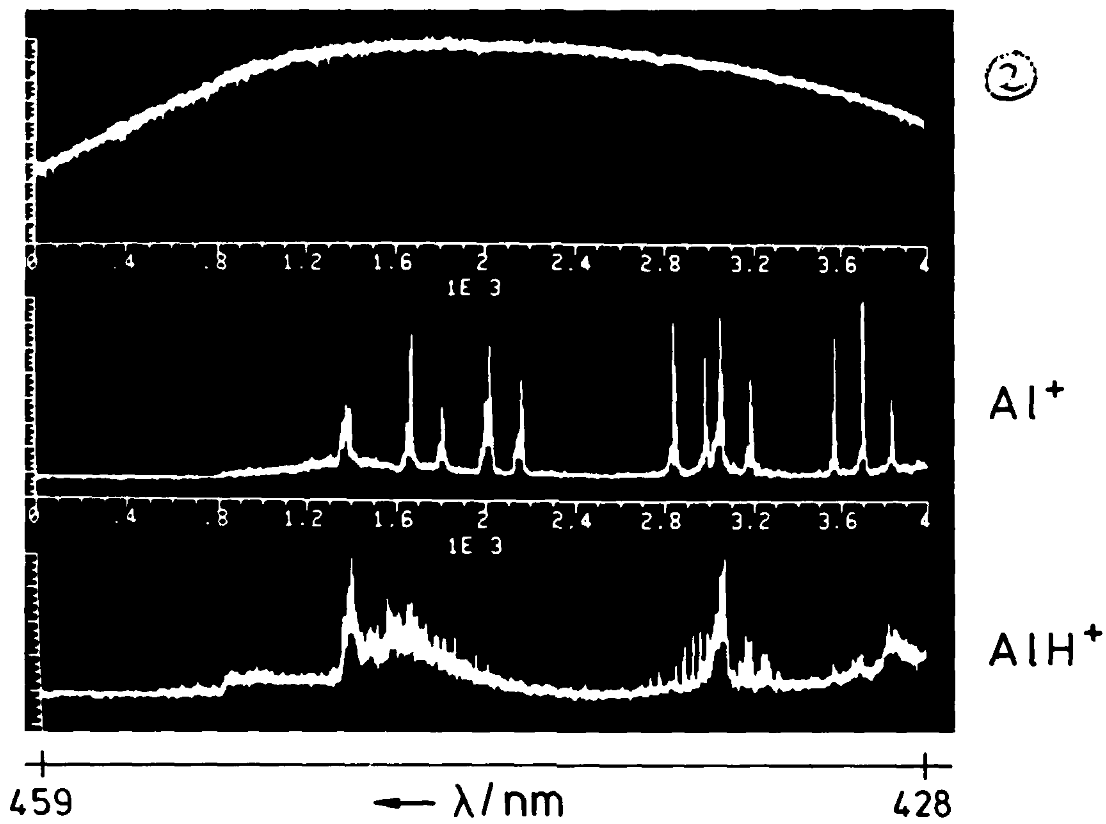

2
0 .4 .8 1.2 1.6 2 2.4 2.8 3.2 3.6 4
1E 3
Al+
0 .4 .8 1.2 1.6 2 2.4 2.8 3.2 3.6 4
1E 3
AlH+
459
← λ/nm
428

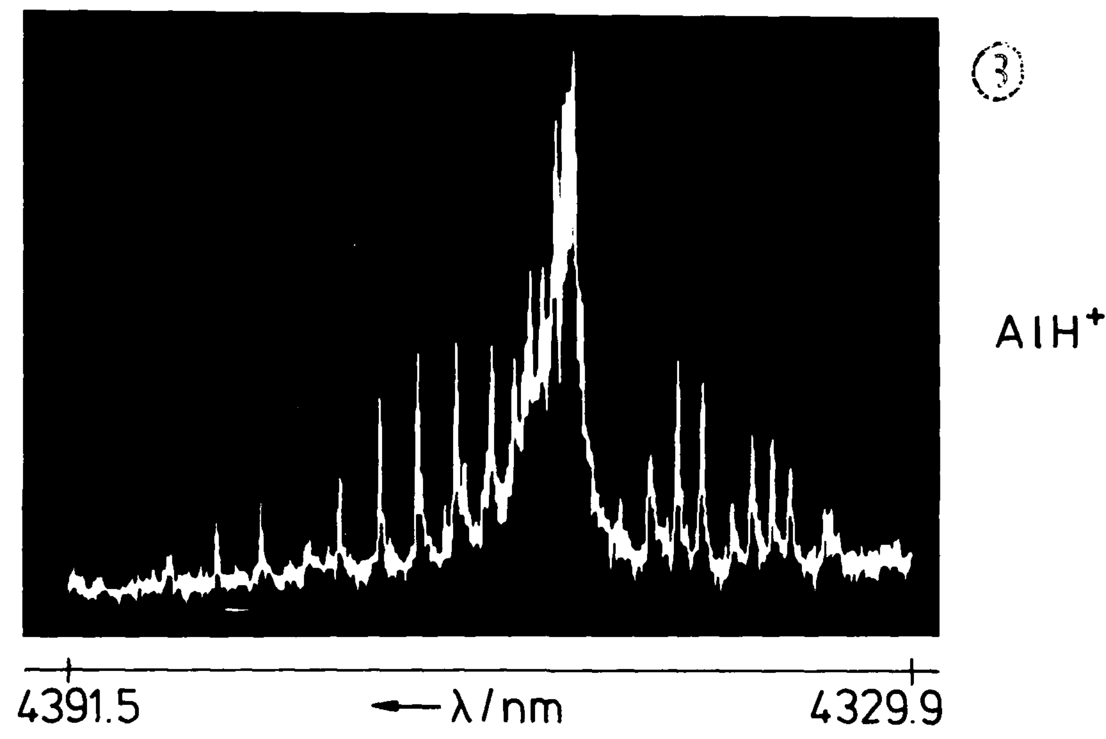

3
AlH+
4391.5
← λ/nm
4329.9

THURSDAY, FEBRUARY 12, 1987

BALLROOM A
3:45 P.M.–4:45 P.M.

ThE1–3

OPTICAL DIAGNOSTICS OF SEMICONDUCTORS-PHOTOLUMINESCENCE

Jean-Claude Diels, University of New Mexico,
Presider

OPTICAL CHARACTERIZATION OF III-V SEMICONDUCTORS

D. C. Reynolds and K. K. Bajaj
AFWAL/AADR, Wright-Patterson AFB OH 45433

During the past several years considerable attention has been focused on artificially structured materials. These materials consist of layered structures of the same or different materials. With the advent of the metal organic chemical vapor deposition (MOCVD) and the molecular beam epitaxy (MBE) growth techniques, atomic layers of one material can be grown on another material with sharp, reproducible interfaces. For layer thicknesses of a few angstroms or less, well defined quasi two-dimensional electronic sub-bands are formed. The confined carriers result in novel electronic and optical properties. The heterostructure system that has received the most extensive investigation is the AlGaAs/GaAs system. The characterization of this system is the focus of the current paper.

In order to exploit fully the potential of the heterostructure technology, it is necessary to be able to fabricate reproducibly abrupt, high-quality interfaces between two materials. This requires both an understanding of the details of the growth process and a characterization technique capable of giving microscopic details about the quality of the interface. High-resolution photoluminescence spectroscopy (PLS) is an important experimental technique that can be used for analyzing the microscopic details of the interfaces.

In order to completely characterize the heterostructure system it is necessary also to be able to characterize the bulk materials from which the system is constructed.

Analysis of GaAs

High quality GaAs is necessary to produce optimum performance in heterostructure systems. To improve the quality requires a knowledge of the residual impurities in undoped material. The acceptors, having relatively large binding energies as compared to the donors (~30 vs. 5.7 meV), can be identified quite easily. The shallow hydrogenic donors, on the other hand, have small binding energies and also have small central-cell corrections. This makes the resolution of different chemical donors difficult.

Recently, shallow residual donors have been identified using high-resolution PLS[1,2]. The optical transitions that were used were those resulting from the collapse of neutral-donor-bound excitons (D,X). The decay of an exciton bound to a donor (acceptor) may have the donor (acceptor) in an excited state. For donor identification, the initial state consists of the exciton bound to the donor. The terminal state is the n = 2 state of the donor. Emission lines have been observed on the high-energy side of the D°,X transition in several materials. A non-rigid-rotator model was proposed[3] that was able to account for the energies of these excited states in InP and GaAs.

We discuss the identification of residual donors in GaAs from the transition involving an exciton bound to the first non-rigid-rotational state. The observation of different residual donor species from this transition is made

possible by performing the experiment in a magnetic field. The magnetic field produces two effects: (a) It separates out states with different orbital angular momentum and (b) it compresses the wave function which sharpens the lines and separates the donors. In the final state the transition can terminate in either the 2S or 2P state. From parity arguments it can be shown that the initial state of the D,X transition has odd parity. The 2S final state will have even parity whereas the 2P final state will have odd parity. The preferential transition, therefore, from the D,X initial state will be to the 2S final state. By similar arguments it can be shown that the preferential transition from the first rotator state will be to the 2P final state.

When an exciton decays from the D^{o},X state in a magnetic field the excited 2S and 2P terminal states are separated. The initial state of the complex consists of two paired electrons and one unpaired hole. The final state of the complex consists of an unpaired electron. The initial state of the complex splits into a quartet and the final 2P state splits into three widely separated states, $2P_{+1}$, $2P_{o}$, and $2P_{-1}$. The magnetic field splitting of the transition going to the $2P^{o}_{-1}$ terminal state at 40 KG is shown in Fig. 1. The inset in Fig. 1 shows the zero-field trace in the n = 2 spectral region of the D,X transition. Here it is seen that the crystal contains residual Si and S donors. The splitting of the $2P_{-1}$ state shows components of these two donors as marked in Fig. 1. The highest-intensity transitions are the spin-conserving transitions. The donors could not be resolved from this transition in zero magnetic field due to broadened lines and the near proximity of the D,X transition.

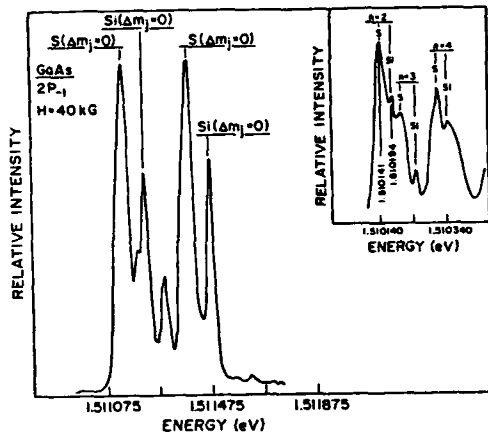

Fig. 1. Components of the $2P_{-1}$ state at 40 KG for both sulfur and silicon donors. The inset shows the same two donors in zero magnetic field resulting from the exciton bound to the second, third and fourth rotational states.

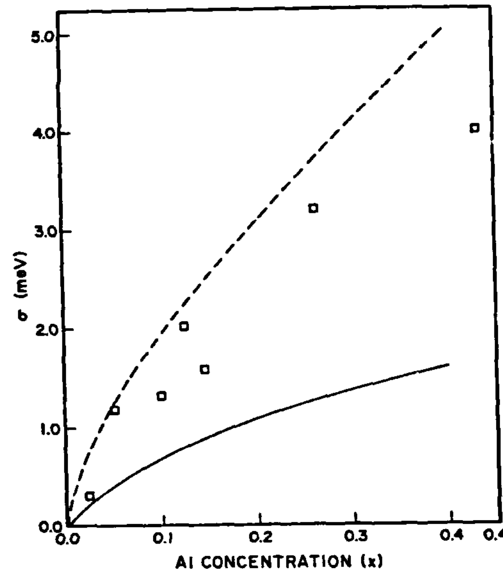

Fig. 2. Variation of σ as a function of X up to X = .43. Dashed and solid curves are theoretical curves.

Analysis of $Al_xGa_{1-x}As$

High quality AlGaAs is also required for optimum performance of the $Al_xGa_{1-x}As$/GaAs heterostructure system. One of the most useful techniques for obtaining information concerning the quality of the alloys is PLS. The shape of the excitonic transition contains a great deal of information about the

quality of the alloy. Generally, the excitonic emission spectra in semiconductor alloys are considerably broader than those observed in their binary components. This broadening has been attributed to compositional disorder present in alloys. An alloy can be random on an atomic scale or on a scale r_c in which case r_c defines the radius of the clusters in the alloys. Gaede, et al.[4] were the first to calculate σ, the full width at half maximum (FWHM) of the excitonic lines as a function of alloy composition in the perfectly random alloys. Subsequently, Singh and Bajaj[5] and Schubert, et al.[6] independently calculated the variation of σ as a function of alloy composition treating the exciton as a classical system. Recently Singh and Bajaj[7] have calculated the variation of σ as a function of alloy composition following a quantum mechanical approach. In Fig. 2 is plotted the values of the widths of the narrowest observed lines in $Al_xGa_{1-x}As$ for several values of X (open squares) along with the variation of σ as calculated, assuming a perfectly random alloy. The dashed curve is obtained by using the expression of Singh and Bajaj[5] and Schubert, et al.[6] treating the exciton as a classical system of volume $V_{ex} = (4/3) R_{ex}^3$ where R_{ex} is the exciton radius. The solid curve represents the results of Singh and Bajaj[7] using a quantum mechanical approach. Their results are about a factor of 3 smaller than those obtained in Rfs. 5 and 6. The observed linewidths are somewhat larger than those calculated using a quantum mechanical approach suggesting a possible improvement in the quality of AlGaAs in the future.

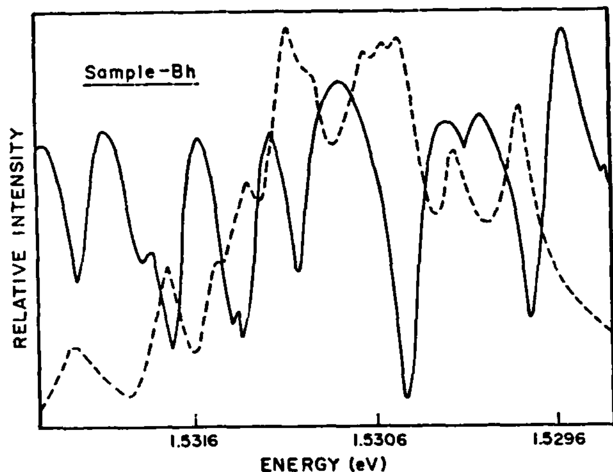

Fig. 3. The heavy-hole free exciton emission (dashed curve) and reflection (solid curve) spectra for a 135-Å MQW.

Analyses of the Interface

High resolution optical spectroscopy is an important experimental technique that can be used to analyze the microscopic details of interfaces. Optical measurements on $Al_xGa_{1-x}As$/GaAs multi-quantum-well (MQW) structures show heavy hole excitonic transitions in emission and both heavy-hole and light-hole exciton transitions in reflection spectra. Considerable structure is observed in the excitonic spectra. In Fig. 3 a sharp 11-line structure is seen in both the PLS and reflection spectra for the heavy hole excitons. A similar 11-line structure is seen for the light-hole excitons in the reflection spectra. The energy spread of the sharp line structure for both the light- and heavy-hole excitons corresponds to well size fluctuations of approximately two monolayers.

The observed fine structure can be attributed to variations in the well width in the MQW structure and the differences in the microscopic quality of the interfaces. To understand the formation of the interfaces related to MQW systems, it is recognized that the heterostructure is grown by allowing the Ga and arsenic (As_2 and As_4) beams to impinge continuously on the growing substrate. The Al flux is shut off during the formation of the well and is allowed to impinge during the growth of the barrier. A perfect interface is one in which the cation layer i is pure Ga and the layer i-1 or i + 1 is

Al_xGa_{1-x} where X is the Al composition in the barrier region. Due to the obvious limits on shutter control and calibration, it is impossible to close or open a shutter when the surface layer is exactly full. In general because of this inherent uncertainty, the surface layer i will have a coverage θ_i (<1) when the shutter is opened or closed to form the interface. The Al composition in the interfacial layer can be expressed as

$$X_i = \theta_i X,$$

when the inverted interface is formed, and

$$X_i = (1-\theta_i)X,$$

when the normal interface is formed. Here X is the concentration of Al in the barrier region. Thus, it is clear that even in the most optimized growth conditions, the Al composition at the interface, will not go from X to 0% over one monolayer, but will change from X to X_i to 0% over two monolayers. This would result in the interfacial microstructure (islands) varying randomly among various configurations.

The above discussion for the interface has definite implications concerning the PL linewidths in quantum wells. When the 2D island size is appreciably larger than the exciton size, the excitons see smooth walls and the exciton transitions are sharp. A theory for the linewidths for the case when the island sizes are comparable to, or smaller than, the exciton size has been reported by Singh et al.(8) For example, for a 100-Å quantum well, if the average island sizes are comparable to the exciton size, the linewidth is ~3 meV; however, if the average island size is approximately 20Å the linewidth is reduced to only 0.15 meV.

The above models for interface formation and PL linewidth predict that different wells, in a MQW structure will emit radiation with different linewidths and different peak positions.

Acknowledgement

We are especially grateful for the high quality AlGaAs samples and quantum-well samples provided by H. Morkoc (University of Illinois).

References

1. R. J. Almassy, D. C. Reynolds, C. W. Litton, K. K. Bajaj and G. L. McCoy, Solid State Commun. 38,1053 (1981).
2. D. C. Reynolds, K. K. Bajaj, C. W. Litton, and E. B. Smith, Phys. Rev. B28,3300 (1983).
3. W. Ruhle and W. Klingenstein, Phys. Rev. B18, 7011 (1978).
4. O. Gaede, L. John, and D. Hennig, Phys. Status Solidi, B89,K183 (1978).
5. J. Singh and K. K. Bajaj, Appl. Phys. Lett. 44, 1975 (1984).
6. E. F. Schubert, E. O. Gobel, Y. Horikosh, K. Ploog, and H. J. Queisser, Phys. Rev. B30,813 (1984).
7. J. Singh and K. K. Bajaj (to be published).
8. J. Singh, K. K. Bajaj, and S. Chaudhuri, Appl. Phys. Lett. 44,805 (1984).

LASER DIAGNOSTICS OF CADMIUM TELLURIDE: CRYSTAL QUALITY AND EXCITON DYNAMICS

Donald E. Cooper, J. Bajaj, P. R. Newman
Rockwell International Science Center
1049 Camino Dos Rios
Thousand Oaks, CA 91360

P. M. Rentzepis and J. Andrew Hutchinson
University of California
Department of Chemistry
Irvine, CA 92717

Cadmium telluride is a II-VI semiconductor of increasing interest because of the use of its ternary alloy HgCdTe as a tunable-bandgap IR detector material. CdTe is often used as a substrate for the growth of HgCdTe epilayers and the detector performance depends upon the purity and crystal quality of both the epilayer and substrate.[1] Laser diagnostics of CdTe make possible the nondestructive screening of detector materials. In many cases electronic properties such as donor and acceptor concentrations can be determined without contact fabrication. Here we present both CW and time-resolved low-temperature spectra of CdTe. The CW spectra are useful for evaluating the crystal quality and the photoluminescence (PL) decays represent the first time-resolved results on single crystal CdTe.

A variety of CdTe samples from different sources were studied. The samples were maintained at 4.2 K and excited by a mode-locked dye laser at about 605 nm, which is well above the CdTe bandgap energy. Temperature effects are observed when the samples are excited with too much intensity, and these are eliminated by attenuating the laser to 10 mW average power and focussing with a cylindrical lens to a spot of about 2 X 0.3 mm. The resulting PL was dispersed by a monochromator and detected by a phototube. For the CW spectra, a chopper modulated the excitation beam for signal detection by a lock-in amplifier. For measurement of the PL decays, the PMT output (with 1.1 ns FWHM response) was sampled and averaged with a Tektronix 7854 oscilloscope with modified sampling plug-ins. In both cases the signal was acquired and stored by a minicomputer. Further signal analysis was performed on the time-resolved data to fit it to a convolution of the PMT impulse response and a model decay function.

The PL spectrum near the band edge of one of the high-quality samples is shown in Fig. 1. The PL is dominated by emission from bound excitons near 778 and 780 nm. The two

peaks have been assigned to excitons bound to donors and acceptors, respectively.[2] At longer wavelengths three weaker peaks are seen. The peak at 783 nm has been attributed to two-electron transitions. The other two peaks are LO-phonon replicas. The largest peak at 790 nm is a replica of the bound exciton emission near 780 nm and the feature with a sharp edge at 787 nm is the replica of the polariton (free exciton) line, which is almost totally reabsorbed at about 776 nm.[3] This sample shows very little donor-acceptor pair recombination, usually seen in the 840-850 nm region, indicating that it is fairly pure.

The band-edge PL spectrum can be used as a diagnostic of crystal quality by analyzing the relative intensity of the polariton emission. Under conditions of either thermal equilibrium or kinetic control by trapping rates the ratio of bound exciton emission to polariton emission should be directly proportional to binding site density. The analysis here is complicated by the presence of two types of binding sites with different binding energies, but a comparison of the data from three samples studied shows a correlation between the PL ratio and concentrations of donors and acceptors as measured by mass spectrometry (Table 1). This correlation is somewhat surprising, since the mass spectrometer is unable to measure concentrations of some of the most common transition metal impurities such as copper, iron and nickel due to mass interference with the CdTe. In addition, native defects such as Cd vacancies are not detectable by mass spec. Further evidence comes from the spectra of samples that have been annealed under a Cd atmosphere, which can reduce the density of Cd vacancy acceptors. In the annealed samples the polariton emission was significantly greater, corresponding to an improvement in crystal quality. Data from these and a wide variety of other samples will be presented and discussed.

TABLE 1

SAMPLE	PL INTEGRATED INTENSITY RATIO (BOUND EXCITONS/POLARITONS)	IMPURITY CONC. (MASS SPEC)
2-47	52	4.2 E 15
1949	143	1.6 E 16
2-48	588	2.2 E 16

Figure 2 shows the PL decay from the polariton replica (dots), together with a calculated fit to the convolution of the PMT impulse response and an exponential decay of 1.9 ns (solid line). The rise time of this signal is limited by

the detector response, indicating that the polaritons are formed from the optically injected carriers on a subnanosecond time scale. The polariton decay is dominated by trapping on donors and acceptors. The PL decays of the bound excitons are displayed in Fig. 3. The donor-bound exciton decay waveform (Fig. 3a) is broader than that of the polariton, but the fitted decay lifetime is identical within the experimental uncertainty. The difference resides in the 0.6 ns rise time that was required for an accurate fit to the data. In this case the indicated waveform decay is determined by the polariton trapping rate and the actual bound exciton lifetime is the waveform rise time, or about 0.6 ns. This behavior has been observed in other II-VI semiconductors.[4]

The PL decay of the most intense line in the PL spectrum is shown in Fig. 3b. This line has been attributed to excitons bound on acceptors and it has the longest lifetime. This waveform also requires a rise time to produce a good convolved fit and the decay time is well resolved by our detection system. The best fit yielded a rise time of 0.9 ns and a decay lifetime of 3.55 ns. The observed lifetime varies with sample and temperature over a range of 2.6-5.0 ns. Results from a variety of samples will be presented and the application to crystal diagnostics will be discussed.

For temporal resolution of 15 ps, similar experiments were also performed using a streak camera. In addition to the CdTe studies, HgCdTe samples were also examined with this technique. These results will be presented in a related paper.

In summary, we have performed photoluminescence measurements on a variety of CdTe samples. The spectrum near the band edge contains information useful for evaluating crystal quality. Furthermore, we have performed the first time-resolved measurements on this system, which give insight into the excitation dynamics.

REFERENCES

1. G.R. Woolhouse, T.J. Magee, H.A. Kawayoshi, C.S.H. Leung, and R.D. Ormund, J. Vac. Sci. Technol., A3, 83 (1985).
2. P. Hiesinger, S. Suga, F. Willmann, and W. Dreybrodt, Phys. Stat. Sol., 67, 641 (1975).
3. E. Cohen, R.A. Street, and A. Muranvich, Phys. Rev. B, 28, 7115 (1983).
4. P. Wiesner and U. Heim, Phys. Rev. B, 11, 3071 (1975). F. Minami and K. Era, Sol. St. Commun., 53, 187 (1985).

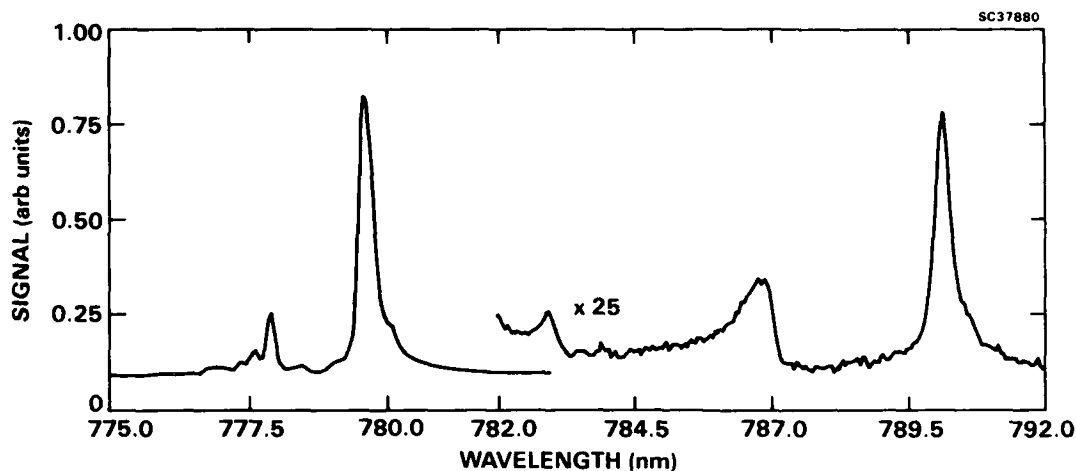

Figure 1 Photoluminescence spectrum of CdTe near the band edge.

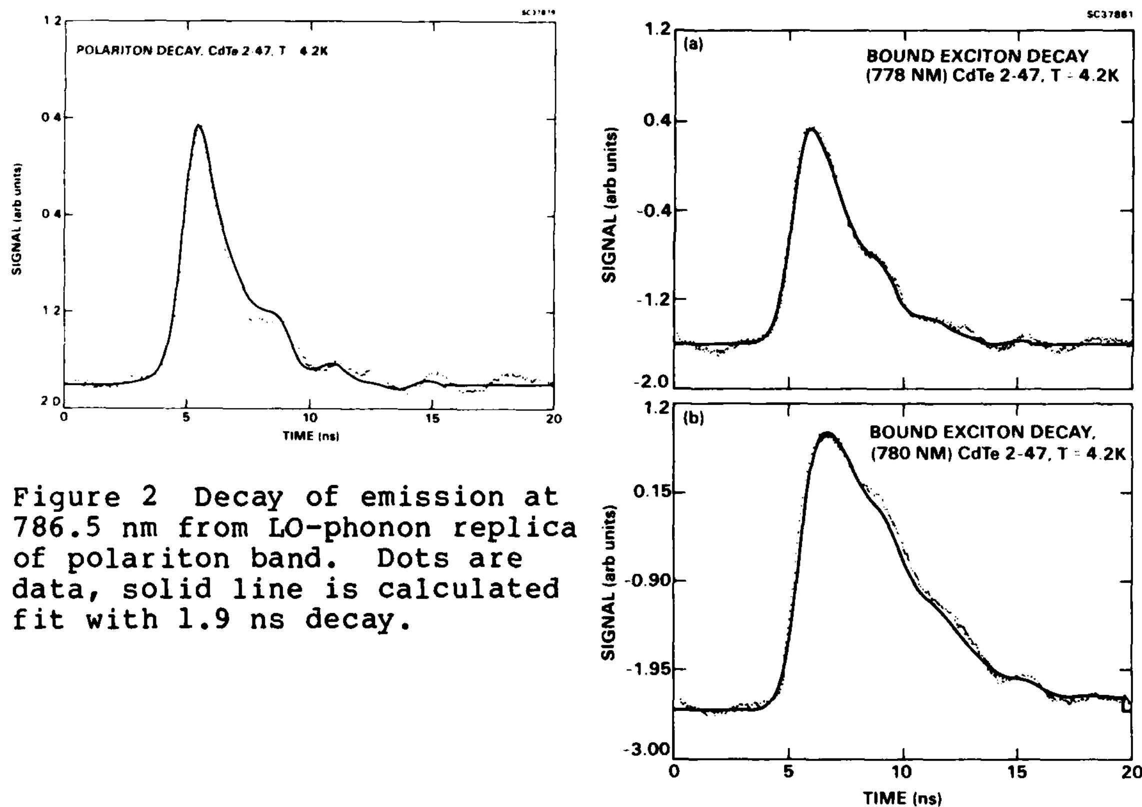

Figure 2 Decay of emission at 786.5 nm from LO-phonon replica of polariton band. Dots are data, solid line is calculated fit with 1.9 ns decay.

Figure 3 Decay of bound exciton emission: A) Emission from excitons bound on donors, 2.0 ns decay and 0.6 ns rise. B) Emission from excitons bound on acceptors, 3.55 ns decay and 0.9 ns rise.

Picosecond Time Resolved Emission of Mercury Cadmium Telluride and Related II - VI Semiconductor Crystals

J. Andrew Hutchinson, T. E. Dutton, P. M. Rentzepis

University of California
Department of Chemistry
Irvine, California 92717

Donald E. Cooper, J. Bajaj and P. R. Newman

Rockwell International Science Center
Thousand Oaks, California 91360

Abstract

Picosecond resolved emission of HgCdTe and CdTe crystals by IR-VIS streak camera shows temperature dependent multiexponential decay kinetics and elucidates the mechanisms of exciton trapping and anihilation.

Summary

The characteristics of II - VI semiconductors as optical detectors are critically dependent upon defect concentration, trapping well depth, temperature, and radiation fluence. From this standpoint, one of the best diagnostic tools for the study of tunable bandgap optical detectors is laser generated fluorescence at cryogenic temperatures. To study exciton dynamics and to verify certain theoretical dynamic models, we have obtained time and wavelength resolved emission spectra of CdTe and HgCdTe (on CdTe substrate) samples at 12-50K[1]. The samples were mounted in a cryotip under high vacuum ($\sim 10^{-7}$ torr) and cooled with liquid He to ~12K, and excited with a mode locked Ar^{+} ion

laser synchronously pumped dye laser tuned to 630 nm (τ_{pulse}=5 psec FWHM, 82 MHz, 40 mW average power, 100 μ spot size). The temporal evolution of the fluorescence emission was obtained using a Hamamatsu streak camera (CdTe samples: S-20 response tube; HgCdTe samples: extended S-1 response tube) with better than 15 ps resolution, and decay kinetics were derived by fit to a first order convolution model.

For the CdTe samples examined (T=8K), the emission showed peaks ranging from ~7756Å to ~8280Å. For wavelengths greater than 8000Å, the fluorescence lifetimes were greater than 5 nsec, the limit of our temporal resolution (15 psec to 5 nsec), and are attributed to donor-acceptor pair recombination. In a sample of high purity, no emission at these wavelengths was observed. The higher energy emission bands were dominated by two bands with maxima at 7786Å and 7810Å (Figure 1a, b), attributed to donor and acceptor bound excitons each of which display approximately biexponential decay rates, a prompt decay (τ≃200 ps) and a long decay (τ≃.8-1.5 nsec) indicating at least two distinct decay paths for these states. The emission bands also exhibit a ~60 psec rise as the excitons become trapped. A weak emission band at 7720Å with ~20 psec rise and ~80 psec decay, corresponding to free exciton formation from free carried combination and subsequent trapping and diffusion, was observed.

The liquid phase epitaxially grown short wave infrared HgCdTe samples (T=12K) showed one principle band at 13250Å, which was comprised of two decays (~250 psec and ~6 nsec) and a prompt rise (~50 psec) (Figure 2a). The relative amounts of these two decays

varied as different parts of the band were examined, indicating the presence of actually two bands that were not spectrally resolved. Raising the temperature of the sample caused the prompt decay to shorten (Figure 2b) and the relative amount of the long component to decrease until, at 50K, only the short component was observed, indicating a well depth of the trapped exciton of less than 100 cal/mole.

References

1. D. E. Cooper, J. Bajaj, P. R. Newman, J. A. Hutchinson, and P. M. Rentzepis, "Laser Diagnostics of Cadmium Telluride Crystal Quality and Exciton Dynamics," Southwest Conference on Optics, Feb 9-13, Albuquerque, NM.

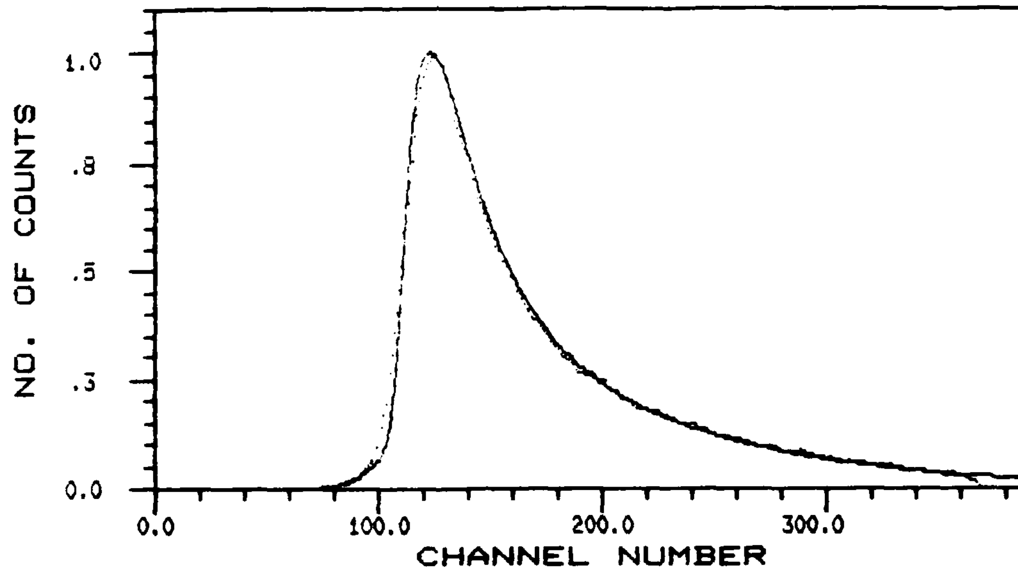

1a. Streak emission (7786 Å) and convolution curve fit for CdTe (λ_{pump}=630 nm, T≈12K, 2.5 ps/channel, t_0=channel 109).

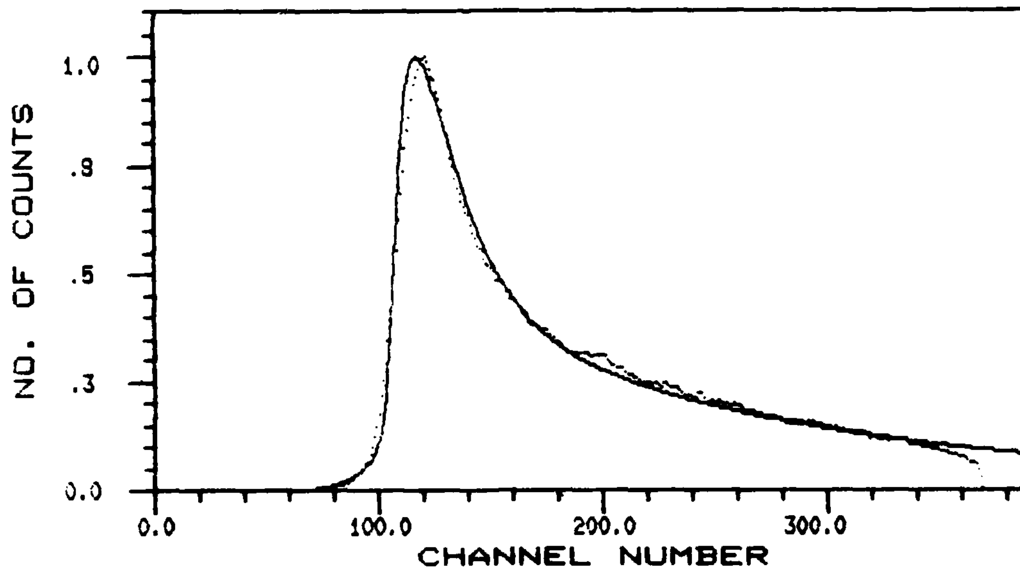

1b. Streak emission (7810 Å) and convolution curve fit for CdTe (λ_{pump}=630 nm, T≈12K, 2.5 ps/channel, t_0=channel 102).

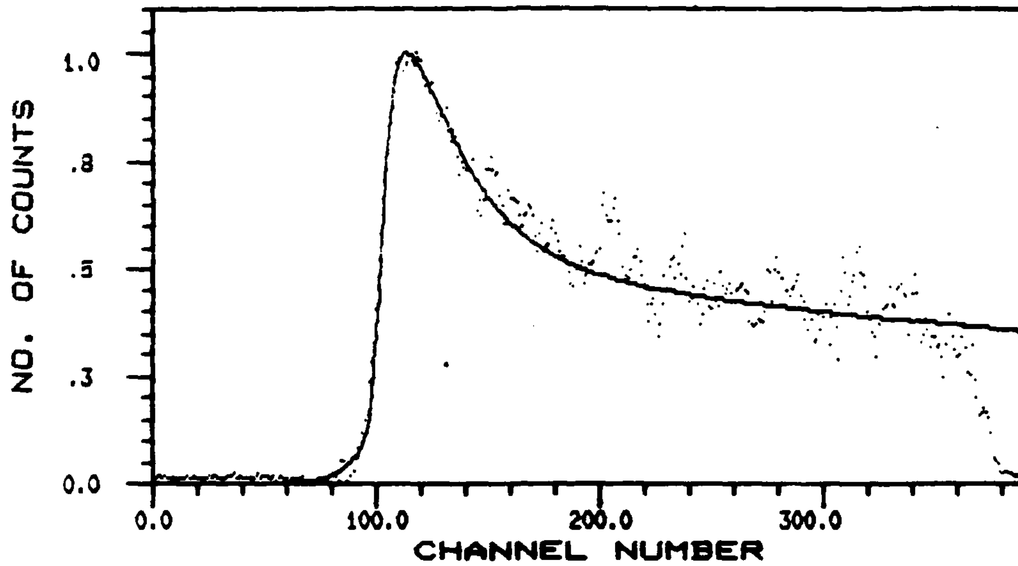

2a. Streak emission (13220 Å) and convolution curve fit for HgCdTe (λ_{pump}=630 nm, T=12K, 2.5 ps/channel, t_0=channel 101).

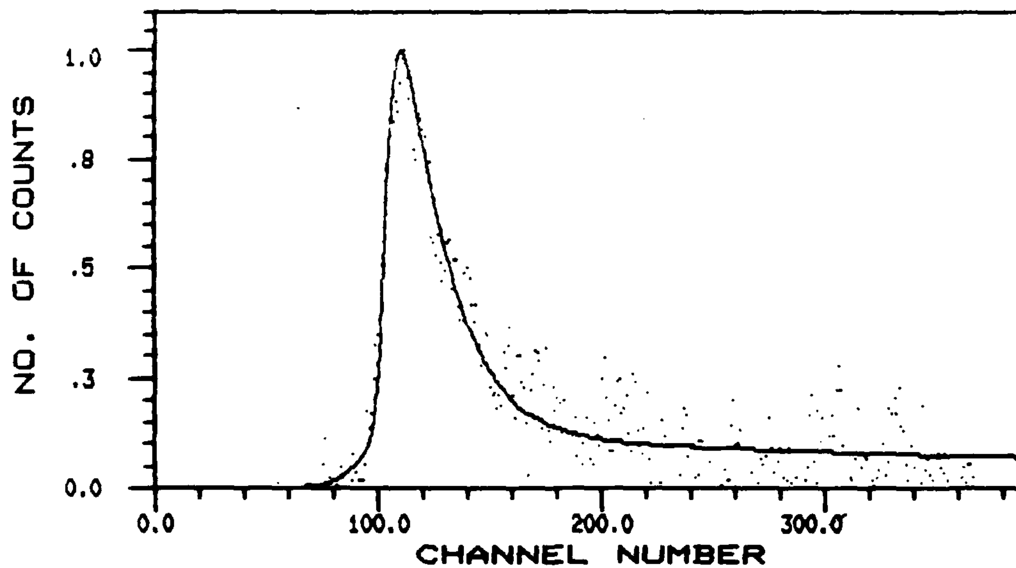

2b. Streak emission (13220 Å) and convolution curve fit for HgCdTe (λ_{pump}=630 nm, T=55K, 2.5 ps/channel, t_0=channel 102).

KEY TO AUTHORS AND PAPERS

Anthes, J. P. — WB3
Aspnes, D. E. — WF1
Atkinson, G. H. — WD2

Bajaj, J. — ThE2, ThE3
Bajaj, K. K. — ThE1
Bass, M. — ThA4
Beck, Steven — WA2
Borsella, E. — ThD2
Breiland, William G. — WD1

Carver, G. E. — WF2
Christie, W. H. — ThC2
Coltrin, Michael E. — WD1, WE2
Cooper, David E. — WD3
Cooper, Donald E. — ThE2, ThE3
Cremers, David A. — WD3

Dreyfus, R. W. — ThD1 ,
Dutton, T. E. — ThE3

Evans, Charles A., Jr. — ThC1

Fauchet, Philippe M. — WA1
Figuera, J. — ThB

Garcia, P. — WB3
Gerardo, J. — WF
Goeringer, D. E. — ThC2
Gottscho, R. A. — WE1
Greenberg, K. E. — ThD

Hammond, R. L. — ThE
Hargis, P. J. — WA3
Herman, Irving P. — ThB1
Hetherington, W. M. III — WC1, WC2
Higgins, K. L. — WA3
Ho, Pauline — WD1, WE
Ho, Z. Z. — WC1, WC2
Hogge, C. B. — WD
Hutchinson, J. Andrew — ThE2, ThE3

Innocenzi, M. — ThA4

Joy, D. C. — WF2

Kay, Bruce D. — WE2
Keller, R. — ThC
Kelly, Roger — ThD1
Koehler, D. R. — WB3
Koenig, E. W. — WC2

Larciprete, R. — ThD2
Lokberg, Ole J. — WB2

Malmo, Jan T. — WB2
Mazely, T. L. — WC1
McNeil, J. R. — WA

KEY TO AUTHORS AND PAPERS—*Continued*

Newman, P. R. — ThE2, ThE3

O'Brien, J. J. — WD2

Padma, Bandu, G. G. — WC1
Podlesnik, D. V. — ThB3

Radziemski, L. — WC
Rao, L. Kameswara — ThB2
Raymond, T. D. — WE2
Renlund, Anita M. — WC4
Rentzepis, P. M. — ThE2, ThE3
Reynolds, D. C. — ThE3
Rosencwaig, Allan — ThA1

Schroeder, Holger — ThA3
Seager, C. H. — ThA
Selvarajan, A. — ThB2
Simard-Normandin, M. — WA4
Srinivasan, R. — ThD1
Stewart, A. F. — WA3
Strand, T. C. — WB1
Stuke, M. — ThD2
Swimm, Randall T. — ThA2, ThA4

Tallant, D. R. — WA3
Tam, Andrew C. — ThA3
Trott, Wayne M. — WC4

Wachter, Joseph R. — WD3
Walkup, R. E. — ThD1
Wessel, John — WA2
Wijekoon, W. M. K. P. — WC1, WC2
Wong, P. T. T. — WA4
Wyant, James C. — WB

Zhang, Y. — ThD2

TOPICAL MEETING ON

LASERS IN MATERIAL DIAGNOSTICS

POSTDEADLINE PAPER

PDP1 "Laser Surface Modification", Ozbayasal, K., and Inal, O. T.
New Mexico Institute of Mining and Technology

LASER SURFACE MODIFICATION

K.Ozbaysal and O. T. Inal

Materials and Metallurgical Engineering Department
New Mexico Institute of Mining and Technology
Socorro, New Mexico 87801

Experimental procedures and preliminary results are presented for laser surface melted mild steel, laser surface alloying and cladding using a CW CO_2laser. Microstructural and EDS analyses of the treated surfaces indicate that a laser beam can locally enhance surface properties. Laser surface alloying offers possibility of selectively modifying a low cost work piece surface to achieve the desired surface properties of high performance alloys. Laser cladding affords the application of high melting temperature carbides onto low melting work pieces as well as the potential of applying ceramics to metallic work pieces. Further studies will provide better understanding for the maximum utilization that can be expected of laser surface treating processes.